Droplet dynamics in mini-channel steam flow condensation

by

Xi Chen

B.S., Wuhan Institute of Technology, 2010
M.S., Wichita State University, 2012

AN ABSTRACT OF A DISSERTATION

submitted in partial fulfillment of the requirements for the degree

DOCTOR OF PHILOSOPHY

Department of Mechanical and Nuclear Engineering
College of Engineering

KANSAS STATE UNIVERSITY
Manhattan, Kansas

2017

Abstract

Power plants are significant water users, accounting for 15% of water withdrawals worldwide. To reduce water usage, compact condensers are required to enable air-cooled condensers and reduce infrastructure costs. Steam flow condensation was studied in 0.952-mm and 1.82-mm hydraulic diameter mini-gaps in an open loop experimental apparatus. The apparatus was validated with single-phase flow. Flow condensation experiments were conducted for a wide range of steam mass fluxes (i.e., 35–100 kg/m^{2}s) and qualities (i.e., 0.2–0.9) in hydrophilic copper and hydrophobic Teflon-coated channels. Water contact angles were 70^o and 110^o on copper and Teflon, respectively, and in general, filmwise condensation was the primary condensation mode in the hydrophilic channel and dropwise condensation was the primary mode observed in the hydrophobic channel. Pressure drops were reduced by 50–80% in the hydrophobic channels. Condensation heat transfer was enhanced by 200–350% in hydrophobic mini-gaps over hydrophilic mini-gap due to dropwise condensation. Droplet dynamics (e.g., nucleation, coalescence and departure) were quantified during dropwise condensation. A model was created which includes droplet adhesion and drag forces for droplet departure diameters which were then correlated to heat transfer coefficients. An overall mean absolute error of 9.6% was achieved without curve fitting. Noncondensable gases can reduce heat transfer in industrial systems, such as power plants due to the additional layer of thermal resistance from the gas. Condensing steam-nitrogen experiments were conducted for nitrogen mass fractions of 0–30%; the addition of nitrogen reduced heat transfer coefficients by up to 59% and 30% in hydrophilic and hydrophobic mini-gaps, respectively. It was found that during dropwise condensation, the noncondensable layer was perturbed by cyclical droplet motion, and therefore heat transfer coefficients were increased by 2–5 times compared with filmwise condensation of the same mass fraction of nitrogen.

Droplet dynamics in mini-channel steam flow condensation

by

Xi Chen

B.S., Wuhan Institute of Technology, 2010
M.S., Wichita State University, 2012

A DISSERTATION

submitted in partial fulfillment of the requirements for the degree

DOCTOR OF PHILOSOPHY

Department of Mechanical and Nuclear Engineering
College of Engineering

KANSAS STATE UNIVERSITY
Manhattan, Kansas

2017

Approved by:

Major Professor
Melanie M. Derby

Copyright

Abstract

Power plants are significant water users, accounting for 15% of water withdrawals worldwide. To reduce water usage, compact condensers are required to enable air-cooled condensers and reduce infrastructure costs. Steam flow condensation was studied in 0.952-mm and 1.82-mm hydraulic diameter mini-gaps in an open loop experimental apparatus. The apparatus was validated with single-phase flow. Flow condensation experiments were conducted for a wide range of steam mass fluxes (i.e., 35–100 kg/m^{2}s) and qualities (i.e., 0.2–0.9) in hydrophilic copper and hydrophobic Teflon-coated channels. Water contact angles were 70^o and 110^o on copper and Teflon, respectively, and in general, filmwise condensation was the primary condensation mode in the hydrophilic channel and dropwise condensation was the primary mode observed in the hydrophobic channel. Pressure drops were reduced by 50–80% in the hydrophobic channels. Condensation heat transfer was enhanced by 200–350% in hydrophobic mini-gaps over hydrophilic mini-gap due to dropwise condensation. Droplet dynamics (e.g., nucleation, coalescence and departure) were quantified during dropwise condensation. A model was created which includes droplet adhesion and drag forces for droplet departure diameters which were then correlated to heat transfer coefficients. An overall mean absolute error of 9.6% was achieved without curve fitting. Noncondensable gases can reduce heat transfer in industrial systems, such as power plants due to the additional layer of thermal resistance from the gas. Condensing steam-nitrogen experiments were conducted for nitrogen mass fractions of 0–30%; the addition of nitrogen reduced heat transfer coefficients by up to 59% and 30% in hydrophilic and hydrophobic mini-gaps, respectively. It was found that during dropwise condensation, the noncondensable layer was perturbed by cyclical droplet motion, and therefore heat transfer coefficients were increased by 2–5 times compared with filmwise condensation of the same mass fraction of nitrogen.

Table of Contents

List of Figures

List of Tables

Acknowledgements

I would like to express my special appreciation to my advisor Dr. Melanie Derby. I would like to thank you for encouraging my research and for allowing me to grow as a research scientist. It has been a transformative four years in the best way I can imagine, actually even beyond your imagination. Your advice, help and support on both research as well as on my career and life are priceless ever. I would also like to thank my committee members, Dr. Amy Betz, Dr. Steven Eckels, Dr. Larry Glasgow and Dr. Stacy Hutchinson for serving as my committee members. I also want to thank you for giving me brilliant comments and suggestions in every research progress reporting presentations. Many thanks to K-State and Wichita State community. Thanks to many good open sources on internet.

A special thanks to my family: my mother-in law, father-in-law, my mother, and father for all of the silent sacrifices that you have made on my behalf. Very special thanks to my mom. Looking back, I just realized how much best you have been devoted for me with a restrained love. I would also like to thank all of my friends who supported me in many ways I do not even deserve. Thanks to Elaine Chan, Michael Ng, Dr. Hamid Lankarani, Song Liu, Daming Wei. At the end I would like express appreciation to my beloved wife Yang Liu and my son David Young Chen for the tremendous joy you give me. You have always given the very best strength.

Chapter 1 Introduction

Steam condensation, due to large latent heat of water [1], is an important process in industries such as thermal power plants [2, 3], desalination [4], fuel cells [5], air conditioning systems [6], water harvesting [7], and electronic device cooling [8]. In the Food-Energy-Water nexus, access to water is essential for the rising population, economic growth, and changes in diets. The energy sector is one of the largest consumers of fresh water which is a finite resource. In 2010, electricity generation sectors accounted for 15% of worldwide water withdrawals (i.e., 583 billion m^3) [9], and in the U.S., thermal power plants were responsible for more than 40% of industrial fresh water withdrawals [10]. According to EPA, more than 1,000 facilities in the U.S., including approximately 500 power plants, withdrew at least 2 million gallons of water each day [11], and approximately 90% of the water intake in the power plants went to condensers to condense steam turbine exhaust into liquid water [9].

Power plant water usage depends on the type of condenser. The traditional water-steam once-through condensers have the lowest infrastructure cost, yet demand the most water intake (i.e. 75-150 m^3/MWh) and create thermal pollution to aqueous organisms [12]. Cooling towers greatly reduce water intake (i.e., 2–28 m^3/MWh) and eliminate thermal pollution to the watersheds. However, cooling towers increase water consumption (i.e., the amount of water not returning to the source) through evaporation increases from 0.8 m^3/MWh in once-through condensers to 2.3 m^3/MWh in cooling towers [2]. Currently, once-through systems and cooling towers constitute 42% and 43% of the power plant condensers, respectively [10, 13]. Air-cooled systems in which heat is rejected from hot steam to air flow nearly eliminates water usage in condensers [14]; however, the performance of air-cooled systems depends on the air dry-bulb temperature, which is higher and fluctuates more than wet-bulb temperatures for cooling towers. Air-cooled systems

typically cost 3.5 to 5 times more than cooling towers and cause the levelized costs of electricity to be about 15% higher [15]. An improved fundamental understanding of steam-side condensation and air-side heat transfer can improve heat transfer performance and reduce infrastructure cost of air-cooled condensers to benefit power generation in the water-constrained future [16].

Chapter 2 Literature review

Condensate forms when vapor contacts a subcooled surface. In flow condensation, convective forces increase heat transfer between the fluid and channel walls, as well as transport fresh fluids to the walls [17]. Flow condensation of steam, steam-air mixtures, organic fluids, and refrigerants have been studied, including flow patterns [18, 19], void fraction [20-25], pressure drops [26-50], and heat transfer performance [51-57]. The heat transfer rate is proportional to surface area and thus channel diameter while the mass flow rate of the fluid is proportional to the cross sectional area and thus the second order of channel diameter. This prompted recent interest in mini-channel condensation (e.g., $D < 3$ mm) compared conventional-sized channels. Reducing channel size potentially decreases the refrigerant charge, reduces overall heat exchanger size, and improves system efficiency. As channel size decreases, the relative influence of gravity, shear, viscous and surface tension differs from conventional channels, thereby affecting flow patterns, pressure gradients, and heat transfer coefficients [58, 59]. Condensation in mini/micro-channels for compact heat exchanger design has been of interest to the HVAC and automobile industries since the late 1990s, yet limited research have explored steam flow condensation in mini/micro-channels.

2.1 Mini- and micro-channel definitions

There is no single size definition for macro-, mini-, and micro-channels. Kandalikar and Grande [60] considered the significance of liquid-solid interface, applicability of no-slip boundary condition, fabrication capability, and experimental errors. Channels with hydraulic diameter greater than 3 mm were considered conventional-sized channels, between 200 μm and 3 mm were mini-channels and between 10 and 200 μm were termed micro-channels. In conventional and mini-

channels, continuum theory is applicable with a no-slip boundary condition, while in micro channels, rarefaction effects take place and the continuum theory needs modification to account for wall slip. These diameters were determined using air at a temperature of 300 K.

Serizawa et al. [61] suggested the Laplace constant $L_c = \sqrt{\frac{\sigma}{g(\rho_l - \rho_v)}} > D_h$ as the criteria for small channels. The Laplace constant measures the stratifying effect of gravity and when $L > D_h$, surface tension dominates over gravity as [62]. Therefore, rather than setting a uniform criterion for macro-, mini- and micro-channels for all fluids at various temperatures, these researchers suggested it is better to using the distinguishing features as identifications. In macro-channels, gravity dominates the flow regimes whereas in mini-channels, shear and viscous effects dominate over gravity in flow regimes, pressure drops, and heat transfer. In micro-channels, surface tension affects bubble and droplet dynamics. For most fluids (i.e. steam and refrigerants), the transition from macro- to mini- channel is between 1 to 10 mm depending on the fluid properties (e.g. density, surface tension, viscosity), which is also the size of many current and near-future engineering applications. In macro-channels (e.g. D_h > 10mm), stratified flow is common due to the influence of gravity whereas in mini/micro-channels (e.g. D_h < 10mm), shear-driven condensation prevails where annular and bubbly/slug flows exist more often.

2.2 Filmwise mini/micro-channel condensation heat transfer

On hydrophilic surfaces such as metal, liquid forms a film on the cooled surface and the film thickness increases along the axis due to the accumulation of condensate. Over decades, research utilizing Nusselt's falling film analysis [63] investigated filmwise flow condensation heat transfer in conventional channels where gravity dominates the flow regime and heat transfer, employing analytical [64, 65], experimental [66] and numerical approaches [67, 68]. In the past

two decades, condensation in mini/micro-channels presented better heat transfer performance than conventional channels to meet the demand for more compact heat exchangers. Shear forces and surface tension thin the liquid film and reduce the thermal resistance.

2.2.1. Refrigerant condensation in mini/micro-channels

In mini/micro-channels, heat transfer coefficients generally increase with decreasing channels sizes [69-71]. Most of the existing research of flow condensation in mini/micro-channels focused on the condensation of refrigerants such as R-134a, R-12, R-22 and R-410A for developing more compact and effective heat exchangers in air-conditioning and heat pump systems; few studies considered steam. Therefore, a brief review of the mini/micro-channel refrigerant literature follows. Table 2.1 tabulates condensation heat transfer of refrigerants and steam in horizontal channels with different cross section shapes and hydraulic diameters of 0.4 to 5 mm at various mass fluxes.

Table 2.1 Experiments of condensation heat transfer in horizontal small channels

Authors	Fluids	Mass fluxes (kg/m^2s)	Channel characteristics
Yan and Lin [45]	R-134a	100, 200	C, 2mm
Matkovic et al. [72]	R-134a, R-32	100 – 1200	C, 0.96mm
Yang and Webb [51]	R-12	400 – 1400	R, 2.64mm MF, 1.56mm
Yang and Webb [73]	R-12, R-134a	400, 1400	C, 1.41mm; MF, 1.56mm
Kim et al. [74]	R-22, R-410A	200 – 600	R, 0.5, 0.7, and 1mm C, 0.5, 0.7, and 1mm
Wang et al. 2002[75]	R-134a	75 – 750	R, 1.46mm
Shin and Kim [69]	R-134a	100 – 600	C, R 0.5 – 1mm
Garimella and Bandhauer [76]	R-134a	150 – 750	C 0.4 – 4.9mm
Derby et al. [77]	R-134a	75 - 450	S, T, semi-C 1mm
Derby et al. [16]	Steam	50 – 200	R, 1mm
Kim and Mudawar [78]	FC-72	118 –367	R; 2mm
Chen and Derby [79]	Steam	50 – 100	R; 1mm

C: Circular, R: Rectangular, S: Square, T: Triangular, MF: Microfined

Yan and Lin [45] investigated the effects of heat fluxes, mass fluxes, vapor qualities, and saturation temperatures of R-134a on condensation heat transfer coefficients and pressure drops of

condensation in a 2-mm-diameter circular tube. Heat transfer coefficients increased with decreasing saturation temperature, increasing steam qualities for higher vapor-liquid interfacial convection, and increasing steam fluxes at high quality-region (i.e. $x > 0.5$). Heat transfer coefficients were not significantly changed by steam mass fluxes in the low-quality region (i.e. $x < 0.3$). Due to the huge difference (i.e. approximately three orders of magnitude) between vapor and liquid, the slip ratio (i.e. the relative velocity between vapor and liquid) greatly decreased and thus the interfacial shear forces decreased, which mitigated effects on heat transfer coefficient by increasing quality at low-quality region. Heat transfer coefficients in 2-mm-diameter circular tubes were 10% higher than in 8-mm circular tubes due to an increased surface to volume ratio and surface tension surface tension effects, which decreased the liquid film thickness and the thermal resistance within it.

Kim et al. [74] studied condensation of R-22 and R-410 in flat aluminum channels with and without micro-fins. The Weber number ($We = \frac{\rho U^2 D}{\sigma}$) of R-22 is smaller than R-407c due to the higher surface tension value of R-22. This resulted in higher heat transfer coefficients of R-22 due to surface tension drainage. Therefore, condensation heat transfer that heat transfer coefficients was independent of steam mass flux. It was hypothesized that the corners thin liquid films in non-circular channels, which reduced thermal resistance of liquid film and increased filmwise heat transfer. Wang and Rose [80-82] analytically studied filmwise condensation of R134a, R22, and R410A in 0.5-mm to 5-mm channels, considering surface tension, interfacial shear stress and gravity. Heat transfer coefficients in non-circular tubes were not necessarily higher than circular tubes depending on flow parameters. Derby et al. [77] reported no significant difference of R-134a condensation heat transfer coefficients in square, triangular and semi-circular mini-channels with hydraulic diameters of approximately 1 mm.

Matkovic et al. [72] studied condensation heat transfer coefficients of R134a and R32 in 0.96-mm diameter circular tube at a wide mass flux range (e.g., 100–1200 kg/m^{2}s). Experimental heat transfer coefficients were compared against four macro-channel correlations: Moser et al. [53] as modified by Zhang and Webb [46], Koyama et al. [83], Cavallini et al. [84], and Cavallini et al. [85]. The Zhang and Webb [46] correlation generally underestimated heat transfer coefficients by 8–25%. The discrepancy increased as quality decreased because the correlation was developed for annular flow. Koyama et al. [83] correlation did not capture the trend of heat transfer coefficients with respect to mass flux and a number of predictions underestimated the data by more than 30%. The Cavallini et al. correlation [84] was developed for mini-channels where shear dominates flow regimes, based on theoretical analysis of Kosky and Staub [86]. The correlation slight overpredicted heat transfer coefficients of R32 and underestimated R134a. The Cavallini et al. [85] correlation is a flow regime-based model developed using condensation data in 3–8 mm tubes. Most of the predictions were within the range of ±15% except those with the lowest mass velocities and qualities, where the association of flow regimes to flow velocity is different compared to macro-channels.

2.2.2. Steam condensation in mini/micro-channels

The surface tension of water is much higher (e.g., approximately 10 times) than most refrigerants (e.g. R-134a, R-22, R-410A), and therefore the effects of surface tension in mini/micro-channels are more significant, which provides great potential for heat transfer enhancements. Reducing channel size may thin liquid water films and therefore increase steam condensation heat transfer. Derby et al. [16] studied steam condensation heat transfer in rectangular copper channels with hydraulic diameters of 1.06 mm and demonstrated the significant shearing effects in mini-gaps. The heat transfer coefficients scaled with respect to mass flux at

higher qualities (i.e. $x > 0.7$). At lower qualities, heat transfer coefficients were independent of steam mass fluxes but greatly dependent on qualities. Zhao and Liao [87] analytically studied filmwise condensation heat transfer in vertical equilateral-triangular microchannel with hydraulic diameters of 1.16, 0.87, and 0.58 mm. This study considered capillary forces caused by special deviation of free liquid film curvature and interfacial shear stress. Liquid on the condensation surface were divided into two zones: on the plain side and in the corners. Compared with circular tubes, triangular channels provided up to three times higher heat transfer coefficients, which were attributed to the greatly thinned liquid film on the side wall and was amplified as the channels size inlet steam velocity and inlet subcooling decreased. Kim and Mudawar [78] amassed 4045 condensation data points of 17 different working fluids, including steam, and developed a condensation heat transfer correlation. The correlation is applicable for annular and slug/bubbly flows which are distinguished by modified Weber number and Martinelli parameter. The overall MAE of the correlation was 16%; 87% of the data were predicted within ± 30% and 98% of the data were predicted within ± 50%.

2.3 Filmwise condensation heat transfer pressure drops

Decreasing channel sizes increases vapor core velocity and vapor-liquid interfacial shear stress, thereby sustaining annular flow. However, higher pressure drops usually accompany these phenomena potentially reducing the overall efficiency [88].

2.3.1. Pressure drop modeling

The Homogeneous Equilibrium Model (HEM) and Separated Flow Model (SFM) are two approaches to predict two-phase pressure drops in conventional tubes. The HEM treats two-phase flow as a uniform single-phase and applies single-phase models for two-phase pressure drops. In

order for the model to work, the two phases are assumed to have same velocity and mixture viscosity and density of mixture is usually averaged on mass basis. It is most applicable for high mass flux cases (e.g., $G > 2000\ \mathrm{kg/m^2s}$) where the two phases are well mixed and the same velocity assumption is more reasonable. Several researchers [89-95] modified the HEM to build the best viscosity correlation for the two-phase mixture Reynolds number. The SFM considers two homogeneous streams in two-phase flow. The resultant pressure drops depend on the individual streams and the interactions between two streams. Lockhart-Martinelli [26] developed a correlation using the separated flow model. It is an empirical correlation expressed in terms of two-phase multipliers to the corresponding single-phase liquid or gas-phase pressure drop (Equation 2.1),

$$\left(\frac{dP}{dz}\right)_{tp} = \phi_l^2 \left(\frac{dP}{dz}\right)_l \qquad \textbf{2.1}$$

where $\left(\frac{dP}{dz}\right)_{\mathrm{tp}}$ is the two-phase pressure gradient, $\left(\frac{dP}{dz}\right)_{\mathrm{l}}$ is the liquid-only pressure gradient and ϕ_{l}^2 is two-phase multiplier. A widely used correlation for the two-phase frictional multiplier was developed by Chisholm and Laird [96]

$$\phi_l^2 = 1 + \frac{C}{X} + \frac{1}{X^2} \qquad \textbf{2.2}$$

$$X = \frac{\left(\frac{dp}{dz}\right)_l}{\left(\frac{dp}{dz}\right)_v} \qquad \textbf{2.3}$$

where C is Chisholm parameter ranging from 5 to 20 and X is Martinelli parameter; both parameters depend on whether the liquid and gas flows are laminar or turbulent.

2.3.2. Experimental and analytical pressure drops

As tabulated in Table 2.2, research studied two-phase refrigerant, air-water, air-nitrogen and steam pressure drops in mini/micro-channels. Two-phase pressure drops in mini/micro-

channels generally do not agree with the extrapolation of predictions for macro-channels, possibly because of poor extrapolation of flow regime predictions or incorrect analyses of pressure drops in small channels [97].

Table 2.2 Experiments of condensation pressure drops in horizontal small channels

Authors	Fluids	Mass fluxes [kg/m^{2}s]	Channel properties
Hinde et al. [98]	R-134a, R-12	149 – 298	C, 4.6 mm
Coleman [99]	R-134a	150 – 750	C, R, 0.4–1.5 mm
Shin [100]	R-134a	100 – 600	C, R, 0.5 – 1 mm
Mitra [101]	R-410a	400 – 800	C, 6.22mm
Andresen [102]	R-410a	200 – 800	C, 0.76, 1.5, 3.05 mm
Quan et al. [103]	Steam	90 – 288	Tr, 0.11, 0.142, 0.151 mm
Marak [104]	Methane	162 – 701	C, 1mm
Huang et al. [105]	R-410a	200 – 600	C, 1.6, 4.18 mm

C: Circular, R: Rectangular, Tr: Trapezoidal

Much research has been devoted to develop new groups of dimensionless number for the Chisholm parameter in order to better represent the flow regime and pressure drops in mini/micro-channels [88]. Dutkowski [106] measured pressure drops of air-water mixture in 1.05 – 2.30 mm tubes. Experimental data showed poor agreement with conventional Lockhart-Martinelli [26] and Friedel [28] correlations. Modification and adjustments for mini-channels were appealed. Choi and Kim [107] investigated adiabatic water-nitrogen flow in rectangular channels with hydraulic diameters of 0.5, 0.32 and 0.15 mm. Reducing aspect ratio reduces film thickness, increases confinement number, and decreases the Chisholm parameter in the Lockhart-Matinelli correlation. Kim and Mudawar [88] amassed 7115 adiabatic and condensing two-phase pressure drop data points of 17 working fluids in mini/micro-channels with hydraulic diameter of 0.0695 to 6.22 mm. They developed a new correlation by modifying the Chisholm parameter using a combination of Reynolds, Weber, Capillary, and Suratman numbers and the density ratio. The new correlation has fairly uniform accuracy for all working fluids and the overall mean absolute error for condensation pressure drops was 17.5%

The discussion above is for frictional pressure drops and there are other pressure drops in flow condensation: deceleration pressure drops ($\Delta P_{tp,A}$) and gravitational pressure drops ($\Delta P_{tp,G}$). Compared with frictional pressure drops, the other pressure drops vary much less and the recommended correlations are respectively [88]:

$$\Delta P_{tp,G} = -\int_0^L [\alpha\rho_v + (1-\alpha)\rho_l] g \, sin\phi \, dz \quad \textbf{2.4}$$

$$\Delta P_{tp,A} = -\int_0^L G^2 D[\frac{\nu_v x^2}{\alpha} + \frac{\nu_l (1-x)^2}{1-\alpha}] \quad \textbf{2.5}$$

where L is the length of the channel, α is void fraction, G is the flow mass flux, x is steam quality, D is the channel hydraulic diameter, v is the specific volume, ρ is the density, and g and f denote saturated vapor and liquid respectively.

Dropwise condensation heat transfer

As reported by Rose [108], Schmidt et al. [109] first recognized 5 –7 times higher heat transfer coefficients in dropwise condensation rather than filmwise condensation. Le Fevre and Rose [110] measured time-averaged heat transfer coefficients at different heights (i.e. 25.4 mm, 28.4 mm, and 101.6 mm from the top) on a 22 mm wide and 127 mm tall vertical plate at ambient pressure, observing an independence of heat transfer coefficients on the location despite different droplet motion. Later research investigated many aspects of dropwise condensation including nucleation site density [111-113], subcooling degree [114], droplet size [115], steam velocity [116], heat flux [116], saturation pressure [117], although these factors are not independent. Lee et al. [113] numerically studied dropwise condensation on a nano-pin-structured surface on which nucleation density was tunable through different nano-pin dimensions and spaces. Higher heat fluxes were achieved as nucleation sites increased. Tanasawa and Ochiai [115] obtained time-averaged steady-state dropwise condensation by wiping the surface periodically. Various

sweeping periods generated different maximum droplet sizes, where higher time-averaged heat transfer coefficients were associated with smaller maximum droplet sizes and higher wiping rates. Extremely high transient heat transfer (greater than $1MW/m^2k$) happened immediately after surface wiping. Tanner et al. [116] promoted dropwise condensation using montan wax on copper surfaces. Heat transfer coefficients increased with increasing heat flux and steam velocity. Hatamiya and Hiroaki [117] experimentally studied dropwise condensation of steam on a gold-plated copper block, ultra-finished gold disk, gold-vapor deposited silicon disk, and chromium plated copper blocks at different saturation pressures. Under same conditions, smaller droplets seemed to be densely populated on the gold-plated surface and provided higher heat transfer coefficients. With similar droplets sizes, similar heat transfer coefficients were observed on two surfaces. Heat transfer coefficients at atmospheric pressure were as much as six times higher than at 1 kPa.

In dropwise condensation, a periodic motion of droplet nucleation, coalescence and departure can be driven by gravity or shear flow. This cyclical process promotes nucleation and reduces the liquid film thermal resistance, which provides significantly higher heat transfer coefficients than filmwise condensation. Heat transfer coefficients were found to decrease with increasing droplet contact angle hysteresis which generally corresponds to higher contact angle and easier droplet rolling [118]. Ma et al. [119] proposed that dropwise condensation heat transfer coefficients were related to the surface free energy difference between the condensate and the solid surface. Lower surface energy, associated with higher contact angle, tended to promote dropwise condensation. Surface modifications such as organic polymer coating [120-126], self-assembled monolayer (SAM) [113, 127-132], ion implantation [133-136], electroplating [137], mini/micro/nano-structures [138-140] and biphilic patterns [16, 114, 141-143] decreased surface

energy and eased droplet roll-off to promote dropwise condensation and increase heat transfer coefficients.

Zhang et al. [126] promoted dropwise condensation on copper substrates with different treatments of organic promoters: polyphenylene sulfide (PPS), polytetrafluoroethylene (PTFE) and self-assembled micro/nano silver (SAM). For the largest number of nucleation sties, the SAM surface provided 1.95, 3.08, and 1.54 times higher heat transfer coefficients over PPS, PTFE and plain copper. Rausch et al. [133, 134] performed steam condensation on N^+ implanted aluminum and titanium surfaces. Alloy inhomogeneity of aluminum reduced dropwise condensation on the implanted aluminum surface and dropwise condensation resulted in a heat transfer enhancement factor of two. The implanted titanium surfaces provided five times higher heat transfer coefficients than the unimplanted surfaces, and stable dropwise condensation was observed over the whole plate despite decreased static contact angle on the surface (75^o) compared to the unimplanted surface (94^o), which was attributed to the nano-scale roughness and surface chemistry effects caused by precipitates. Surface wettability can be improved or suppressed through roughness and physical textures on the surface [144].

Wenzel [145] and Cassie [146] proposed different wetting behavior of surfaces with different textures. Dietz et al. [147] applied cupric hydroxide nanostructures and obtained a superhydrophobic surface (contact angle of 150^o). Compared to Rain-X coated hydrophobic surfaces, the superhydrophobic surface facilitated droplet departure and altered the droplet size distribution. The predicted heat transfer coefficients based on Le Fevre and Rose correlation [148] were 2 times higher on the superhydrophobic surfaces. Peng et al. [114] performed steam condensation on surfaces with hydrophilic strips of PFA/Cr_2O_3 or SAMs of different width and spaces on copper disks of 13.25-mm radius. Liquid water was presumed to travel spontaneously

for the surface energy differences between hydrophilic and hydrophobic parts. Maximum droplet size was altered by the width and space of the strips and up to 1.18 times heat transfer coefficients over pure hydrophobic surface was observed on patterned surfaces.

2.4 Dropwise condensation modeling

In dropwise condensation, saturated vapor deposits on condensation surfaces and forms small droplets, which grow until external forces (i.e. gravity or shear forces) sweep them away [148]. Le Fevre and Rose [148] analyzed condensation heat transfer through a single droplet using an electrical resistor analogy. They also proposed the idea of integrating heat transfer rates through single droplets over the range of droplet size distribution to obtain the average heat transfer rate on condensation surfaces. Le Fevre and Rose [148] visualized dropwise condensation and correlated a power-law function for droplet size distribution with heat transfer coefficient obtained in their previous work [110], through which they developed the first dropwise condensation heat transfer coefficient correlation with four experimentally determined coefficients. Graham and Griffith [149] derived the minimum stable droplet size through mechanics and thermodynamics analysis,

$$r_{min} = \left(\frac{2T_s\sigma}{h_{lv}\rho_l}\right)\frac{1}{\Delta T} \qquad \textbf{2.6}$$

where T_s is saturation temperature, σ is surface tension of liquid, h_{fg} is evaporative enthalpy, ρ_l is the density of liquid, and ΔT is the difference in saturation and surface temperatures.

Tanaka [150] observed that the power-law function works well for droplets growing through coalescence but not for smaller one growing through direct condensation. Population theory [111, 118, 150-152] considers conservation of droplet numbers in certain ranges of droplet sizes as well as sweeping effects. In the following decades, single droplet heat transfer models

improved to include the effect of thermal resistance of surface promoter, contact angle, and subcooling degree; droplet size distribution models evolved to consider nucleation site density. This research develops the first model for internal dropwise condensation where shear forces drive droplet incipient motion. Detailed derivations and cited works are in section 4.3.

2.5 Condensation heat transfer with noncondensable gases

In thermal power stations and seawater desalination systems, degradation of condensation due to the presence of noncondensable gases is a common problem. Two sources of noncondensables are the penetration of gas through small leaks of pipe and tube fittings if the system operates at vacuum, and the outgassing of oxygen, nitrogen and CO_2 in the evaporator [153]. Since Othmer [154] identified a great decrease of condensation heat transfer performance in the presence of NCG, the degradation effects of various gases (e.g. air, oxygen, nitrogen, hydrogen, CO_2, helium) have been investigated experimentally.

Table 2.3 lists the experimental work on condensation heat transfer in presence of noncondensable gases.

Table 2.3 Experiments of flow condensation in presence of noncondensable gases

Authors	Fluids	Gases	Gas mass fraction %	Orientation	Steam Velocity
Lee and Rose [155]	R-113	air/hydrogen	0.02 – 32	Horizontal	0.3 – 26 m/s
Wu and Vierow [156]	steam	air	0–20	Horizontal	8.2 – 38 m/s
Chantana and Kumar [157]	steam	air	3–12	Horizontal	1.8–5.5 m/s
Siddique et al. [158]	steam	air/helium	10 – 35	Vertical	7.9 – 31.9 kg/h
Kuhn [159]	steam	air/helium	0 – 4	Vertical	N/A
Akaki et al. [160]	steam	air/helium	0 – 24	Vertical	9.0–58.0 kg/h
Park and No [161]	steam	air	10–40	Vertical	7.6 – 40 kg/h
Kim [162]	steam	air	0–30	Vertical	N/A
Al-Shammari et al. [163]	steam	air	47–97	Vertical	5.24–11.3 kg/h
Oh and Revankar [164]	steam	air	0–10	Vertical	9.0–19.8 kg/h
Zhu et al. [165]	steam	air	34–81	Vertical	1.08–10.8 m/s
Park et al. [166]	steam	nitrogen	N/A	Vertical	0–0.22 kg/s
Lee and Kim [59]	steam	nitrogen	0–40	Vertical	6.5–28.2 kg/h
Su et al. [167]	steam	air/helium	<80	Vertical	N/A
Caruso and Vitale [168]	steam	air	0–26	Vertical	0.828–8.28 kg/h

Wu and Vierow [156] measured local heat transfer coefficients of steam/air mixtures in a horizontal 27.5-mm tube. Heat transfer coefficients dropped by an order of magnitude from the inlet to the outlet. The liquid resistance was dominant at the inlet where the heat transfer coefficients were higher on the top and lower at the bottom. As air accumulated between vapor and liquid, the air thermal resistance dominated over the liquid thermal resistance. Lee and Kim [59] studied experimentally heat transfer coefficients of steam/nitrogen condensation in a 13-mm-diameter vertical tube. Unlike in larger tubes, 3% of nitrogen by mass in steam did not affect heat transfer. Different gases impose different inhibiting effects. With the same mole fraction, air mitigates heat transfer coefficients more than helium while at the same mass fraction it is the opposite [158]. As discussed previously, liquid condensate on hydrophobic surfaces bead up to form dropwise condensation and enhancement condensation heat transfer. Ma et al. [169] experimentally, numerically, and visually investigated the flow velocity field in filmwise and dropwise condensation of steam with 0 – 5% air by mass on vertical plate in confined chamber. Cyclic nucleation, coalescence and departure of droplets perturbed accumulation of air near the condensation and created eddy flow and perpendicular motion of vapor-air mixture through which heat transfer enhancement was expected.

To understand and predict condensation heat transfer performance in presence of noncondensables, two theoretical frameworks have been developed; the boundary layer model and diffusion layer model are mainly for gravity-driven natural condensation on vertical plate, using mass, momentum and energy transportation equations provided physical and mathematical insight in to the phenomena. In the boundary layer model, vapor-gas mixtures are considered static and have no slip at the contact of the liquid condensate film. In gravity-driven condensation on vertical plate, the film travels down and condensate accumulates in which an air boundary layer forms in

the vapor-gas mixture near the condensate film [170-176]. The diffusion layer model considers the diffusion process through the noncondensable layer formed by the accumulation of noncondensable gas near liquid condensate during vapor condensation. The diffusion process hinders condensation and reduces the heat transfer performance [177, 178].

Due to the complexity of accurately modeling condensation heat transfer performance in the presence of noncondensables, researchers developed empirical correlations for engineering purposes. Vierow and Schrock [179] and Kuhn et al. [180] developed correlations using a degradation factor by comparing condensation heat transfer coefficients with and without noncondensable gases. Lee and Kim [59] modified the correlation by taking shear stress into consideration.

Table 2.4 Degradation factor models for condensation in presence of noncondensbale gases

Authors	Model
Vierow and Schrock [179]	$F = (1 + aRe_g^b)(1 - cY_a^d)$
Kuhn et al. [180]	$F = \frac{\delta_{exp}}{\delta_{Nu}}(1 + aRe_l)(1 - bY_a^c)$
Lee and Kim [59]	$F = \tau_g^{*0.3124}(1 - 0.964Y_a^{0.402})$

where a, b, c, and d are coefficients, and Y_a depends on the flow conditions and mass fractions and properties of noncondensalge gas.

Caruso et al. [168] observed a dependence of heat transfer coefficients on mixture Reynolds number, liquid Reynolds number, and nitrogen content during steam-air condensation experimental in near-horizontal tubes of 12.6, 20 and 26.8-mm diameters at atmospheric pressure. They developed the following heat transfer coefficient correlation by fitting the experimental data,

$$Nu_v = 18.8Re_m^{0.592}Re_l^{-0.13}\left(\frac{\omega_N}{1-\omega_N}\right)^{-0.357} \quad \textbf{2.7}$$

where Nu_v is vapor Nusselt number ($Nu_v = \frac{hD}{k_v}$), Re_m is mixture Reynolds number ($Re_m = \frac{G(\omega_N+\omega_v)D}{\mu_m}$), Re_l is liquid Reynolds number ($Re_l = \frac{G(1-x)(1-\omega_g)D}{\mu_l}$), μ_m is the mass averaged gas mixture viscosity ($\mu_m = \mu_v \frac{\omega_v}{\omega_g+\omega_v} + \mu_g \frac{\omega_g}{\omega_g+\omega_v}$) and ω_v and ω_N are the mass fraction of vapor and noncondensable gas in the flow, respectively.

2.6 Conclusions from literature

Analytical, numerical, and experimental studies have revealed heat transfer coefficients and pressure drops of filmwise condensation in conventional and mini/micro-channels. Dropwise condensation on hydrophobic surfaces reduced the liquid film thermal resistance through facilitating droplet departure while the lower surface energy of hydrophobic material provided the potential of reduced pressure drops in internal dropwise condensation. Droplet formation and motion perturbs the noncondensbale layer of thermal resistance and improves condensation heat transfer. The following conclusions can be drawn from the literature:

- In mini/micro-channels, a higher surface to volume ratio increased the effects of shear forces and surface tension so that annular flow prevails, and liquid film thickness were reduced compared with conventional channels.
- Hydrophobic surfaces have lower surface energy for which droplets form; therefore, in dropwise condensation, the liquid thermal resistance was reduced and heat transfer coefficients was enhanced.
- Heat transfer coefficients in dropwise condensation were highly connected to the droplet size distribution, which correlated to droplet departure size. Surfaces facilitated droplet departure improved heat transfer coefficients.

- Noncondensable gas forms a static layer between vapor and liquid in condensing flows. In shear drivens flow in mini/micro-channels, the gas layer was thinned and therefore impacts on heat transfer were slightly reduced. It was also presumed that the gas layer would be perturbed in droplet condensation for the periodic formation and motion of droplets.

2.7 Research objectives

However, few research have investigated quantitatively and visually dropwise condensation in mini-channels with and with presence noncondensable gases. The objectives of this research are:

- Condense steam in hydrophilic and hydrophobic mini-gaps while measuring heat transfer coefficients, pressure drops, and visualizing flow regimes.
- Observe droplet formation, growth, and departure in dropwise condensation in the hydrophobic mini-gap
- Model the relationship between droplet dynamics and heat transfer in the hydrophobic mini-gap
- Study the effects of noncondensable nitrogen on hydrophilic and hydrophobic condensation.

Chapter 3 Experimental design

3.1 Experimental apparatus

Simultaneous heat transfer, pressure drop, and flow visualization were obtained in an open loop system for a wide range of steam mass fluxes and qualities (Figure 3.1). Steam was provided by the campus facility; a regulator reduced steam pressure from at 550 kPa to approximately 250 kPa. A separation tank removed excess liquid condensate and subsequently small particles, rust, and contaminants were removed in three parallel 60-μm pore filters. High-quality steam entered the pre-heater with a 500W cartridge heater and was heated to 20–30^{o}C above saturation temperature in order to determine enthalpy through measured temperature and absolute pressure. The superheated steam then entered the tube-in-tube counterflow pre-condenser where a constant temperature chiller (Neslab RTE-221) provided cooling water to partially condense the steam. Cooling water flow rates were measured using Coriolis flow meter (Micro Motion^{TM} F-series sensor and 2700 transmitter) and the inlet and exit pre-condenser temperatures were measured using T-type thermocouples. The change of steam enthalpy in pre-condenser was calculated suing energy balance in cooling water. Steam entered the test section in a superheated or two-phase state. In the test section, inlet and exit temperatures, inlet pressure, and differential pressure were directly measured and the flow was visualized through a glass window using a Leica Z16 APO macroscope and a FASTEC IL3 high-speed camera (maximum space resolution of 1280 x 1024 at 500 fps and reduced resolution for up to 20,000 fps rate). In the post-condenser, steam was fully condensed and passed through a rotameter for visual confirmation of flow stability. The condensate mass flow rate was measured using an electronic scale and timer.

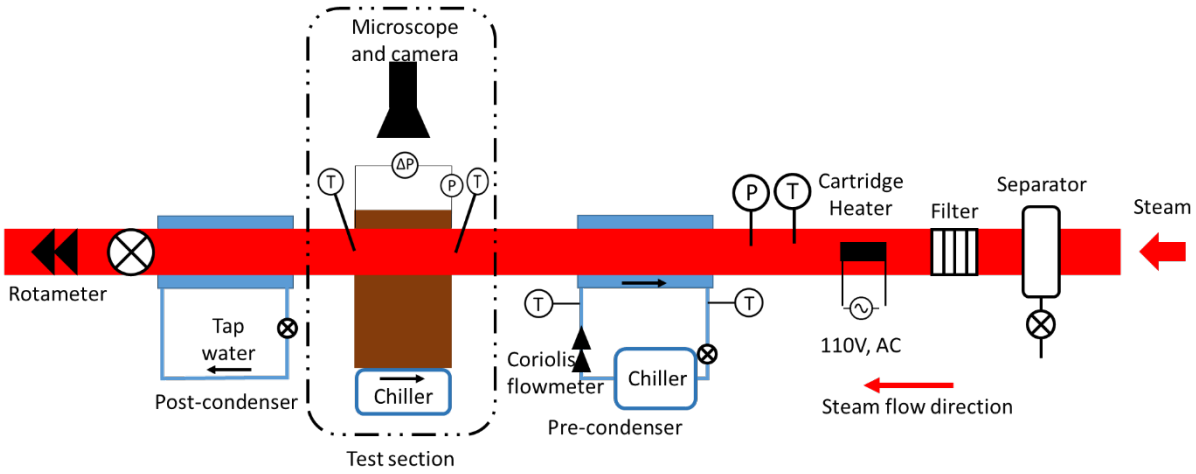

Figure 3.1 Diagram of the open-loop system for steam condensation experiments

3.2 Test section

The test section consisted of a cover plate, glass viewing window, interchangeable coupon with mini-gap, oxygen-free copper block for heat flux measurements, a PEEK block with flow inlet and exit, and an aluminum cooling pad (Figure 3.2). The mini-gap was milled into an oxygen-free copper coupon. Two mini-gaps were used in experiments. Both had a width of 10 mm, an inlet-outlet length of 40 mm with depths of 0.5 and 1 mm, creating hydraulic diameters of 0.952 and 1.818 mm, respectively.

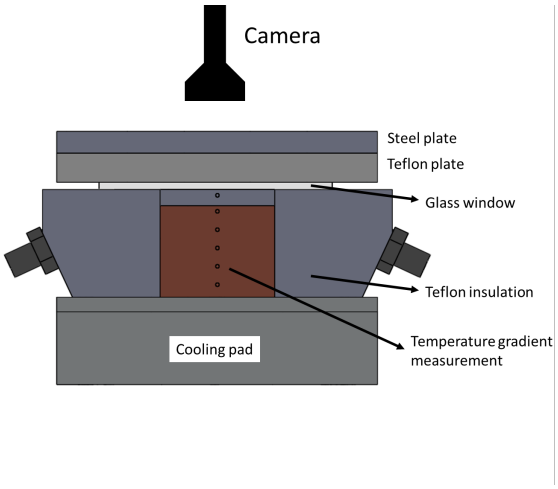

Figure 3.2 Test section for heat transfer, pressure drop measurement and visualization

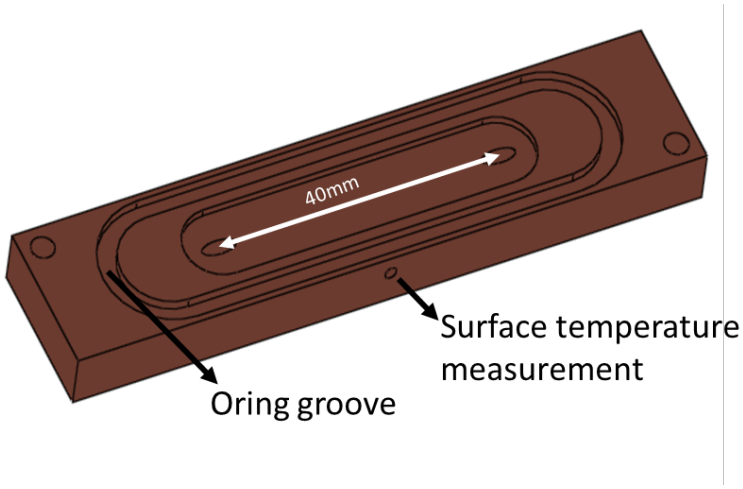

Figure 3.3 Steam flow condensation mini-gap of two hydraulic diameters

Steam flowed through the PEEK block after leaving the pre-condenser. The entering and exiting channels connected to mini-gap were at an angle of 20^{o} from the horizontal plane. The coupon inlet and outlet were sealed to the PEEK block with O-ring seals in the horizontal plane. Indium thermal interface material connected the coupon to the oxygen free copper block for accurate heat flux measurement due to well-documented and uniform thermal conductivity. The 20 x 40 x 40 mm copper block had five holes with diameters of 1.59 mm, spaced 8 mm apart vertically, for temperature measurements. The ends of the holes were on the virtual vertical centerline of the coupon. To measure the temperature gradient, T-type thermocouples with diameters of 1.59 mm were inserted into each hole, and a thermocouple was installed in the coupon 0.5 mm from the bottom of the mini-gap to determine wall temperature. To ensure good contact between thermocouple and the copper material, thermocouples were dipped in thermo paste (Omega Thermo 201) before installation. Heat flux was determined using Fourier's law for the heat transfer coefficient and steam quality change in the test section. Thermal paste was used to maintain contact between the copper heat flux block and the aluminum cooling pad. Cooling water from the water bath flowed through serpentine channels in cooling pads with a total temperature change of less than 2 ^{o}C, ensuring a constant temperature boundary condition.

Flow visualization was accomplished from the top of the test section with the microscope (Leica^{TM} Z16 APO) through a 3.175-mm-thick tempered glass viewing window. The window was sealed to the coupon via an O-ring seal, and a cover plate on the top glass window provided pressure for sealing. The entire test section was clamped with five bolts from the cover plate to the cooling pads; bolts were torqued to 0.7 N·m in a diamond pattern to reduce contact resistance and improve O-ring sealing.

3.3 Surface preparation

Flow condensation experiments were conducted on a bare copper, hydrophilic coupon and a Teflon AF^{TM}-coated hydrophobic coupon. On the bare copper surface, a goniometer measured the contact angle of a water droplet to be 70 ± 3^{o} (Figure 3.4). A copper mini-gap was dip-coated to become hydrophobic [16]. The coupon was initially put into a UV cleaner (ProCleaner^{TM} 110) for 30 minutes to remove contaminants and then soaked in isopropanol for 10 mins to remove small particles and the oxide layer. The coupon was then dipped twice in a solution of DuPont Teflon AF^{TM} Grade 400s2-100-1 and FC-40 solvent at a volumetric ratio of 1:20. Subsequently, the coupon was baked at 105 ^{o}C for 1 hr to remove the solvent and then 165 ^{o}C (the glass transition temperature) for 72 hours to create a uniform coating. An additional copper sample was dip-coated using the same procedure as the mini-gap. After the dip-coating process, the contact angle was measured to be 110 ± 3^{o} on the Teflon-coated copper sample (Figure 3.4).

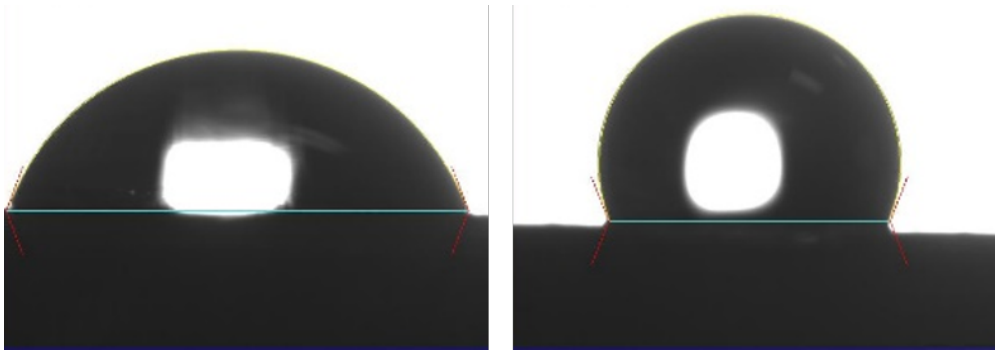

Figure 3.4 Contact angles on bare copper (70^o, left) and Teflon coated surfaces (110^o, right)

3.4 Data reduction and uncertainty analysis

The least squares approach (Equation 3.1) calculated the temperature gradient in the copper block using evenly spaced (8mm) temperature measurements in vertical centerline,

$$\frac{dT}{dy} = \frac{5\sum T_i y_i - \sum T_i \sum y_i}{\sum y_i^2 - (\sum y_i)^2} \qquad \textbf{3.1}$$

where T_i is the temperature measure from individual thermocouples with index i increasing from top to the bottom hole, y_i is the distance of ith thermocouple tip to the condensation surface making positive direction of y axis vertically downward.

Due to the importance of temperature measurements, all thermocouples were calibrated to reduce uncertainties. Seven temperature points in water bath (NESLAB™ RTE-111) plus ice point and boiling point calibrated the T-type thermocouples against a thermometer (Omega™ HH41) with an accuracy of ±0.05 ^{o}C. Calibration provided a resultant temperature measurement uncertainty of ±0.2 ^{o}C. The Kedzierski and Worthington [181] equation was used to calculate the temperature gradient uncertainty,

$$w_g = \sqrt{w_{Ti}^2 + \left(\frac{q''D}{6k_{cu}}\right)^2}\sqrt{\frac{1}{\sum_{i=1}^{N}(y_i - \bar{y})^2}} \qquad \textbf{3.2}$$

where w_{Ti} is the calibrated thermocouple uncertainty, y_i is the distance of the ith thermocouple from the condensation surface, and $\bar{y}$ is the average distance of the thermocouple from the

condensation surface. Due to the high conductivity (i.e. 390 W/mK) of oxygen-free copper, large spacing (i.e. 8 mm) between holes, and the small diameter of the holes (i.e. 1.59 mm), the maximum temperature gradient uncertainty was ± 2%.

Fourier's law calculated the heat flux in the copper block:

$$q"_{bl} = -k_{cu}\frac{dT_{bl}}{dy} \quad \textbf{3.3}$$

where $q"_{bl}$ is the heat flux in the copper block and k_{cu} is the thermal conductivity of oxygen free copper.

As seen from conservation of energy, the heat transfer rate in the copper block equals the condensation heat transfer rate. Equation 3.4 was used to calculate heat flux through condensation surface that is composed of the bottom surface and sidewalls of the racetrack shape mini-gap (Equation 3.5). The copper block cross sectional area (perpendicular to heat transfer direction) was 800 mm^2 (20 mm × 40 mm rectangle). The condensation areas of the 0.5 and 1.0 mm deep mini-gap were 214.25 and 269.96 mm^2, respectively,

$$q"_{cond}A_{cond} = q"_{bl}A_{bl} \quad \textbf{3.4}$$

$$A_{cond} = A_{side} + A_{bottom} \quad \textbf{3.5}$$

where $q"_{cond}$ is condensation heat flux, A_{cond} is condensation surface area, A_{bl} is copper block cross sectional area.

Newton's law of cooling was used to evaluate heat transfer coefficients in Equation 3.6 using condensation heat flux ($q"_{cond}$) and the difference between fluid temperature (T_f) and condensation surface temperature (T_s).

$$h = \frac{q"cond}{T_f - T_s} \quad \textbf{3.6}$$

The uncertainty in heat transfer coefficients comes from the uncertainty of condensation heat flux (q''_{cond}), fluid temperature (T_f), and temperature (T_s). Condensation heat flux was calculated in Equation 3.1. Fluid temperature was obtained using two-phase pressure drop correlation. In test section, inlet pressure and differential pressure between inlet and outlet were both measured. Kim and Mudawar [78] frictional pressure drop correlation (Equation 2.1, 2.2, and 2.3) was utilized to calculate the pressure drop from the inlet to the center point of the mini-gap and thus find the saturation pressure and therefore saturation temperature. The pressure drop correlation was developed based on the Lockhart-Martinelli method with modifications to Chisholm constant *C* using liquid- and gas-phase flow regimes (i.e. laminar or turbulent). Pressure drops across the test section were also predicted using the correlation and compared with the experimental data. Measurements of block and channel dimensions showed that the uncertainty in these areas were less than 2%. Therefore the propagation of uncertainty in heat transfer coefficients is:

$$w_h^2 = \left(\frac{A_{bl}}{A_{cond}}\right)^2 \left\{ \left(\omega_{k_{cu}}\right)^2 \left(\frac{\frac{dT}{dy}}{T_f - T_s} \right)^2 + \left(\omega_g\right)^2 \left(\frac{k_{cu}}{T_f - T_s}\right)^2 + \left[\left(\omega_{T_f}\right)^2 + \left(\omega_{T_s}\right)^2 \right] \left(\frac{k_{cu}}{\left(T_f - T_s\right)^2} \right)^2 \right\} \qquad \textbf{3.7}$$

Superheated steam entered precondenser at known temperature, pressure and thus the specific enthalpy. Equation 3.8 evaluated cooling rate ($\dot{Q}_{pre}$). A Coriolis flowmeter measured the cooling water mass flow rate ($\dot{m}_{cooling}$) with ± 0.1% uncertainty. The specific heat of water (C_p) within the temperature range of 20 – 70 ^{o}C varies negligibly from 4.18 kJ/kgK and is considered constant. The temperature of water entering (T_{in}) and exiting (T_{out}) precondenser were measured with calibrated Type-T thermocouple,

$$\dot{Q}_{pre} = m_{cooling} C_p (T_{out} - T_{in}) \qquad \textbf{3.8}$$

With steam mass flow rate ($\dot{m}_{st}$) measured at the end of the open-loop system, Equation 3.9 calculated the change of steam specific heat in precondenser from which the specific enthalpy at test section inlet ($i_{ts,i}$) was obtained using Equation 3.10.

$$\Delta i_{pre} = \frac{\dot{Q}_{pre}}{\dot{m}_{st}} \quad \textbf{3.9}$$

$$i_{ts,i} = i_{pre,i} - \Delta i_{pre} \quad \textbf{3.10}$$

where $i_{pre,i}$ is the specific enthalpy of superheated vapor entering test section and Δi_{pre} is the change of steam specific enthalpy in precondenser.

The specific enthalpy of superheated vapor was obtained through measured temperature and pressure; the pressure transducer provided a ± 0.25% of full scale uncertainty (i.e. ±0.86 kPa). During the experiments, the fluctuations of superheated vapor temperature and pressure were within ± 0.3^{o}C and 1 kPa. Therefore, the uncertainty in the enthalpy of the superheated vapor was negligible. The Kline and McClintock [182] approach was used to calculate the uncertainty in the change of specific enthalpy in pre-condenser,

$$w_{\Delta h_{pre}}^2 = \left(\omega_{T_{in}}\right)^2 \left(\frac{m_{cooling} C_p}{\dot{m}_{st}}\right)^2 + \left(\omega_{T_{out}}\right)^2 \left(\frac{m_c C_p}{\dot{m}_{st}}\right)^2 \quad \textbf{3.11}$$

where $\omega_{T_{in}}$ and $\omega_{T_{out}}$ are the both the uncertainty of Type-T thermocouple (i.e. $\pm 0.2^{o}C$). The heat transfer rate and steam mass flow rate determined the enthalpy change of steam in the tests section:

$$\dot{Q}_{ts} = q"_{cond} A_{cond} \quad \textbf{3.12}$$

$$\Delta i_{ts} = \frac{\dot{Q}_{ts}}{\dot{m}_{st}} \quad \textbf{3.13}$$

$$i_{ts,o} = i_{pre,i} - \Delta i_{ts} \quad \textbf{3.14}$$

Steam quality is the mass fraction of vapor divided by the total mass and thus affects heat transfer coefficients significantly. Steam qualities at the test section inlet and outlet were

determined from two-phase enthalpies and pressures. The steam quality at the center of the mini-gap is assumed the average of steam qualities at the inlet and outlet of test section:

$$\bar{x} = \frac{x_{ts,i} + x_{ts,o}}{2} \qquad \textbf{3.15}$$

where $x_{ts,i}$ and $x_{ts,o}$ are respectively the inlet and outlet steam quality of test section. The inlet steam quality was obtained through an energy balance on the pre-condenser.

Chapter 4 Results and discussion

4.1 Single-phase validation tests

Single-phase tests validated heat transfer rate measurements in the cooper block, heat losses from the glass window, and heat transfer coefficient measurements. In the first single-phase test, the pre-condenser fully condensed the two-phase steam into liquid water and the single-phase energy balance in the condensate side was compared to the heat flux in the copper block obtained via Fourier's law. The test section heat transfer rate ranged from 40 to 80 W (Figure 4.1) corresponding to water inlet temperatures ranging from 75 to 110 ^{o}C. Cooling side temperature was maintained constant (35^{o}C) and therefore the higher inlet temperature corresponds to higher heat flux and larger temperature drop in the test section. The agreement was very good at most heat fluxes (Figure 4.1) but was reduced when single-phase condensate temperature drops across the mini-gap approached 40 ^{o}C at the highest condensate inlet temperature and highest heat transfer rate. At a fluid temperature drop of 40^{o}C, it is possible that axial conduction affected heat transfer measurements in the copper block. However, temperature drops during two-phase steam condensation experiments were less than 5^{o}C.

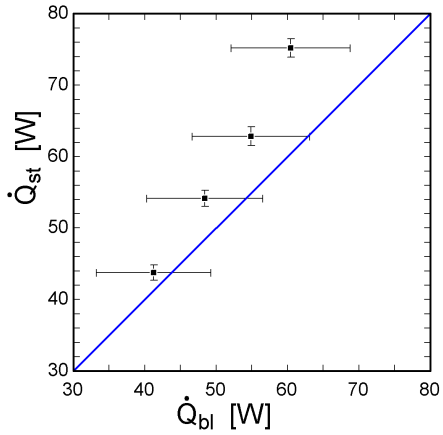

Figure 4.1 Comparison of steam-side and cooling-side heat removal rate measurements

Insulation on the top surface was removed for imaging and tests were conducted to determine heat losses through the top viewing window. The heat transfer rate in the copper block with and without an insulation cover was compared for single-phase water at various inlet water temperatures (e.g., 70–110 ^{o}C). Heat losses were always less than 2W and 5% of the single-phase heat transfer rate (Figure 4.2). In the condensation tests, steam temperatures were in the range of 120 to 130 ^{o}C. Heat losses through the visualization window decreased steam quality by less than 0.001 and were therefore considered negligible. Glass fiber insulation insulated the window during heat transfer data recording periods and was removed for visualization. Negligible heat losses through the glass window resulted in a minimal steam quality change from removing the insulation cover for visualization.

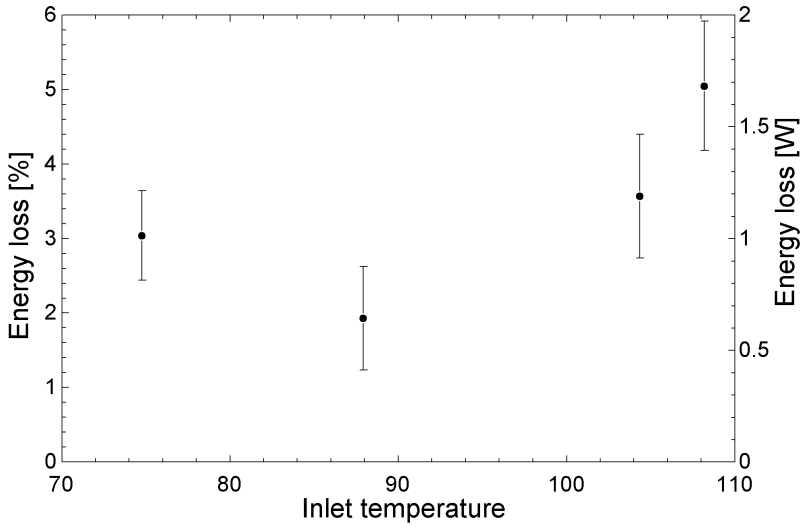

Figure 4.2 Absolute and relative energy loss through visualization window

For further validation of heat transfer measurements in the test section with 0.5-mm deep mini-gap, single-phase Nusselt numbers were evaluated experimentally for laminar flows (Figure 4.3). Due to the high aspect ratio of the channel (20:1), the experimental data were compared against the theoretical case for flat plates with one plate insulated (i.e. Nu=4.86) and the resulting agreement was very good.

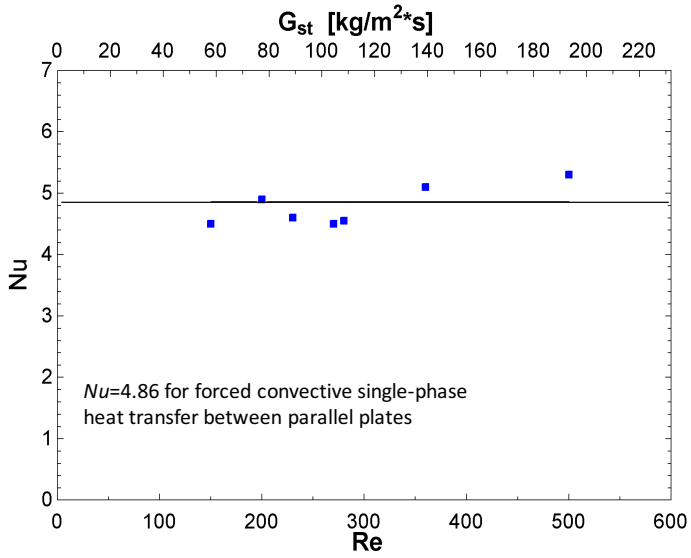

Figure 4.3 Nusselt numbers of single-phase cooling at various steam flow rate in test section

4.2 Steam condensation in hydrophilic mini-channels

After the validation of the experimental apparatus, condensation heat transfer and flow visualization experiments were conducted in the bare copper hydrophilic mini-gaps at mass fluxes of 50, 75, and 100 kg/m^{2}s and at 35, 50, and 75 kg/m^{2}s in the 0.5-mm and 1-mm deep mini-gaps, respectively. Except for the different depth, two mini-gaps had the same dimensions and the hydraulic diameters were 0.952 and 1.818 mm, respectively. Due to small condensation areas (i.e. 534.35 and 589.95 mm^2), quality changes were low (≤ 0.2) through the mini-gap, although quality changes were slightly higher at the lowest mass flux of 50 kg/m^{2}s in 0.5-mm deep mini-gap. For all cases, filmwise condensation was observed in the hydrophilic mini-gap.

Figure 4.4 plots the heat transfer coefficients at various mass fluxes and steam qualities in both hydrophilic mini-gaps. The heat transfer coefficient increased with increased steam qualities and mass fluxes, corresponding thinner condensate films. At steam mass fluxes of 50 and 75 kg/m^{2}s, in 0.5-mm deep mini-gap, the differences in heat transfer coefficients decrease with

increasing steam quality, indicating that the benefit of reducing thermal resistance through increasing steam mass flux was mitigated by increasing steam quality associated with decreasing amount of liquid. In the 1-mm deep mini-gap, similar trends were observed. Yet the enhancements of heat transfer coefficients from increasing mass flux were consistent for the whole steam quality span. As the hydraulic diameter increases, the surface tension effects decrease and therefore the effects of increasing interfacial shear stress from increasing mass fluxes were sustained at higher steam qualities.

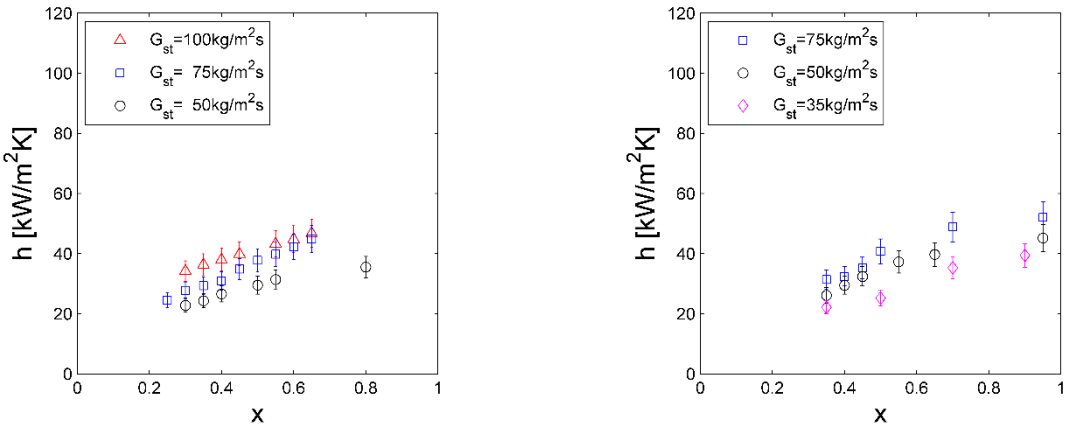

Figure 4.4 Heat transfer coefficients in 0.5mm (left) and 1mm (right) deep hydrophilic mini-gaps with respect to mass flux and steam quality

Pressure drops were recorded simultaneously with heat transfer coefficients. Pressure drop increased with increased steam qualities or mass fluxes, corresponding to increased superficial or average velocities (Figure 4.5). Pressure drops increased faster with steam quality at higher mass fluxes in the 0.5-mm deep mini-gap while the slope of pressure drops over steam quality were similar for three mass fluxes in 1mm deep mini-gap. Generally, at the same steam mass flux and quality, pressure drops in 0.5-mm deep mini-gap were about 2–4 times higher than those in the 1-mm deep mini-gap.

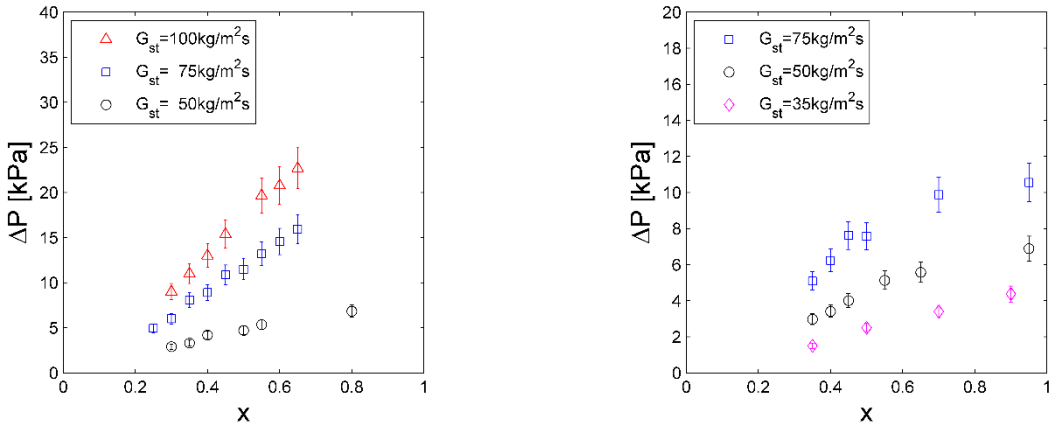

Figure 4.5 Steam condensation pressure drops in 0.5mm (left) and 1mm (right) deep hydrophilic mini-gap at various steam mass fluxes and steam qualities.

For tests in the hydrophilic mini-gap, condensation heat transfer data were compared to the Kim and Mudawar [183] correlation for filmwise condensation in mini/micro-channels. The correlation was developed for many working fluids, primarily refrigerants, for diameters ranging from 0.424 to 6.22 mm. The correlation was assessed using Mean Absolute Error (MAE), defined as:

$$MAE = \frac{1}{n}\sum_{i=1}^{n}\left|\frac{h_{pred} - h_{exp}}{h_{exp}}\right| \qquad \textbf{4.1}$$

where h_{pred} is the heat transfer coefficient obtained from the Kim and Mudawar [183] correlation, h_{exp} is the experimentally measured heat transfer coefficient, and n is the total number of data points. The MAEs of experimental results from the Kim and Mudawar model [183] were 20.19% for 0.5-mm deep mini-gap (Figure 4.6, left) and 15.6% (Figure 4.6, right) for 1-mm deep mini-gap, demonstrating good predictions of the experimental data for the hydrophilic mini-gaps. The experimental results were higher than the model, particularly at lower qualities, with several possible contributing factors.

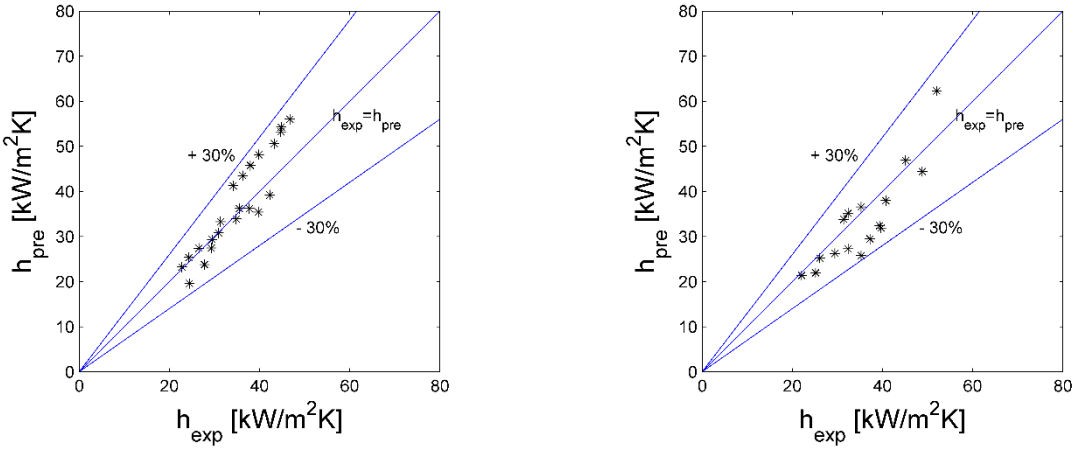

Figure 4.6 Comparison of experimental predicted heat transfer coefficients in 0.5mm (left) and 1mm (right) deep mini-gaps

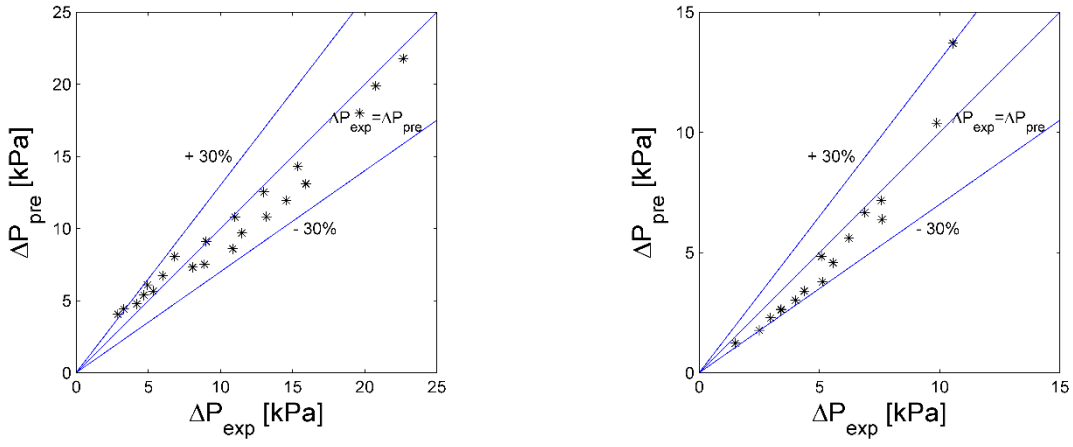

Figure 4.7 Comparison of experimental and predicted pressure drops in 0.5mm (left) and 1mm (right) deep mini-gaps

First, the correlation was developed primarily for refrigerants, but water has a higher surface tension value. Surface tension may cause condensate to gather in sharp mini-channel corners, thereby thinning the liquid film around the perimeter and increasing heat transfer, although this liquid film thinning is dependent on the fluid and geometry [184-187]. With the reduction of aspect ratio from 20:1 to 10:1 and increase of hydraulic diameter from 0.952 mm to 1.818 mm, the surface tension effects may decrease and the disagreement between experimental and prediction results dropped from 20.19% to 15.6%. Overall, the prediction obtained from Kim

and Mudawar [183] correlation agreed with the heat transfer coefficients measured in the hydrophilic mini-gap.

4.3 Steam condensation in hydrophobic mini-channels

Steam condensation was performed at mass fluxes of 50–100 kg/m^{2}s and 35–75 kg/m^{2}s in 0.5-mm and 1-mm deep hydrophobic mini-gaps, respectively. Unlike filmwise condensation observed in hydrophilic mini-gaps (Figure 4.8 a), dropwise condensation was observed in the hydrophobic mini-gap at all steam mass fluxes and qualities (Figure 4.8).

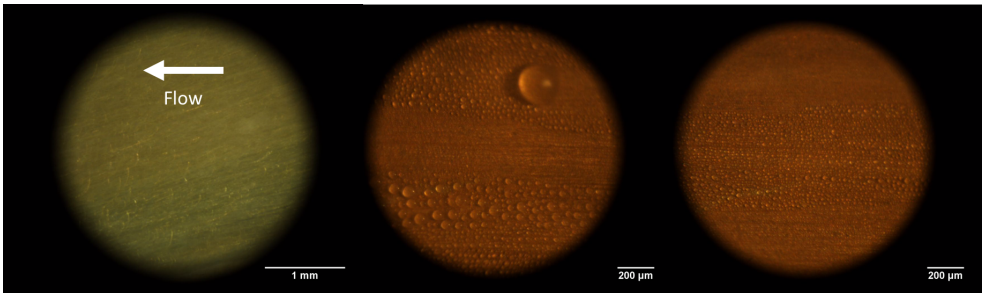

Figure 4.8 Filmwise flow condensation in hydrophilic mini-gap and dropwise flow condensation in hydrophobic mini-gap

In dropwise condensation, periodic droplet nucleation, coalescence, and departure were observed in hydrophobic mini-gaps (Figure 4.9). Tiny droplets nucleated on the bare surface and then grew continuously through direct condensation. Coalescence with neighboring droplets followed the droplet growth phase, creating larger droplets. Droplets of the departure size were swept by vapor flow; droplet departure sizes depended on the steam mass flux and steam quality. Additionally, droplets were shed by sweeping droplets from upstream. Water condensate in the hydrophobic mini-gap completely covered the surface with small droplets or formed larger droplets and rivulets depending on the quality and interfacial shear force associated with steam mass fluxes. Heat transfer in dropwise condensation is correlated with droplet sizes, which determines the thermal resistance of condensate; small droplets account for the largest portion of

heat transfer [188-190]. Steam mass flux and quality determined the velocity of vapor relative to the droplet and thus affected the droplet departure sizes. The largest droplets (i.e. ~500 μm in diameter) were observed for the lowest flow rate (i.e., 50 kg/m^{2}s), lowest steam quality (i.e., x = 0.2) in the 0.5-mm deep mini-gap, and droplet departure size decreased as mass flux and shear forces increased.

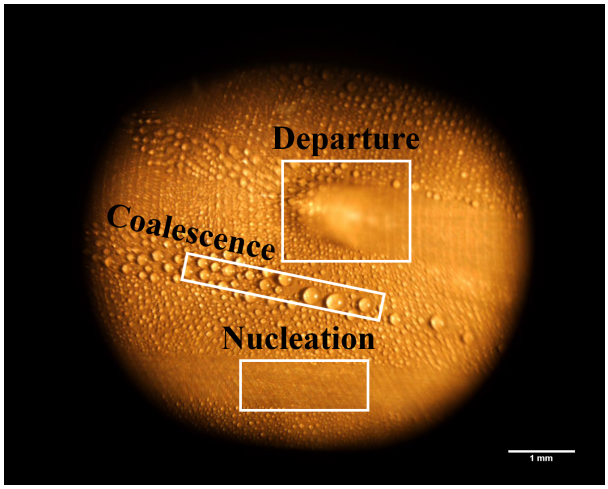

Figure 4.9 Stages of droplet nucleation, coalescence, and departure in dropwise flow condensation

Videos were analyzed at the center point for conditions of identical average quality ($\bar{x}$ = 0.42) and differing mass fluxes. Videos were taken at 250 –500 fps depending on sweeping periods and associated lighting conditions and droplet analyses were conducted frame by frame using ImageJ^{TM} and PFV^{TM} (Photron FASTCAM Viewer) software. The cycle began with nucleation, followed by coalescence, and ended at the frame at which the droplets departed. Table 4.1 tabulates the droplet departure size, sweeping periods, and heat transfer coefficients at steam mass flux of 50 kg/m^{2}s and various steam qualities of 0.35 s, 0.42 s, and 0.55 s.

Table 4.1 Droplet departure size and sweeping periods in dropwise flow condensation at various steam qualities of 0.35, 0.42 and 0.55 and steam mass flux of 50 kg/m^{2}s

Steam quality	Droplet departure size (μm)	Sweeping periods (s)	h (kW/m2K)
0.35	32 ± 16	32	84,420
0.42	13.7 ± 4.5	28	87,908
0.55	10.6 ± 1.0	16	98,884

Table 4.2 Droplet departure size and sweeping periods in dropwise flow condensation at various steam qualities of 0.42 and steam mass fluxes of 50, 75 and 100 kg/m^{2}s

Steam mass flux (kg/m2s)	Droplet departure size (μm)	Sweeping periods (ms)	h (kW/m2K)
50	13.7 ± 4.5	28	84,420
75	12.9 ± 4.0	24	95,673
100	10.3 ± 1.0	17	105,409

Dropwise condensation increased condensation heat transfer coefficients compared to filmwise condensation in the hydrophilic mini-gap. Condensation heat transfer coefficients are presented in Figure 4.10. Uncertainties in the condensation heat transfer coefficient were ± 4.5%– ± 10.1%. Based on flow visualization, droplet departure diameters were smaller for high mass fluxes at the same quality due to higher vapor shearing velocities. Droplet size distribution had been found correlated to droplet departure sizes [110], which determines the thermal resistance of liquids in the mini-gap. The reduction in droplet departure size and, therefore, liquid film resistance was likely responsible for the increase in heat transfer coefficients with respect to mass flux. Increasing mass flux and steam quality both increased interfacial shear forces between vapor and droplets. Therefore, heat transfer enhancement from increasing steam quality was reduced at higher steam mass fluxes. Likewise, the enhancement from increasing steam mass flux was reduced at higher steam qualities.

a b

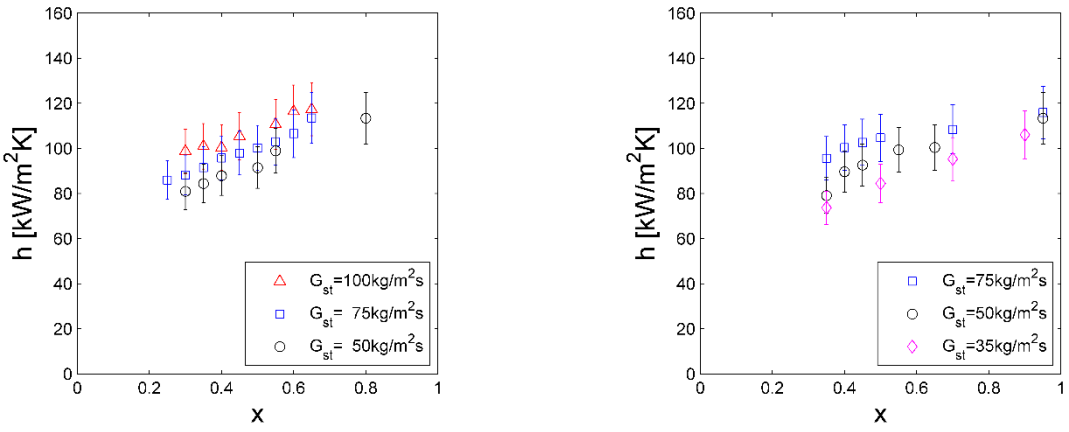

Figure 4.10 Heat transfer coefficients in 0.5mm and 1mm deep hydrophobic mini-gap

Flow condensation heat transfer coefficients in the hydrophobic gap were compared to the measured filmwise condensation heat transfer coefficients in the hydrophilic gap (Fig. 16). Heat transfer coefficient enhancement is defined as

$$\epsilon = \frac{h_{phobic}}{h_{philic}} \qquad \textbf{4.2}$$

where ϵ is the ratio of experimental data over predicted data, h_{phobic} is the experimentally measured heat transfer coefficient in the hydrophobic gap, and h_{philic} is the corresponding heat transfer coefficient in a hydrophilic gap for a specific mass flux, G, and steam quality, x. The hydrophobic mini-gaps showed 200%–350% enhancement over the hydrophilic mini-gaps. The highest enhancements were observed at the lowest qualities, in which the liquid film created the highest liquid film resistance.

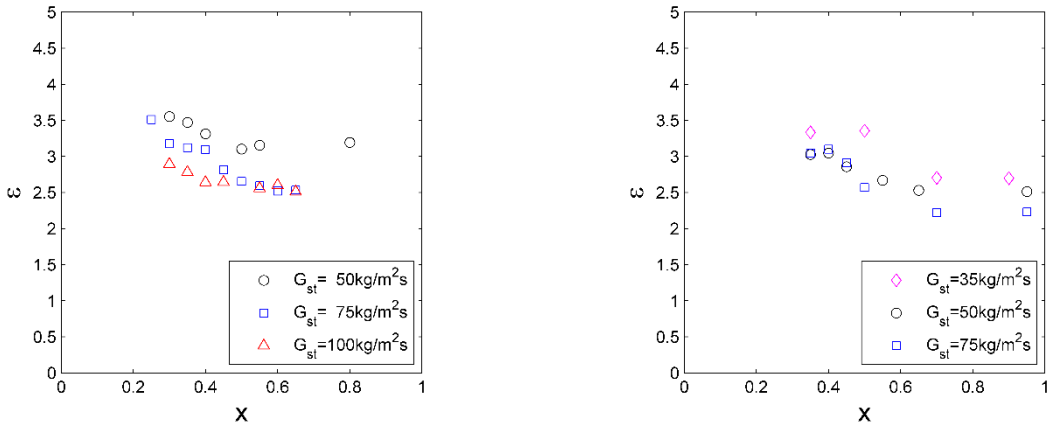

Figure 4.11 Heat transfer coefficient enhancements in 0.5-mm (left) and 1-mm (right) deep hydrophobic mini-gaps

As expected, higher pressure drops in dropwise flow condensation occurred at higher steam mass fluxes and steam qualities, corresponding to higher interfacial velocities. At higher mass fluxes, pressure drops increased with steam quality at a steeper slope. Pressure drops in hydrophobic mini-gap were reduced by 50–80%, compared to the hydrophilic mini-gaps. In the 1-mm deep mini-gap, the slope of pressure drop to steam quality was less affected than the 0.5-mm deep mini-gap.

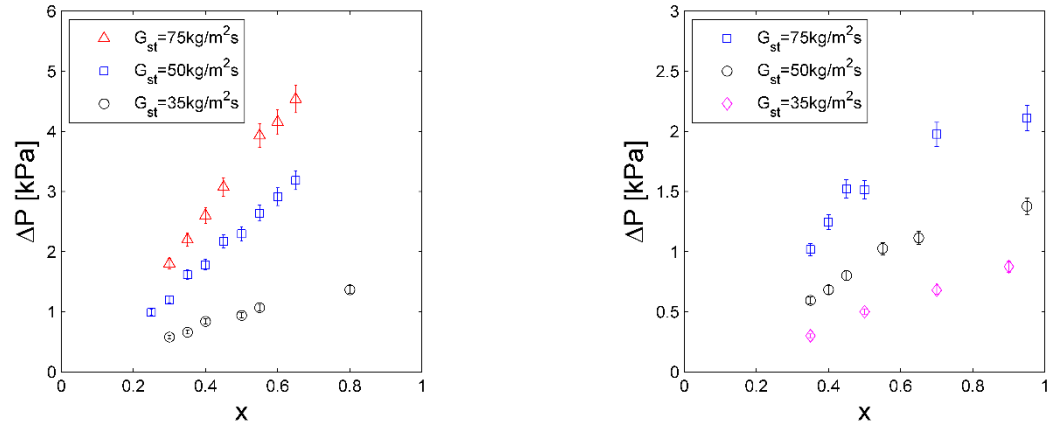

Figure 4.12 Pressure drops of Heat transfer coefficient enhancements in 0.5mm (left) and 1mm (right) hydrophobic mini-gap

4.4 Dropwise flow condensation heat transfer modeling

4.4.1. Modeling approach

The previous sections have shown the advantages of dropwise condensation over filmwise condensation for heat transfer enhancement and pressure drop reduction. In dropwise condensation, a liquid-vapor mixture enters the condensation channel and thus the liquid streams or rivulets (vapor-liquid interface has infinite curvature) cover part of the condensation area. A predictive heat transfer correlation will be developed for dropwise condensation. To predict heat transfer coefficient of dropwise flow condensation, stream/rivulet-covered area is considered to undergo filmwise condensation (Figure 4.13), and the rest of the area undergoes dropwise condensation.

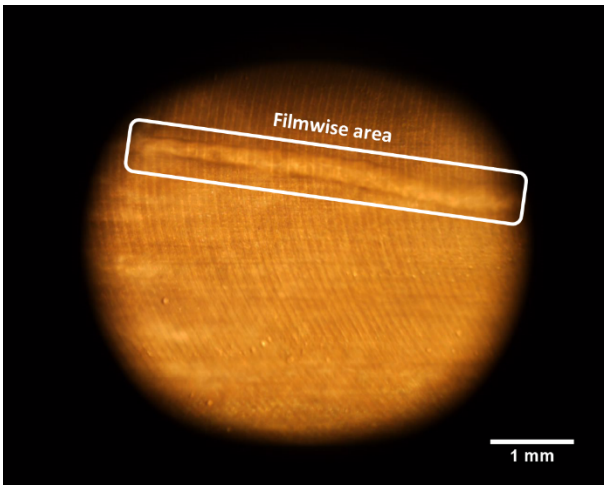

Figure 4.13 Filmwise condensation region and dropwise condensation region during steam condensation on hydrophobic surfaces

The filmwise and dropwise condensation areas (A_{FWC}) are estimated using void fraction (i.e. $A_{FWC} = (1-\alpha)A_{cond}$ and $A_{FWC} = \alpha A_{cond}$) where A_{cond} is the total condensation area and α is the void fraction obtained using Lockhart-Martinelli correlation (Equation 4.3) assuming

turbulent liquid and turbulent vapor [57, 191]. Figure 4.14 depicts void fractions of vapor changes with steam quality at steam temperature of 130 ^{o}C.

$$\frac{1-\alpha}{\alpha} = 0.28\left(\frac{1-x}{x}\right)^{0.64}\left(\frac{\rho_v}{\rho_l}\right)^{0.36}\left(\frac{\mu_l}{\mu_v}\right)^{0.07} \quad \textbf{4.3}$$

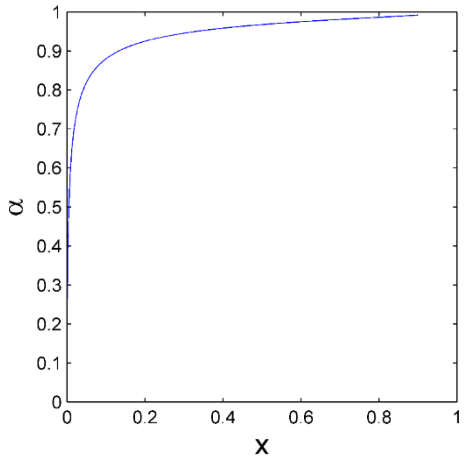

Figure 4.14 Void fraction in flow condensation using Lockhart-Martinelli correlation [191]

The average condensation heat transfer coefficient is a weighted average of filmwise and dropwise heat transfer coefficients,

$$\bar{h} = \frac{A_{DWC}h_{DWC}+A_{FWC}h_{FWC}}{A_{cond}} = (1-\alpha)h_{FWC} + \alpha h_{DWC} \quad \textbf{4.4}$$

where h_{DWC} is the dropwise condensation heat transfer coefficient and h_{FWC} is the filmwise condensation heat transfer coefficient obtained from Kim and Mudawar [78] correlation. In mini/micro-channels, Kim and Mudawar [78] proposed annular flow for $We^* > 7\mathrm{X}_{tt}^{0.2}$ and slug-bubbly flow for $We^* < 7\mathrm{X}_{tt}^{0.2}$ where We^* is modified Weber number defined by Soliman [192] and X_{tt} is turbulent-turbulent Lockhart-Martinelli parameter. Kim and Mudawar [78] proposed Equation 4.5 for annular flow and Equation 4.6 for slug/bubbly flow,

$$h_{FWC} = \frac{k_l}{D_h}\left[\left(0.048Re_l^{0.69}Pr_l^{0.34}\frac{\Phi_v}{X_{tt}}\right)^2\right]^{0.5} \quad \textbf{4.5}$$

$$h_{FWC} = \frac{k_l}{D_h}\left[\left(0.048Re_l^{0.69}Pr_l^{0.34}\frac{\Phi_v}{X_{tt}}\right)^2 + (3.2\times10^{-7}Re_l^{-0.38}Su_{vo}^{1.39})^2\right]^{0.5} \quad \textbf{4.6}$$

where $Re_l = \frac{G_{st}(1-x)D_h}{\mu_l}$ is the liquid Reynolds number, $G_{st} = \frac{m_{st}}{A}$ is the steam only mass flux, $\mathrm{Pr_l} = \frac{C_p\mu_l}{k_l}$ is liquid Prandtl number, X_{tt} is turbulent-turbulent Martinelli parameter,

$$\phi_g = 1 + CX + X^2 \quad \textbf{4.7}$$

where X is the Lockhart-Martinelli parameter, and C is Chisholm constant. Both depend on the flow regime (i.e. laminar or turbulent) of liquid phase and vapor phase.

In dropwise condensation, the droplet departure sizes and sweeping periods associated with flow conditions (i.e. steam mass flux and steam quality) affect the thermal resistance of liquid and therefore regulate dropwise condensation heat transfer. In horizontal channels, vapor-droplet interfacial shear stresses induce droplet shedding, while gravity dominates drop departure in quiescent flows. Le Fevre and Rose [148] first developed a model for heat transfer coefficients of gravity-driven, quiescent dropwise condensation on vertical plate. Heat transfer was first solved for single droplets for the droplet size distribution on the surface. Integrating heat transfer through the range of condensing droplets generates the total heat flux. In this work, a similar methodology is applied to create a dropwise condensation model which includes nucleation size, nucleation density, heat transfer through single droplet, droplet size distribution, and droplet departure size,

$$q"_{DWC} = \int_{r_{min}}^{r_{max}} q"_{drop}(r)A(r)dr \quad \textbf{4.8}$$

$$h_{DWC} = \frac{q"_{DWC}}{f-T_s} \quad \textbf{4.9}$$

where $q"_{drop}(r)$ is the heat flux through the base (droplet-solid contact area) of one droplet with radius r, $A(r)dr$ is the differential area fraction occupy by droplets with radius of r to $r + dr$, r_{max} and r_{min} are respectively the largest and the smallest droplet radius on the condensation

surface, T_v is the vapor saturation temperature and T_s is condensation surface temperature. The droplet departure radius is considered to be the largest droplet radius.

4.4.2. Heat transfer through single droplet

Across a single droplet, thermal resistances are between the constant vapor flow temperature (T_f) and constant surface temperature (T_s), interfacial thermal resistance from the droplet curvature (R_{lv}) conduction thermal resistance in the droplet (R_{drop}) and conduction thermal resistance of the Teflon™ coating (R_{coat}). Since these resistances are in series, the general equation for heat flux through a droplet of radius *r* is:

$$q"_{drop}(r) = \frac{T_v - T_s}{R_{lv} + R_{drop} + R_{coat}} \qquad \textbf{4.10}$$

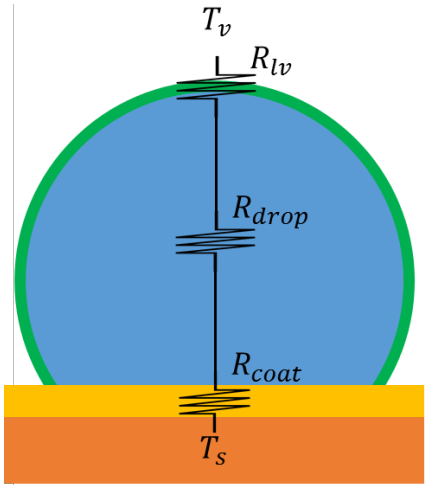

Figure 4.15 Resistor analogy for condensation heat transfer through a droplet

Le Fevre and Rose [148] first developed heat flux through the base of a hemispherical cap using the resistance analysis (Figure 4.15) and neglected the thermal resistance in the surface promoter,

$$q"_{drop}(r) = \frac{T_v - T_s - \frac{2\sigma T_v}{r\rho_l i_{lv}}}{\frac{T_{sat}}{\rho_v h_{lv}^2}\left(\frac{\gamma+1}{\gamma-1}\right)\left(\frac{R_g T_{sat}}{2\pi}\right)^{\frac{1}{2}} + \frac{r}{k_l}} \qquad \textbf{4.11}$$

$$P_2 - P_1 = \frac{2\sigma}{r} \quad \textbf{4.12}$$

$$P_2 - P_1 = \frac{P_1 \nu_1}{\nu_2} ln\,(\frac{P_1}{P_{sat} T_{12}}) \quad \textbf{4.13}$$

where $\frac{2\sigma T_v}{r\rho_l i_{lv}}$ is the subcooling of the droplet surface for condensation of vapor on a curved surface derived from Equation 4.12 for the mechanical equilibrium at the drop interface and Equation 4.13 for the thermodynamic equilibrium, $\frac{T_{sat}}{\rho_v i_{lv}^2}\left(\frac{\gamma+1}{\gamma-1}\right)\left(\frac{R_g T_{sat}}{2\pi}\right)^{\frac{1}{2}}$ is the vapor-liquid interfacial thermal resistance derived using normal stress difference between the inner and outer faces of surface of drop, $\frac{r}{k_l}$ is the thermal resistance of conduction in the droplet.

where the subscript 1 and 2 respectively denote inner and outer surfaces of the curved interface, ν is specific volume. The required subcooling degree increases for smaller droplets because it requires a larger pressure difference across a stable droplet surface. Bonner [193] modified the Le Fevre and Rose model by adding contact angle effects to conduction in the droplet as $\frac{r(1-cos\theta)}{k_{coat} sin\theta}$, where $r(1 - cos\theta)$ is the height of the droplet with contact angle of θ and sinθ in the denominator accounts for the change of the base area. Abu-Orabi [111] investigated and added the resistance of surface promoter layer as $\frac{\delta_{coat}}{k_{coat}}$ for hemispherical droplets condensing on hydrophobic surface. Kim and Kim [112] considered thermal resistance and used $\frac{1}{2(1-cos\theta)h_i}$ for liquid-vapor interfacial thermal resistance, where h_i liquid-vapor interfacial thermal resistance for hemispherical droplet [194] and $\frac{1}{2(1-cos\theta)}$ accounts for the shape effect.

$$h_i = \frac{2\alpha}{2-\alpha}\frac{1}{\sqrt{2\pi R_V T_{sat}}}\frac{i_{lv}^2}{v_v T_{sat}} \quad \textbf{4.14}$$

where α is the accommodation coefficient ($0 < \alpha \leq 1$). It is very similar to the term used in Le Fevre and Rose model except for the accommodation coefficient for different fluids. In the current model, the Bonner model is modified by adding $\frac{\delta_{coat} sin\theta}{k_{coat}}$ as the thermal resistance in Teflon™ layer where $sin\theta$ accounts for the base area reduction.

Table 4.3 Thermal resistance in curved surface, liquid-vapor interface, liquid droplet, and surface promoter using three models by Le Fevre and Rose [148], Bonner [193] and Kim and Kim [112]

	Curvature	Interfacial	Droplet	Surface promoter
Le Fevre and Rose [148]	$\frac{2\sigma T_v}{r\rho_l i_{lv}}$	$\frac{T_{sat}}{\rho_v i_{lv}^2}\left(\frac{\gamma+1}{\gamma-1}\right)\left(\frac{R_g T_{sat}}{2\pi}\right)^{\frac{1}{2}}$	$\frac{r}{k_l}$	N/A
Modified Bonner [193]	$\frac{2\sigma T_v}{r\rho_l i_{lv}}$	$\frac{T_{sat}}{\rho_v i_{lv}^2}\left(\frac{\gamma+1}{\gamma-1}\right)\left(\frac{R_g T_{sat}}{2\pi}\right)^{\frac{1}{2}}$	$\frac{r(1-cos\theta)}{k_l\, sin\theta}$	$\frac{\delta_{coat} sin\theta}{k_{coat}}$
Kim and Kim [112]	$\frac{2\sigma T_v}{r\rho_l i_{lv}}$	$\frac{1}{2(1-cos\theta)h_i}$	$\frac{r(1-cos\theta)}{k_l\, sin\theta}$	$\frac{\delta_{coat} sin\theta}{k_{coat}}$

Figure 4.16 compares the Le Fevre and Rose [148], Bonner [193], and Kim and Kim [112] models for heat fluxes through droplets of different radius at same thermal conditions. Results from the Rose model are significantly larger than the other two, perhaps because the thermal resistance in promoter layer was not included. As the droplet size decreases, the significance of promoter layer arises. Leach et al. [195] experimentally and numerically investigated growth rates of droplets with different sizes. Small droplets (e.g., radius < 25 μm) provides 15 times average higher heat fluxes than the larger droplets and therefore they contributed equivalent condensation rates although they occupied only 5% of the condensation surface. As a result, the Bonner model [193] with thermal resistance of surface promoter added, is adopted in this research.

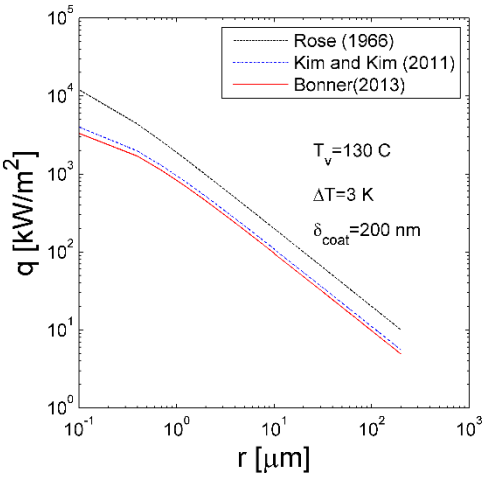

Figure 4.16 Heat flux through droplet bases using three models developed by Rose [148], Kim and Kim [112] and Bonner [193] at saturation temperature of 130°C, subcooling of 3°C and surface promoter thickness of 200 nm

Leach et al. [195] studied growth rate of condensing droplets at different radii and found that droplets (radius smaller than 25 μm) have the same growth rate (volumetric growth rate per unit area). Therefore, heat flux through the base of droplet with radius smaller than 25μm is the same. Bonner model is further modified to consider all the droplets with radius equal to or smaller than 25 μm having the same heat flux through the base. The model for heat flux through a droplet base depends on droplet size:

$$q"_{drop}(r) = \frac{T_v - T_s - \frac{2\sigma T_v}{r\rho_l i_{lv}}}{\frac{T_{sat}}{\rho_v i_{lv}^2}\left(\frac{\gamma+1}{\gamma-1}\right)\left(\frac{RgT_{sat}}{2\pi}\right)^{\frac{1}{2}} + \frac{r(1-cos\theta)}{k_l\, sin\theta} + \frac{\delta_{coat} sin\theta}{k_{coat}}} \quad for\ r > 25\mu m \qquad \textbf{4.15}$$

$$q"_{drop}(r) = \frac{T_v - T_s - \frac{2\sigma T_v}{r_0\rho_l i_{lv}}}{\frac{T_{sat}}{\rho_v i_{lv}^2}\left(\frac{\gamma+1}{\gamma-1}\right)\left(\frac{RgT_{sat}}{2\pi}\right)^{\frac{1}{2}} + \frac{r_0(1-cos\theta)}{k_l\, sin\theta} + \frac{\delta_{coat} sin\theta}{k_{coat}}} \quad for\ r \leq 25\mu m \qquad \textbf{4.16}$$

where $r_0 = 25\ \mu m$.Figure 4.17 depicts the heat flux through the droplet base of radius ranging from 0.1 to 200 μm at the vapor saturation temperature of 130 °C, surface subcooling degree of 3 °C, and surface coating thickness of 200 nm.

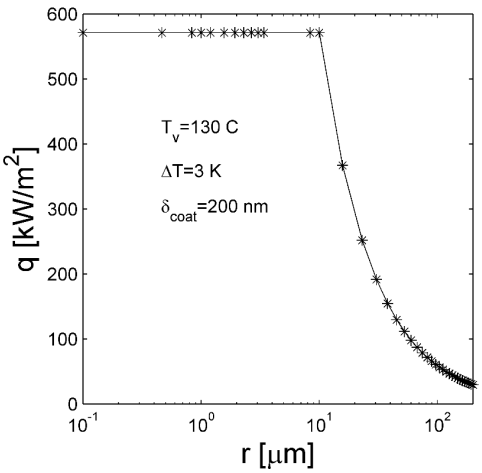

Figure 4.17 Heat flux through the base of droplet with different sizes

4.4.3. Droplet size distribution

From Figure 4.17, heat flux through the base of a droplet depends on the droplet size. To obtain the mean dropwise condensation heat flux, it is necessary to know the droplet size distribution, which describes the largest and smallest droplet sizes as well as the number of droplets of different sizes between them. Le Fevre and Rose [110] and Rose and Glicksman [196] conducted dropwise steam condensation experiments on vertical plates and identified the power-law function (Equation 4.17) to describe the size distribution of visible droplets.

$$f(r^*) = 1 - (r^*)^{\frac{1}{3}}\,;\, r^* = \frac{r}{r_{max}} \qquad \textbf{4.17}$$

where $f(r)$ is the area fraction occupied by droplets of radius larger than r to r_{max}. Figure 4.18 demonstrates the power law distribution of droplet sizes.

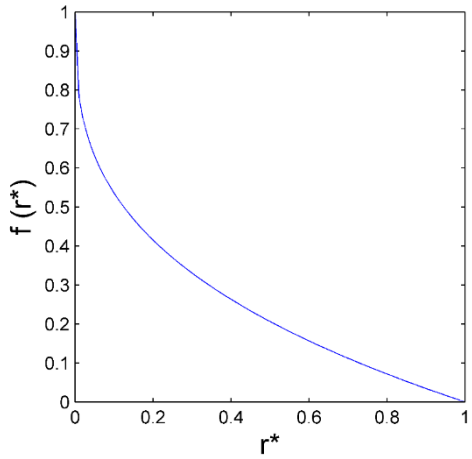

Figure 4.18 Fractional area occupation by droplet with radius greater than r*

However, this power law relationship generally only describes the size distribution of large droplets well; large droplets refer to the sizes obtained through coalescence and small droplets refer to those sizes mainly through direct condensation of vapor on the droplet surface [150]. Wu and Maa [151] defined the cutoff size (r_e) to distinguish small and large droplets as half the distance between neighboring nucleation sites.

$$r_e = (4N_s)^{-1/2} \tag{4.18}$$

where N_s is the number of nucleation sites on a unit area of condensation surface. Rose [197] assumed a random distribution of nucleation sites on the condensing surface and developed a correlation for droplet nucleation density:

$$N_s = \frac{0.037}{r_{min}^2} \tag{4.19}$$

where r_{min} is the nucleation size derived by Graham and Griffith [149] using heterogeneous droplet nucleation theory.

$$r_{min} = \frac{2T_{sat}\sigma_{lv}}{\rho_l i_{lv} \Delta T_{sub}} \tag{4.20}$$

where ΔT_{sub} is the subcooling degree of condensation surface. In this research, the steam saturation temperature is approximately 130 ^{o}C (403.15 K) and the subcooling degree is 3 ^{o}C. The nucleation density from Equation 4.19 is 10^{14} m^{-2} and the nucleation size is 10 nm.

Wu and Maa [151] proposed a population balance method for the size distribution of small droplets. It described the size distribution of droplets with the minimum radius to cutoff radius. The population balance method assumed a stable dynamic droplet size distribution and the number of droplets is constant in the radius ranged from r to r+Δr. Therefore, the number of droplets entering the range of r to $r+\Delta r$ through growth must equal the number of droplets leaving this range of r to $r+\Delta r$. Droplets leave this radius range by two mechanisms: being swept by upstream droplets or dislodged by drag forces. The left side of Equation 4.21 is the number of droplets grown from smaller than a radius of r to equal or larger than r. The right side is the number of droplets grow out of $r+\Delta r$ by condensation (An_2G_2dt) and being swept by upstream droplet ($Sn_{1-2}\Delta rdt$),

$$An_1M_1dt = An_2M_2dt + Sn(r)\Delta rdt \quad \textbf{4.21}$$

where M_1 and M_2 are the growth rate of droplets (i.e. heat transfer rate) with radius of r_1 and r_2, $n(r)$ is the number of droplet with radius r per unit area, A is an arbitrary area, and S is the sweeping period. Instead of an experimental evaluation, the sweeping periods were calculated by the continuity of droplet size distribution at the cutoff size (r_e). Let f(r) be the area fraction occupied by droplets of radius between r and r_{max} and $a(r)$ be the differential area fractions occupied by droplets with radius from r to $r+\Delta r$, subscript l and s respectively denote large droplets and small droplets.

$$f(r) - f(r+dr) = a(r)dr \quad \textbf{4.22}$$

Therefore,

$$a(r) = \frac{f(r)-f(r+dr)}{dr} = -\frac{df(r)}{dr} \quad \textbf{4.23}$$

In addition, as n(r) is the number of droplets with radius of r in a unit area, the fraction area occupied by droplets with radius of *r* equal to the number of droplets in a unit area times the area occupied by each droplet.

$$a(r) = n(r)\pi r^2 \sin^2\theta \quad \textbf{4.24}$$

For the large droplets (i.e. $r>r_e$), from Equation 4.17 and Equation 4.22, the fraction area occupied by droplet of radius r is:

$$a_l(r) = n\frac{1}{r_{max}}\left(\frac{r}{r_{max}}\right)^{-\frac{2}{3}} \text{ for } r > r_e \quad \textbf{4.25}$$

Equation 4.21 and Equation 4.24 (i.e. equation group for droplet size distribution of small droplets) were solved for continuity at $r=r_e$ (cutoff for small and large droplets) with Equation 4.17 (i.e. droplet size distribution function for large droplets) so that the droplet size distribution function is continuous throughout the whole droplet size range from r_{min} to r_{dept}. Therefore the area fraction occupied by droplets of r in the range of r_{min} to r_e is:

$$a_s(r) = \frac{1}{3r_e^3 r_{max}}\left(\frac{r_e}{r_{max}}\right)^{-\frac{2}{3}}\frac{r^3(r_e-r_{min})}{r-r_{min}}\frac{A_2 r+A_3}{A_2 r_e+A_3} exp\,(B_1+B_2) \quad \textbf{4.26}$$

where A_1, A_2, B_1, and B_2 are coefficients:

$$A_2 = \frac{\theta(1-cos\theta)}{4k_{coat}sin\theta} \quad \textbf{4.27}$$

$$A_3 = \frac{1}{2h_i} + \frac{\delta_{coat}(1-cos\theta)}{k_{coat}sin^2\theta} \quad \textbf{4.28}$$

$$B_1 = \frac{A_2}{\tau A_1}\left[\frac{r_e^2-r^2}{2} + r_{min}(r_e-r) - r_{min}^2 ln\left(\frac{r-r_{min}}{r_e-r_{min}}\right)\right] \quad \textbf{4.29}$$

$$B_2 = \frac{A_3}{\tau A_1}[r_e - r - r_{min} ln\,(\frac{r - r_{min}}{r_e - r_{min}})] \quad \textbf{4.30}$$

$$\tau = \frac{3r_e^2(A_2 r_e + A_3)^2}{A_1(11A_2 r_e^2 - 14A_2 r_e r_{min} + 8A_3 r_e - 11A_3 r_{min})} \quad \textbf{4.31}$$

Combining the heat flux through small and large droplets provides the mean dropwise condensation heat flux through the surface

$$q"_{DWC} = \int_{r_{min}}^{r_e} q"(r)a_s(r)dr + \int_{r_e}^{r_{max}} q"(r)a_l(r)dr \quad \textbf{4.32}$$

Therefore, the dropwise condensation heat transfer coefficient is:

$$h_{DWC} = \frac{q"_{DWC}}{\Delta T} = \frac{1}{\Delta T}(\int_{r_{min}}^{r_e} q"(r)a_s(r)dr + \int_{r_e}^{r_{max}} q"(r)a_l(r)dr) \quad \textbf{4.33}$$

Figure 4.19 presents heat transfer coefficients obtained using different droplet departure sizes; droplet departure size is also assumed to be the maximum droplet radius. Increasing droplet departure radius, decreases condensation heat transfer coefficient as it increases the thermal resistance in the droplet. Hence, it is important to predict droplet departure size for predicting heat transfer coefficient in flow condensation.

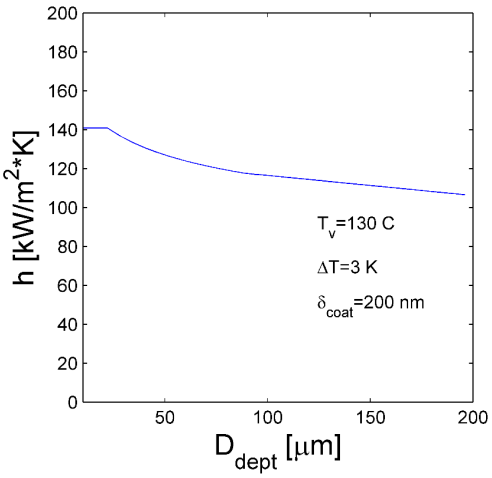

Figure 4.19 Heat transfer coeffceints with respect to droplet departure size

4.4.4. Droplet adhesion forces

Unlike gravity-driven dropwise condensation on vertical plates, droplet departure in shear flow is primarily dominated by interfacial shear stress caused by the difference in vapor and liquid velocities. Evaluation of the integral for heat flux of dropwise condensation (Equation 4.32) requires droplet departure size. There are many challenge of multi-phase flow modeling: droplet-solid adhesion forces involving van der Waals, electrostatic, solvation and polymer-mediated interactions [198]. Additionally, the incipient motion of contact line is not well understood [199]. Eral et al. [200] analyzed the physical phenomenon of contact angle hysteresis and found no promising numerical models predicted droplet dynamics well. Therefore, in this research, drag forces and adhesion forces are analyzed separately to predict droplet departure size.

Droplets move when the drag force exceeds the adhesion force between the droplet and solid surface. Drag forces increase faster than adhesion forces with increasing droplet size to continuously deform droplets and increase contact angle hysteresis [201]. At critical droplet sizes, contact angle hysteresis reaches its maximum value and droplets move from the original sites [201]. Adhesion is the tendency of unlike particles or surfaces clinging to one another. Adhesion forces depend on liquid surface tension and dynamic and static contact angles. In the gas-liquid-solid three-phase system, the Young-Dupre equation [202] describes solid-liquid interfacial tension on the contact line of droplets in static equilibrium:

$$\gamma_{sv} = \gamma_{ls} + \gamma_{lv} cos\theta \qquad \textbf{4.34}$$

where γ_{sv} is solid-vapor interfacial tension, γ_{ls} is liquid-solid interfacial tension, γ_{lv} is the liquid-vapor interfacial tension (liquid surface tension), and θ is the equilibrium contact angle. A droplet deforms when vapor flows over the droplet. Therefore, along the vapor-liquid-solid three-phase contact line, contact angle varies. The largest and smallest contact angles are respectively termed

the advancing and receding contact angle (Figure 4.20) and the corresponding contact points are the advancing and receding points. Contact angle hysteresis is the difference between advancing and receding contact angles.

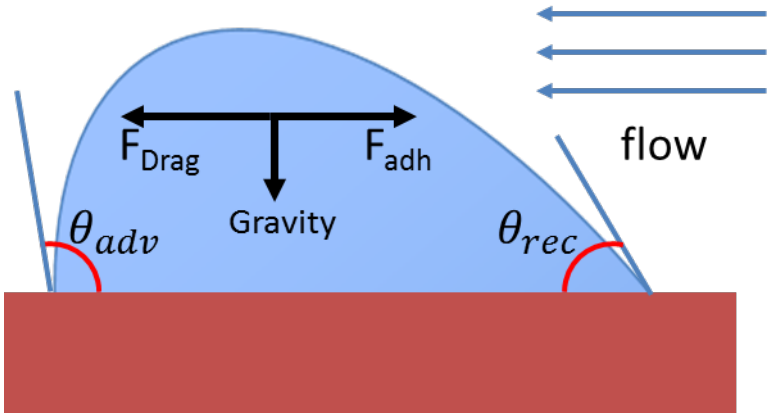

Figure 4.20 Force balance of droplet deformed by shearing flow

Contact angle hysteresis can correlate with the adhesion force between the droplet and surface. Researchers [203-207] investigated contact angle hysteresis and the resultant adhesion force between droplets and surfaces. Antonini et al. [207] modified the Brown et al. [208] prediction and obtain the following model for adhesion forces of droplets on solid surface:

$$F_{adh} = -\gamma \int_0^{2\pi} cos\theta cos\phi r d\phi \qquad \textbf{4.35}$$

where ϕ is the azimuthal angle starting from receding point ($\phi_{rec} = 0, \phi_{adv} = \pi$) and r is the radius of the contact area (droplet base). The base area is not affected by the deformation of the droplet (static contact line). Therefore,

$$r = Rsin\theta \qquad \textbf{4.36}$$

where R is the radius of a spherical cap with equivalent volume of the droplet (V) and static contact angle θ.

$$R = \left(\frac{3V}{2\pi(1-cos\theta)}\right)^{-\frac{1}{3}} \quad \textbf{4.37}$$

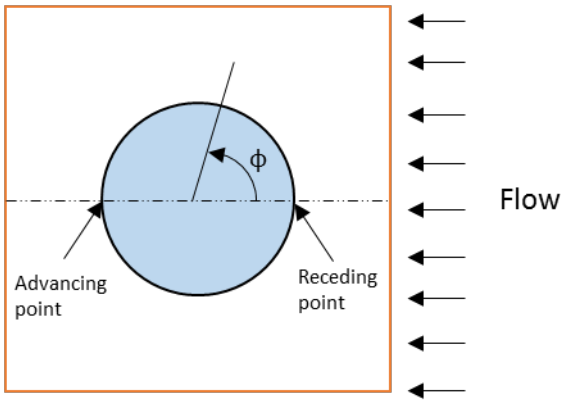

Figure 4.21 Diagram (top view) advancing and receding point, and azimuthal angle

4.4.5. Droplet drag force

At different flow conditions (i.e. steam mass flux and steam quality), the relatively velocities of vapor over droplets vary. Droplet sweeping occurs when the shear forces imposed on the droplets by the shearing vapor exceeds the maximum adhesion force. Shear forces are estimated using the drag force equation:

$$F_d = \frac{1}{2} C_d \rho_v A_p U_v^2 \quad \textbf{4.38}$$

where C_d is drag coefficient, ρ_v is vapor density, A_p is area of droplet surface projected to flow direction, U_v is vapor velocity calculated with vapor void fraction (α) taken into consideration using Equation 4.39.

$$U_v = \frac{Gx}{\rho_v \alpha} \quad \textbf{4.39}$$

The drag force is proportional to the projected area of the droplet to the flow direction. Droplets are deformed under shearing flow and cannot be assumed to be a perfect spherical cap. El Sherbini and Jacob [209] proposed a two-circle-fitting method for projected area. The model is a parabolic function of droplet radius. Comparison with experiments of droplets on inclined and

vertical plate validated the model and greatly reduced the error from assuming spherical cap for the projected area and droplet volume,

$$A_p = \frac{1}{2}\frac{L_1^2\theta_{adv}}{(sin\beta)^2} + \frac{1}{2}\frac{L_1^2}{tan\beta} + \frac{1}{2}\frac{L_2^2\theta_{rec}}{(sin\theta_{rec})^2} - \frac{1}{2}\frac{L_2^2}{|tan\theta_{rec}|} \quad \textbf{4.40}$$

$$L_f = \frac{sin\theta_{adv}(1+cos\theta_{rec})}{sin\theta_{rec}(1-cos\theta_{adv})} \quad \textbf{4.41}$$

$$L_1 = \frac{2r\,L_f}{1+L_f} \quad \textbf{4.42}$$

$$L_2 = \frac{2r}{1+L_f} \quad \textbf{4.43}$$

where r is droplet radius, $\beta_1 = \pi - \theta_{adv}$, and L_1, L_2 and L_f are coefficients determined using proceeding equations.

CFD (Computation Fluid Dynamics) studies were conducted using FLUENT^{TM} to evaluate the drag forces applied to solid spherical caps of same projected area as deformed ones. Studies investigated droplet radius of 12.5 to 50 μm and vapor velocities of 5 to 25 m/s, which are equivalent to flow conditions for steam mass fluxes of 35 – 100 kg/m^{2}s and qualities of 0.2 – 0.8. Geometry modelling was completed in ANSYS design modeler, where the channel was divided into multiple zones for multi scale meshing (Figure 4.22 and Figure 4.23). The sweeping mesh method created the most structured elements from inlet and outlet approaching the small block cut with two diagonal lines. To obtain a smooth transition from cuboid elements to spherical elements, two cylindrical zones were created from the top of the droplet. The outer one had a radius of 0.5 mm which is greater than the droplet radius and the inner one had a radius $r_i = r_{drop}cos45^o$. For the calculation of boundary layer, thirty and ten inflation layer were created for bottom and top surfaces respectively. Ultimately, there were 1 – 3 million elements for different sizes of droplets.

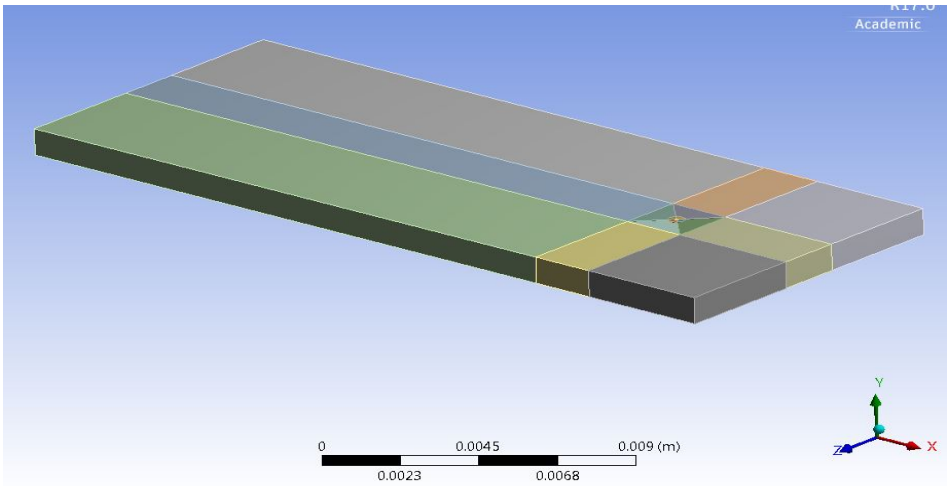

Figure 4.22 Multi-zone model for droplet in mini-gap in FLUENT

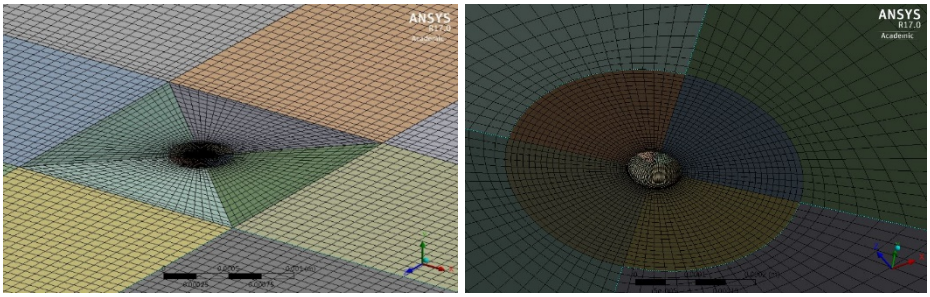

Figure 4.23 Mulit-scale meshing in FLUENT for determining drag force on droplet

The κ-ω SST model low-Re correction was employed for the model as it solves the confined flow and near-wall field the best. Drag force simulations ran for droplet radiuses of 12.5, 25 and 50 μm, at flow velocities of 5, 10, 15, 20, 25 and 30 m/s for each droplet size. FLUENT calculated the drag force exerted on the droplet surfaces and drag coefficients (C_d) were calculated using $C_d = \frac{2F_d}{\rho_V A_p U_v^2}$. The average values of drag coefficients at six velocities were all approximately 0.45 with average percentage variances of 8.7%, 7.4% and 5.1% for droplet radiuses of 12.5, 25 and 50 μm respectively (Figure 4.24).

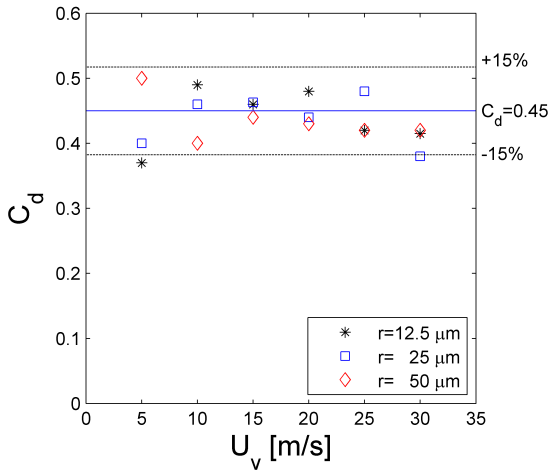

Figure 4.24 Drag coefficients of vapor flow on droplet at various velocity and droplet sizes

Sommers et al. [201] studied critical velocities required to sweep droplets from vertical surfaces and determined the drag coefficient (C_d) using two-circle method (Equation 4.40) for projected area. Milne and Amirfazli [204] evaluated drag coefficients by investigating incipient motion of droplet on hydrophilic, hydrophobic and super hydrophobic surface under shearing air flow in wind tunnel. Both studies saw a consistent drag coefficient between 0.44 and 0.45. Volynskii [210], Lane [211] and Morsi [212] observed same similar drag coefficients (i.e., 0.44-0.45) of deformable droplets and rigid spheres. Combined with the FLUENT simulations, a constant drag coefficient of 0.45 is assumed. Figure 4.25 compares the drag forces from simulation and drag force equation using a constant drag coefficient of 0.45.

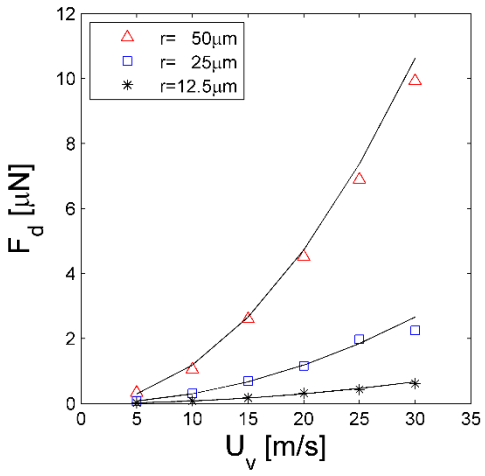

Figure 4.25 Comparions of drag forces from prediciton and numerical computation

4.4.6. Droplet departure sizes

Droplet forces are proportional to projected areas of droplets, which are second order of droplet radius. Adhesion forces are proportional to droplet radiuses according to Equation 4.35. Therefore, drag forces increase faster than adhesion forces with increasing droplet size. At the critical radius that satisfies $F_d = F_{adh}$, drag force initiates droplet motion. Figure 4.26 depicts predicted droplet departure sizes at steam mass fluxes of 35–200 kg/m^{2}s and steam quality of 0.2–0.9. Increasing steam mass fluxes and steam qualities increase vapor velocity and in turn decrease droplet departure size.

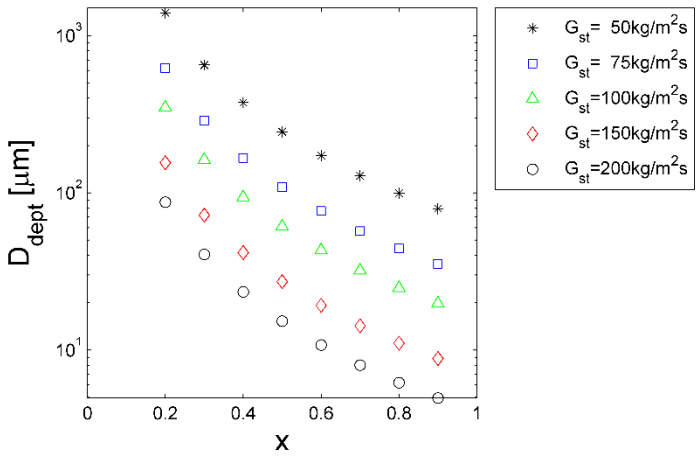

Figure 4.26 Droplet departure size at various steam mass fluxes and steam qualites

Droplet departure sizes visualized in experiments at a mass flux of 50 kg/m^{2}s and steam qualities of 0.35, 0.45, and 0.65, validate the predictions. To ensure shear-induced departure, size measurements were performed on droplets completing the series of nucleation, growth, coalescence and departure. The nominal departure sizes are the average of lengths in axial and lateral directions. The predicted departure size is averagely 6.5% smaller than the mean value of the two principal sizes. The uncertainty of the measurements was ± 4 pixel, which is equivalent to ±11.2 μm with the magnification of 5.0 in the lens and camera pixel size of 14 μm.

a

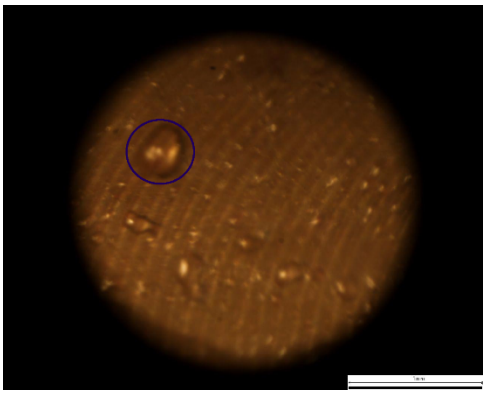

G = 50 kg/m^{2}s and x = 0.65
Predicted departure size: 364μm
Nominal departure size: 370 ± 11.2 μm
Measured principle sizes: 336 μm and 404 μm

b

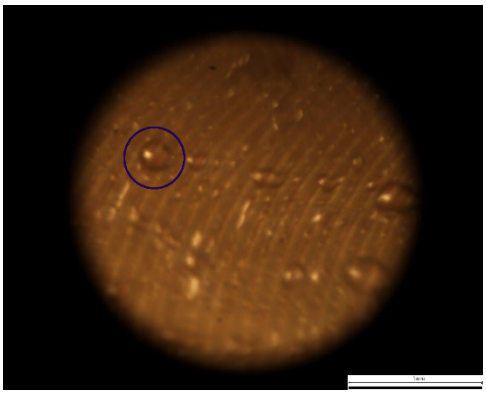

G = 50 kg/m^{2}s and x = 0.65
Predicted departure size: 225μm
Nominal departure size: 231 ± 11.2 μm
Measured principle sizes: 235 μm and 227 μm

c

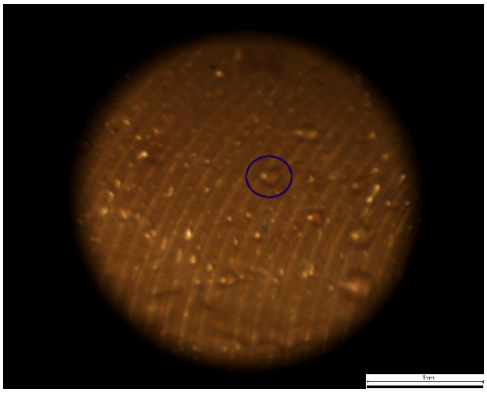

G = 50 kg/m^{2}s and x = 0.65
Predicted departure size: 111μm
Nominal departure size: 131 ± 11.2 μm
Measured principle sizes:142 μm and 120 μm

Figure 4.27 Comparison of dropelt departues sizes in experiments and predicitons

4.4.7. Dropwise condensation heat transfer coefficient correlation

With droplet departure size is known from the balance of drag and adhesion forces, the dropwise condensation heat transfer coefficients are predictable using Equation 4.33. Thereby, estimates the average flow condensation heat transfer coefficients in hydrophobic mini-gap. Figure 4.28 plots predicted heat transfer coefficients with steam qualities of 0.2–0.9 and steam mass fluxes of 35–200 kg/m^{2}s in the 0.5-mm deep mini-gap. It should be noted that this model is not designed

for conditions of steam quality lower than 0.2, where the void fraction changes dramatically to change the flow pattern from annular to slug/bubbly. Increasing steam mass flux and steam quality always increases heat transfer coefficients since increasing interfacial shear decreases droplet departure size. Smaller departing droplets correspond to lower thermal resistance. As steam mass flux increases, heat transfer coefficients become less dependent on steam quality because most droplets are within the radius range of 25 μm where heat transfer coefficients are independent of droplet sizes.

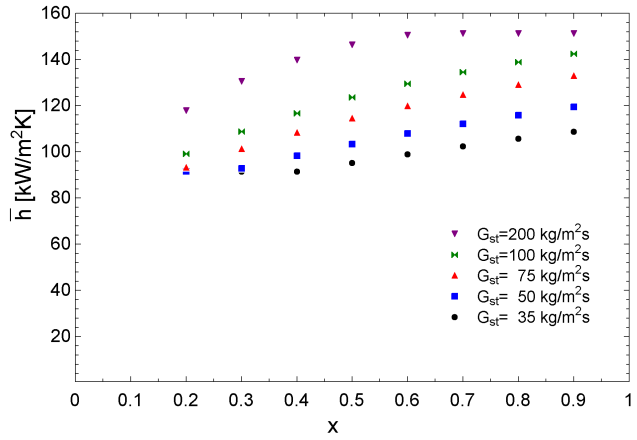

Figure 4.28 Predicted heat transfer coeffcients at different mass fluxes and qualities

With no curve fitting made to the model, the comparison of heat transfer coefficients with experiments results in Figure 4.29 presents great agreement that all the predictions are all within -30% to 30% range of relative errors (RE) and most of the data points are within ± 15%. The mean absolute errors (MAE) for the 0.5-mm and 1-mm deep mini-gaps are 9.6 % and 8.8%, respectively,

$$RE = \frac{h_{pre} - h_{exp}}{h_{exp}} \times 100\% \qquad \textbf{4.44}$$

$$MAE = \frac{\sum_{i=1}^{n} |RE_i|}{n} \times 100\% \qquad \textbf{4.45}$$

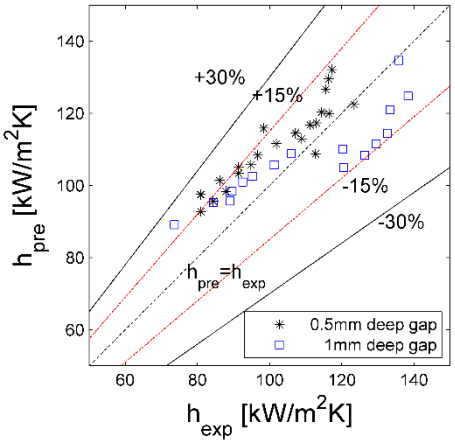

Figure 4.29 Comparison of heat transfer coefffcient from correlation and experimental resutls

4.5 Steam-nitrogen condensation in mini-gaps

As mentioned in the literature review, the degradation of heat transfer performance by the presence of noncondensable gas has been observed since the 1930s [171, 174, 213]. Ma et al. [214] hypothesized that in dropwise condensation, the periodic sweeping of droplets can mitigate heat transfer degradation by perturbing the accumulated noncondensable layer between the vapor and liquid condensate. This part of the research studies quantitatively the degradation of heat transfer coefficients in internal filmwise condensation and the mitigation of noncondensable gas effects in dropwise condensation by condensing nitrogen-steam mixture in hydrophilic and hydrophobic mini-gap. Shown in the box branch of Figure 4.30, ultra-pure nitrogen (mass purity > 99.9%, Matheson) is injected to two-phase steam exiting the pre-condenser at a known steam quality. A pressure regulator provides nitrogen from the nitrogen cylinder to the steam pipe line at a stable pressure and flow rate and an acrylic volumetric flow meter (Omega^{TM} FL7211) enables flow stability visualization and measurements of volumetric flow rate. Since nitrogen goes through the flow meter at a known temperature and pressure (measured with a thermocouple and pressure

transducer, respectively), the conversion equation translates volumetric flow rate to mass flow rate. At the T-joint, a valve fully mixed nitrogen and steam.

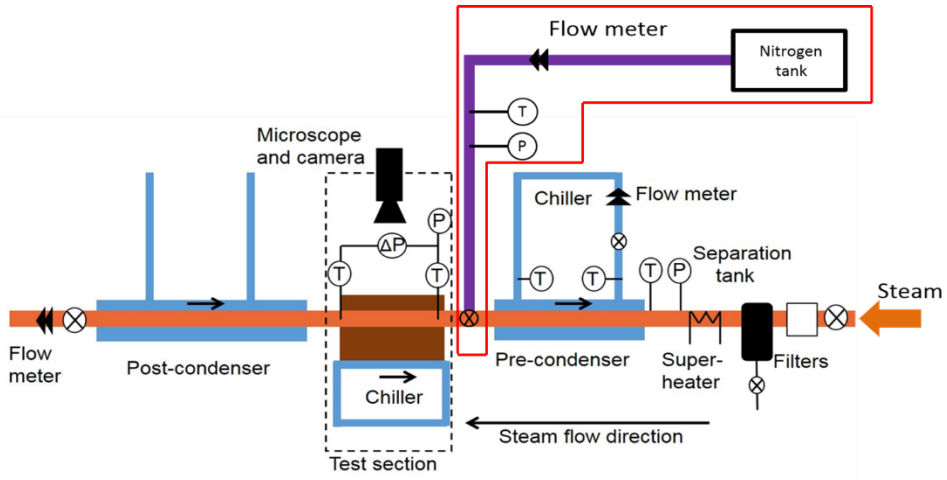

Figure 4.30 Experimental apparatus for steam condnesation in presence of nitrogen

The coupon with 1-mm deep mini-gap was used in these experiments. Fluid temperatures in the condensing mini-gap are required for calculating heat transfer coefficients. However, due to the presence of nitrogen, models for two-phase pressure drops cannot estimate fluid pressure or temperature. Therefore, a type-T micro-thermocouple (TC Direct^{TM} 206-494) was inserted at the center of the mini-gap to measure fluid temperature. The micro-thermocouple had a 0.508-mm radius with a rubber gasket near the tip. The glass cover compressed the rubber gasket on the bottom surface of the mini-gap to position the micro-thermocouple at the center of the mini-gap. Validation tests evaluate the effects of micro-thermocouple on heat transfer coefficients. For validation, condensation experiments at steam mass flux of 50 kg/m^{2}s and steam qualities of 0.3 – 0.9 were performed and compared with previously validated results whose fluid temperatures were estimated using two-phase pressure drop model. Figure 4.31 compares the results of heat transfer coefficients obtained using different mechanisms for fluid temperature. The good agreement demonstrates the credibility of using micro-thermocouple for measuring fluid temperatures.

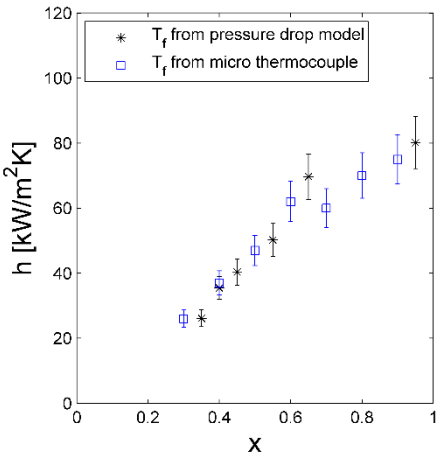

Figure 4.31 Validation of fluid temperature measurements using micro-thermocouple

Three sets of steam condensation experiments at steam mass fluxes of 35, 50 and 75 kg/m^{2}s were used to study effects of nitrogen mass fractions at steam qualities of 0.35 – 0.9. In each set of experiments, steam mass flux ($G_{st} = \frac{\dot{m}_{st}}{A_x}$) remains the same. Increasing nitrogen mass fraction increased flow mass flux ($G_f = \frac{\dot{m}_f}{A_x} = \frac{\dot{m}_{st}+\dot{m}_N}{A_x}$). Nitrogen mass fraction in the three-component flow quantifies the amount of nitrogen:

$$\omega_N = \frac{\dot{m}_N}{\dot{m}_f} = \frac{\dot{m}_N}{\dot{m}_v+\dot{m}_l+\dot{m}_N} \qquad \textbf{4.46}$$

where $\dot{m}_N$ is the nitrogen mass flow rate, $\dot{m}_f$ is the three-phase mixture mass flow rate, $\dot{m}_v$ is the vapor phase mass flow rate, and $\dot{m}_l$ is the liquid mass flow rate.

4.5.1. Steam-nitrogen condensation in hydrophilic mini-gaps

Condensing steam-nitrogen heat transfer coefficients in the hydrophilic copper mini-gap are graphed in Figure 4.32 at steam mass fluxes of 35, 50 and 75 kg/m^{2}s. The experimental conditions covered steam mass fluxes of 35–75 kg/m^{2}s, steam qualities of 0.35–0.9, and nitrogen mass fractions of 0–30%. The resultant heat transfer coefficients ranged from 10,000 to 80,000

W/m^2K. Hence, steam mass flux, steam quality and nitrogen mass fraction are potentially strong factors affecting heat transfer coefficients of condensing steam-nitrogen mixture.

For the same steam mass flux and quality, increasing the nitrogen mass fraction (ω_N) consistently decreased heat transfer coefficients significantly. Adding nitrogen increased the relative velocity between liquid phase and gaseous mixture (i.e. vapor and nitrogen) to thin the liquid film and decrease the thermal resistance in the liquid film. However, the presence of nitrogen introduced additional thermal resistance and suppressed steam condensation.

At each of three steam mass fluxes, increasing steam quality with the same nitrogen mass fraction increases heat transfer coefficients, which is similar to the observations of steam condensation without presence of nitrogen. Increasing steam quality is essentially replacing liquid condensate partly with steam vapor, which increases void fraction and reduces liquid film thickness and thermal resistance within. Meanwhile, flow velocity greatly increases with increasing steam quality due to the huge density differences betweem liquid and vapor. Increased mass fraction of vapor in vapor-nitrogen mixture for increasing steam quality, enhance steam condensation from the perspective of kinetic theory. Comparison of a, b and c in Figure 4.32 shows that higher steam mass fluxes are associated with higher heat transfer coefficients with the same nitrogen mass fraction and steam quality for the increasing steam velocity and thus the flow Reynolds number.

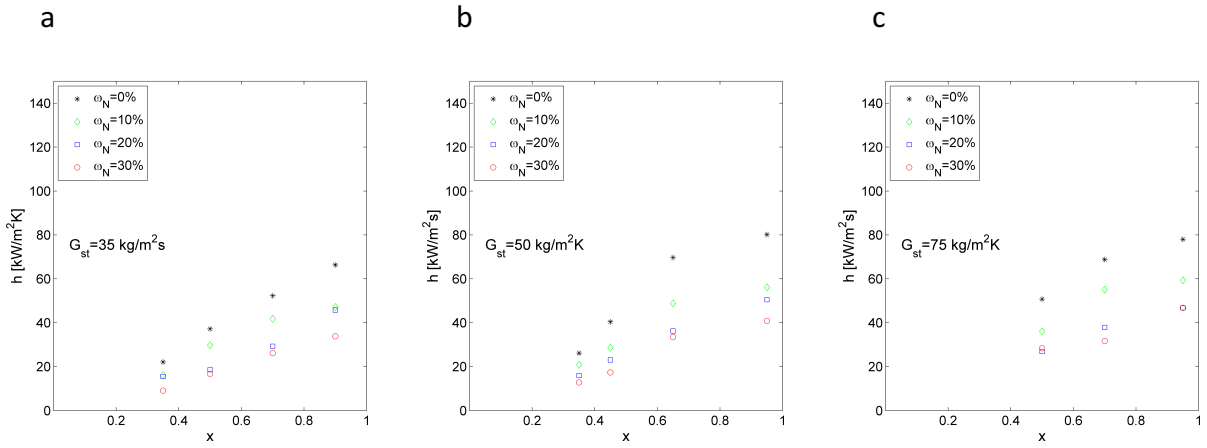

Figure 4.32 Heat transfer coeffceint in 0.5mm deep mini-gap at steam mass fluxes of (a) 35, (b) 50, and (c) 75 kg/m^{2}s

Heat transfer coefficient degradation factors ($\varepsilon_{de,htc,x}$) compare heat transfer coefficients of condensing steam-nitrogen mixture with nitrogen mass fraction to those of condensing steam without nitrogen. Smaller degradation factors means more degradation,

$$\varepsilon_{de,x} = \frac{h_{st} - h_x}{h_{st}} \times 100 \qquad \textbf{4.47}$$

where $\varepsilon_{de,x}$ is the heat transfer coefficient degradation factor h_{st} is the pure-steam condensation heat transfer coefficient and h_x is the steam-nitrogen condensation heat transfer coefficient, x denotes nitrogen mass concentration percentage (x%). Table 4.4 presents the degradation factors obtained from adding a certain percentage of nitrogen to the steam. Each data point averages degradation factors of different steam qualities with same steam mass flux and nitrogen mass fraction.

Table 4.4 Degradation of heat transfer coefficients due to presence of nitrogen

G_{st} (kg/m^{2}s)	35	50	75
$\varepsilon_{de,htc,10}$	28%	38%	52%
$\varepsilon_{de,htc,20}$	28%	38%	51%
$\varepsilon_{de,htc,30}$	27%	38%	44%

Boundary layer theory [170-173] and diffusion layer theory [177, 179, 215] agree that noncondensable gases play a significant role at the vapor-liquid interface by adding a layer of

thermal resistance and suppressing condensation on the liquid film by reducing vapor concentration near the condensation interface. The mass fraction of vapor is a combination of nitrogen mass fraction and steam quality, which are important parameters,

$$\omega_v = \frac{\dot{m}_v}{\dot{m}_f} = x(1 - \omega_N) \qquad \textbf{4.48}$$

As steam quality increases and nitrogen mass fraction decreases, vapor mass fraction increases, which follows the same trend of heat transfer coefficient. Figure 4.33 plots heat transfer coefficients against vapor mass fraction (ω_v). As the thermal conductivity of nitrogen is an order of magnitude lower than the conductivity of liquid water, liquid condensate thickness is less significant in the system of steam-nitrogen mixture than that of steam only. Therefore, heat transfer coefficient is greatly strong function of vapor mass fraction.

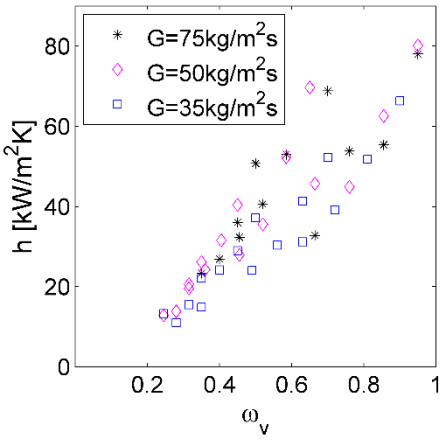

Figure 4.33 Heat transfer coefficient of steam-nitrogen mixture with respect to mass fraction of steam vapor at three mass fluxes

4.5.2. Comparisons of heat transfer coefficients with correlations

Caruso et al. [216] studied condensation of steam-air mixture in near-horizontal (i.e., 7^o inclination) copper tubes of 12.6, 20 and 26.8-mm diameters. The experimental conditions cover inlet noncondensable gas mass fractions (ω_N) of 5%–60% and mixture Reynolds numbers (Re_m)

of 500–20,000, which fully envelops the conditions of this research. Heat transfer coefficients in terms of vapor Nusselt number were curve fitted using vapor-nitrogen Reynolds number (Re_g), liquid Reynolds number (Re_l) and nitrogen mass fraction (ω_N).

$$Nu_v = 18.8\, Re_g^{0.592}\, Re_l^{-0.13} \left(\frac{\omega_N}{1-\omega_N}\right)^{-0.357} \quad \textbf{4.49}$$

$$Re_g = \frac{G_g D_h}{\mu_g} \quad \textbf{4.50}$$

$$Re_l = \frac{G_l D_h}{\mu_l} \quad \textbf{4.51}$$

where D_h is hydraulic diameter ($D_h = \frac{4A}{Pe}, A\ is\ wetted\ area\ and\ Pe\ is\ wetted\ perimeter$), μ_g is vapor-nitrogen mixture viscosity, calculated using Gambill correlation [217]:

$$\mu_g = \left(\frac{\lambda_{v,g}}{\mu_v} + \frac{\lambda_{N,g}}{\mu_N}\right)^{-1} \quad \textbf{4.52}$$

where $\lambda_{v,g}$ and $\lambda_{N,g}$ are respectively the mass fraction of vapor and nitrogen in the vapor-nitrogen mixture.

a

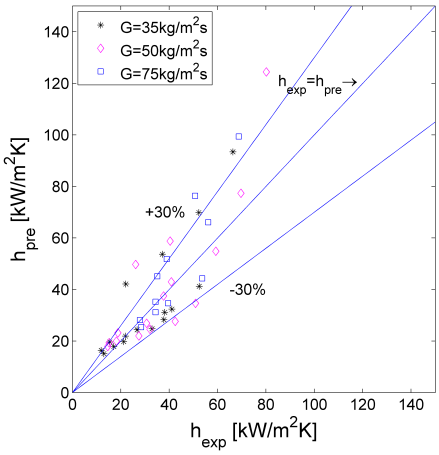

b

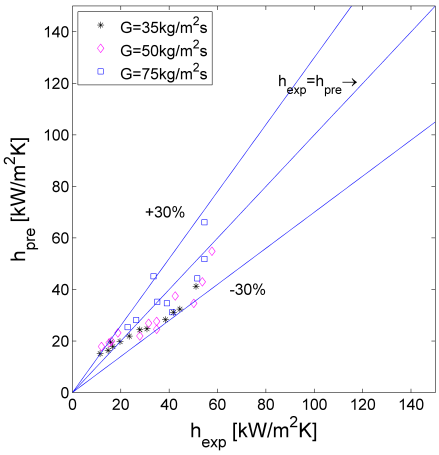

Figure 4.34 Comparison of experimental and predicted steam-nitrogen condensation heat transfer coefficients (a) with scenarios of $\omega_N = 0$ (b) with scenarios of $\omega_N > 0$ only

Figure 4.34 (a) compares experimental results (including non-nitrogen cases) with Caruso et al. [216] correlation. The term $\left(\frac{\omega_N}{1-\omega_N}\right)^{-0.357}$ goes to infinity when ω_N approaches zero. Therefore, $\omega_N = 1\%$ was used for the non-nitrogen cases. Overall, the estimates from the model and the experimental results agreed with an MAE of 27%, although there are some cases that correlation overestimate heat transfer coefficients for more than 30%. Figure 4.34 (b) eliminates non-nitrogen data points. The Caruso et al. [216] correlation tends to predicted steam-nitrogen mixture condensation better with an MAE of 18% with no preference on mass fluxes. The MAEs are 17%, 20% and 15% at mass fluxes of 35, 50 and 75 kg/m^{2}s, respectively.

Different experiments were conducted to evaluate the effects of nitrogen on pressure drops in the condensation mini-gap. Three sets of experiments at three flow mass fluxes $\left(G_f\right)$ evaluated the effects of nitrogen on pressure drops. In Figure 4.35, ω_g denotes the mass fraction of gas mixture (i.e. vapor and nitrogen) in the vapor-liquid-nitrogen flow (Equation 4.53)

$$\omega_g = \frac{\dot{m}_g}{\dot{m}_f} = \frac{\dot{m}_v + \dot{m}_N}{\dot{m}_v + \dot{m}_N + \dot{m}_l} \qquad \textbf{4.53}$$

These experiments tested the effects of replacing vapor partly with nitrogen on pressure drops in the mini-gap. At all three flow mass fluxes and gas mixture mass fractions, replacing vapor with nitrogen has minimal effect on pressure drops in the mini-gap. When $\omega_N = 0\%$, $\omega_v = \omega_g = x$, where ω_v stands for the mass fraction of vapor. Intuitively, increasing flow mass flux from 35 to 75 kg/m^{2}s, pressure drops increases for each data point of gas mass fraction (ω_g).

$$\omega_v = \frac{\dot{m}_v}{\dot{m}_f} = \frac{\dot{m}_v}{\dot{m}_v + \dot{m}_N + \dot{m}_l} \qquad \textbf{4.54}$$

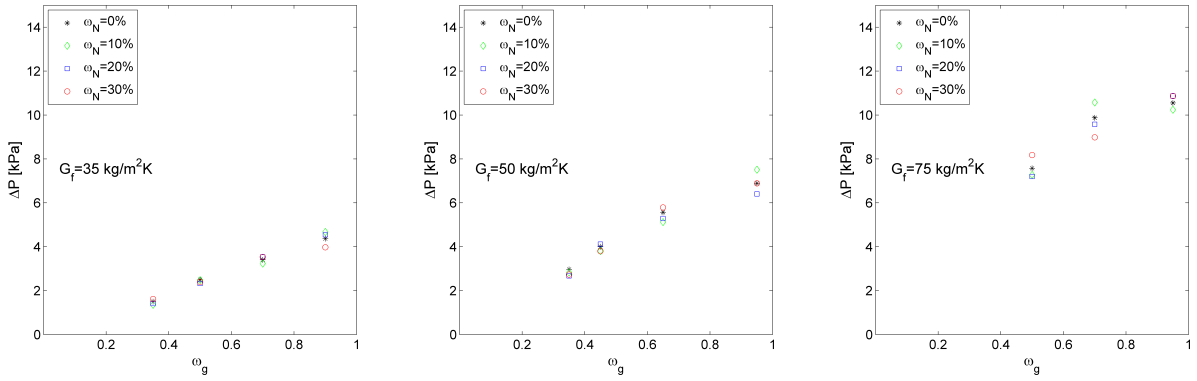

Figure 4.35 Pressure drops of steam-nitrogen condensation in 1mm deep mini-gap

Mini/micro-channels enhance filmwise condensation by thinning the liquid film and reducing the thermal resistance in the film for the dominance of surface tension over [60]. Derby et al. [77] found similar condensation heat transfer performance of R134a in 1-mm square, triangular and semi-circular mini-channels. Therefore, to test the effects of aspect ratio on heat transfer and pressure drops in mini-gaps, experiments were conducted in another mini-gap with similar hydraulic diameter but different aspect ratio (AR) investigates the influence of channel shape on steam condensation in presence of nitrogen. This mini-gap had a 3-mm width and 1.5-mm depth to obtain a hydraulic diameter of 2 mm and aspect ratio of 2, which is slightly larger than the hydraulic diameter with the 1-mm depth (i.e. 1.82 mm in hydraulic diameter and 10 in aspect ratio). Experiments at steam mass flux of 75 kg/m^{2}s and nitrogen mass fractions of 0, 10 and 30% test the effect of different aspect ratios. Figure 4.36 compares heat transfer coefficients in these two mini-gaps. Similar heat transfer coefficients were observed at each nitrogen mass fraction for steam qualities between 0.4 and 0.6. The higher aspect ratio provided slightly higher heat transfer coefficients. It is hypothesized that smaller height increases the vapor-liquid superficial velocity and therefore thins the liquid film to reduce thermal resistance in liquid film to enhance heat transfer.

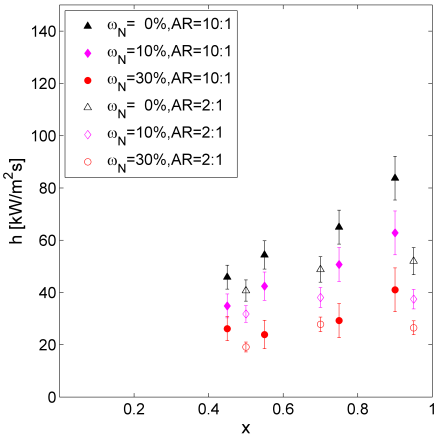

Figure 4.36 Heat transfer coeffcient of steam-nitrogen mixture in mini-gaps of two aspect ratios at steam mass flux of 75 kg/m^{2}s

Figure 4.37 presents pressure drops of steam-nitrogen condensation in mini-gaps of two aspect ratios and similar hydraulic diameters at steam mass fraction of 75 kg/m^{2}s, nitrogen mass fraction of 0, 10 and 30%. Decreasing mini-gap aspect ratio from 10:1 to 2:1 greatly reduces pressure drops in the mini-gap by an order of magnitude. Like the effects on heat transfer coefficients, higher aspect ratio increase the interfacial shear stress. Meanwhile, the high-aspect-ratio mini-gap has larger cross sectional area and therefore higher mass flow rate, which impose more entering and exiting effects as well.

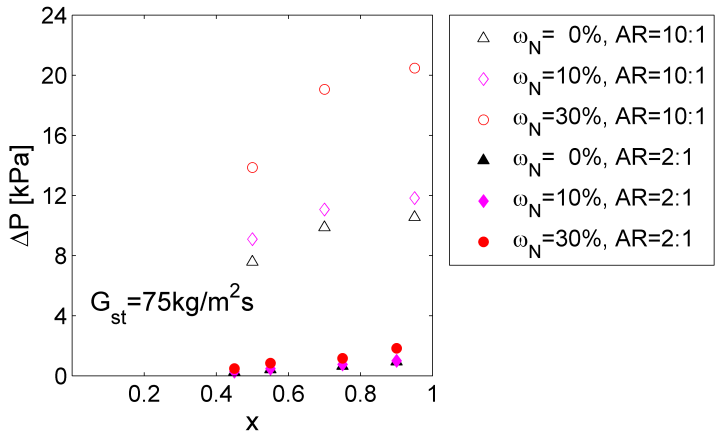

Figure 4.37 Pressure drops in 1mm and 1.5mm deep channesl at steam mass flux of 75 kg/m^{2}s and steam quality range of 0.5 to 0.95.

4.5.3. Steam-nitrogen condensation in hydrophobic mini-gaps

In steam condensation, a hydrophobic mini-gap promoted dropwise condensation in which liquid condensate formed droplets. The periodic sequence of nucleation, growth, coalescence and departure keeps refresh and expose solid surface to vapor. The thermal resistance in liquid condensation was reduced and therefore heat transfer coefficients were enhanced. Steam-nitrogen condensation were performed in Teflon AF™ coated 1-mm deep hydrophobic mini-gap for heat transfer coefficients and pressure drops at the flow conditions tested in the 1-mm deep hydrophilic mini-gap. Figure 4.38 presented steam-nitrogen condensation heat transfer coefficients at three mass fluxes of 35, 50 and 75 kg/m^{2}s. Like in hydrophilic min-gap, heat transfer coefficients increase with increasing steam mass fluxes and steam qualities. Increasing nitrogen mass fraction decreased heat transfer coefficients as well.

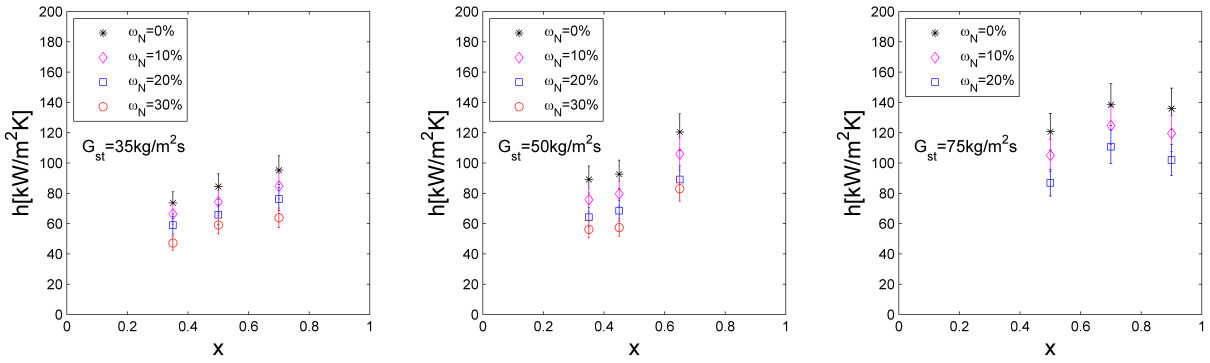

Figure 4.38 Heat transfer coeffcients of steam-nitrogen condensation in hydrophobic mini-gap

As observed in Figure 4.38, steam-nitrogen condensation heat transfer coefficients were influenced by steam mass flux, steam quality, and nitrogen mass fraction. Vapor mass fraction in flow, as used in Figure 4.33, represented steam quality and nitrogen mass fraction. It increases with increasing steam quality and decreasing nitrogen mass fraction. Figure 4.39 presents heat transfer coefficients with respect to vapor mass fraction at three mass fluxes. Heat transfer

coefficients generally increase with increasing vapor mass fraction and increasing steam mass fluxes. In dropwise condensation, heat transfer coefficients are associated with droplet sizes. Increasing steam mass flux significantly increased vapor-liquid interfacial shear stress and thus increased heat transfer coefficient. Increasing nitrogen mass fraction suppressed nucleation as the presence of nitrogen reduces partial pressure of vapor near the condensation surface and decreased heat transfer coefficients.

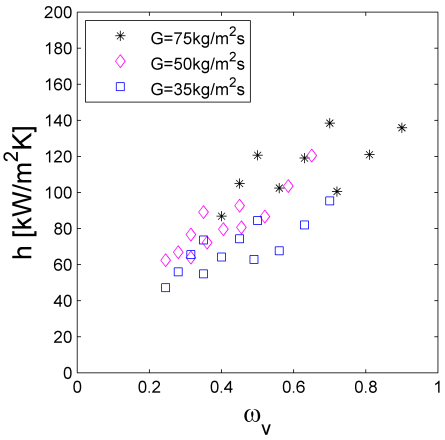

Figure 4.39 Heat transfer coeffcients with respect to vapor mass fraction of steam-nitrogen condensation hydrophobic mini-gaps

Ma et al. [169] proposed that droplet formation and motion perturbates the noncondensable layer between vapor and the condensation surface to enhance condensation heat transfer in presence of noncondensable gases. Figure 4.40 compares steam-nitrogen condensation heat transfer enhancement in hydrophobic mini-gap and hydrophilic mini-gap at same flow conditions using ε, defined as:

$$\varepsilon = \frac{h_{phobic}}{h_{philic}} \qquad 4.55$$

where h_{phobic} and h_{philic} are respectively heat transfer coefficients in hydrophobic and hydrophilic mini-gaps at the same flow condition. The heat transfer coefficients in hydrophobic

mini-gap were 2–5 times higher in hydrophobic channels depending on the steam quality and nitrogen mass fraction. The enhancements decrease with increasing steam quality and nitrogen mass fraction. Increasing steam quality decrease the amount of liquid and the thermal resistance in liquid. Increasing nitrogen mass fraction increase thermal resistance in the nitrogen layer. Although hydrophobic mini-gap promotes dropwise condensation, the cyclic formation and motion of droplets reduces thermal resistance in liquids and perturbs the nitrogen layer, the advantages diminishes when depression of nucleation from nitrogen and convection in vapor dominate the thermal resistance.

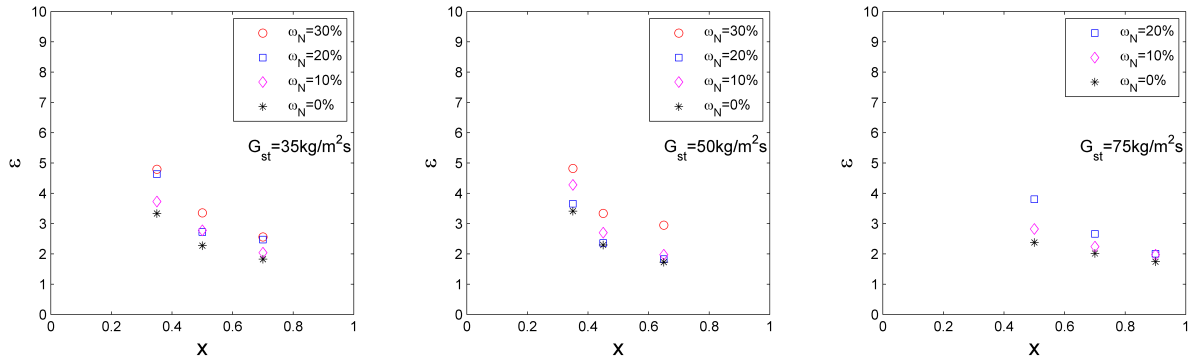

Figure 4.40 Heat transfer coefficient enhancement of steam-nitrogen condensation in hydrophobic mini-gap compared to hydrophilic mini-gap

Experiments investigated the effects of nitrogen mass fraction on pressure drops. With each of three flow mass fluxes, experiments studied the effects of nitrogen mass fractions on pressure drops at various gas fractions (i.e. mass fraction of steam and nitrogen in the flow). There was no significant change in pressure drops with same steam-nitrogen mixture mass fraction and increasing nitrogen mass fraction (Figure 4.41**).** The main contributor to pressure drops was the interfacial shear stress and therefore replacing vapor with the same amount of nitrogen in mass did not change the pressure drop. Increasing mass fluxes and steam quality increases flow velocity,

interfacial shear stress, and therefore the pressure drops. The error bars in Figure 4.41 show the standard deviation of pressure drops during tests.

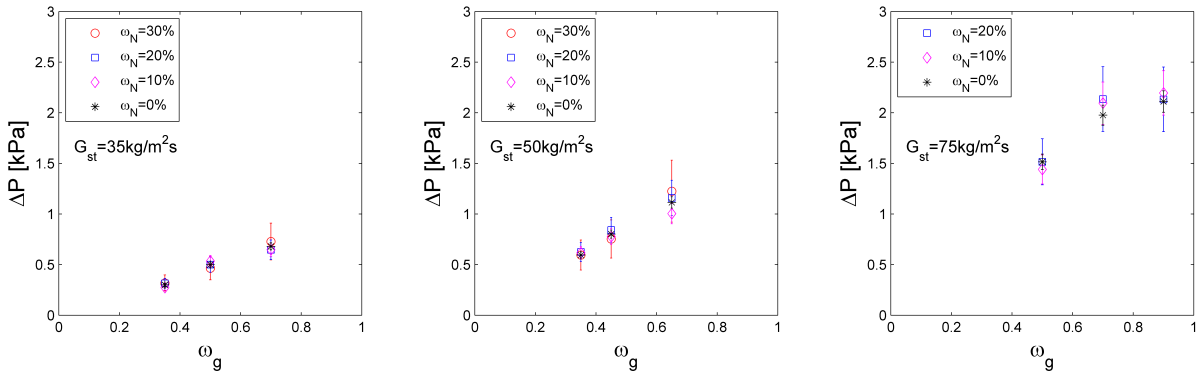

Figure 4.41 Pressure drops of steam-nitrogen condensation in hydrophobic mini-gap

Compared to hydrophilic mini-gap at the same flow conditons, the pressure drops were decreased by about 80% in hydrophobic mini-gap for most cases (Figure 4.42)

$$\eta = \frac{\Delta P_{phobic}}{\Delta P_{philic}} \qquad 4.56$$

where η is the ratio of pressure drop in hydrophobic mini-gap to that in hydrophilic mini-gap at the same flow conditons.

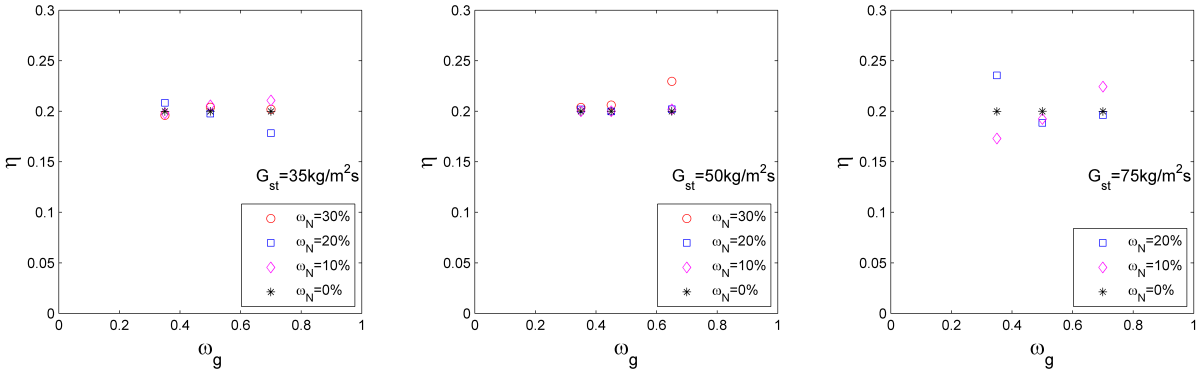

Figure 4.42 Ratio of pressure drops in hydrophobic mini-gap to hydrophili mini-gap

Chapter 5 Conclusions and future work

A research plan was designed and open-loop experimental apparatus was constructed with to measure heat transfer, pressure drops, and visualize steam condensation for a wide range of mass fluxes and qualities with or without the presence of nitrogen. Single-phase cooling experiments validated the systems for heat transfer and pressure drop measurements. Steam condensation were conducted in hydrophilic (contact angle of 70^{o}) and hydrophobic (contact angle of 110^{o}) rectangular mini-gaps of 0.952-mm and 1.818-mm hydraulic diameter.

Filmwise condensation was observed in hydrophilic copper mini-gaps. Comparison of condensation heat transfer coefficients and pressure drops in hydrophilic mini-gap with the Kim and Mudawar [78] correlation presented good agreement. In Teflon-coated hydrophobic mini-gaps, dropwise condensation was observed with periodic nucleation, growth, coalescence and departure of droplets. Droplet departure sizes depended on flow conditions (i.e. mass flux and quality) for the associated interfacial shear forces. Droplet sizes correlated to heat transfer coefficients for they determined the liquid phase thermal resistance. Due to the reduction of thermal resistance in the liquid, dropwise condensation provided 200–350% heat transfer enhancements while reducing pressure drops by 50–80% for less water-solid adhesion induced by the lower surface energy of Teflon.

A correlation for dropwise condensation heat transfer coefficients on hydrophobic surfaces was built through investigation of heat transfer through single droplets and droplet size distributions. Droplet size distributions depended on the droplet departure sizes, which were predicted by analyzing adhesion and shear forces in analytical work and numerical calculations

using FLUENT. Without any curve fitting to the correlation, an overall MAE of 9.6% was obtained.

Filmwise and dropwise condensation of steam-nitrogen flows were observed in hydrophilic and hydrophobic mini-gaps, respectively. Heat transfer coefficients decreased with increasing nitrogen mass fraction. Vapor mass fraction in the liquid-vapor-nitrogen mixture highly correlated to heat transfer coefficients. Periodic formation and motion of droplets perturbed the nitrogen layer between vapor and solid surface. Compared with filmwise condensation in hydrophilic mini-gaps, dropwise condensation increased heat transfer coefficients by 200–500% while pressure drops were reduced by about 80%.

There are some opportunities for future work emerging from this research. For example, experimental data of filmwise and dropwise condensation heat transfer coefficients with four-side-cooling would be beneficial. For four-sided cooling, correlations for the dropwise condensation could incorporate the droplet dynamics on the top surface, which could change the flow regime. More investigation of contact angle hysteresis and droplet-solid adhesion forces during condensation experiments are desired.

Nomenclature

a(r)	fractional area occupied by droplet of radius r
A	area, m^2
C	Chisholm constant, dimensionless
C_d	drag coefficient
Cp	specific heat, kJ/(kgK)
D	diameter, m
D_h	hydraulic diameter, m
F	force, N
F_d	drag forece, N
G	mass flux, kg/(m^2s)
h	heat transfer coefficient, W/(m^2K)
i	specific enthalpy, kJ/kg
i_{lv}	specific evaporation enthalpy, kJ/kg
k	thermal conductivity, W/(mK)
L	length, m
L_c	Laplace number
$\dot{m}$	mass flow rate, kg/s
M	droplet growth rate, kg/s
N_s	Nucleation density, /m^2
Nu	Nusselt number
P	pressure, kPa
Pr	Prandtl number

$\dot{Q}$	heat transfer rate, W
q”	heat flux, W/m^2
R	thermal resistance, m^2k/W
r_e	cutoff size between small and large droplets, m
Re	Reynolds number
S	sweeping period, s
T	temperature, ^oC
t	sweeping period, s
W	width, m
w	uncertainty
We	Webber number
x	quality
y	vertical location, m
z	characteristic length, m

Greek:

α	void fraction
γ	interfacial tension, N/m
δ	thickness, m
ϵ	heat transfer coefficient enhancement ratio
η	pressure drop reducing factor
θ	contact angle, rad
$\boldsymbol{\lambda}$	mass fraction of individual phase in vapor-nitrogen flow
μ	dynamic viscosity, PaS

ν	specific volume, m^3/kg
ρ	density, kg/m^3
σ	surface tension, N/m
Φ	two-phase pressure drop multiplier
ϕ	azimuthal angle, rad
χ	Lockhart-Martinelli parameter
ω	mass fraction of individual phase in steam-nitrogen flow

Subscripts:

adh	adhesion
adv	advancing
rec	receding
bl	block
cond	condensation
cooling	cooling water of precondenser
cu	copper
DWC	dropwise condensation
exp	experimental result
f	fluid
FWC	filmwise condensation
g	temperature gradient
i	inlet
l	liquid
m	steam-nitrogen mixture

o	outlet
philic	hydrophilic
phobic	hydrophobic
pre	precondenser
pred	predicted result
s	surface
sat	saturation
st	steam
sub	subcooling
ts	test section
TP	two phase
w,ins	with insulation
wo,ins	without insulation

References

1. Moran, M.J., H.N. Shapiro, D.D. Boettner, and M.B. Bailey, *Fundamentals of engineering thermodynamics*. 2011.
2. Bustamante, J.G., A.S. Rattner, and S. Garimella, *Achieving near-water-cooled power plant performance with air-cooled condensers.* Applied Thermal Engineering, 2016. **105**: p. 362-371.
3. Beér, J.M., *High efficiency electric power generation: The environmental role.* Progress in Energy and Combustion Science, 2007. **33**(2): p. 107-134.
4. Bacha, H.B., M. Bouzguenda, M. Abid, and A. Maalej, *Modelling and simulation of a water desalination station with solar multiple condensation evaporation cycle technique.* Renewable energy, 1999. **18**(3): p. 349-365.
5. Zhang, F., X. Yang, and C. Wang, *Liquid water removal from a polymer electrolyte fuel cell.* Journal of the Electrochemical Society, 2006. **153**(2): p. A225-A232.
6. Liu, L. and A.M. Jacobi, *The effects of hydrophilicity on water drainage and condensate retention on air-conditioning evaporators.* 2006.
7. Lee, A., M.-W. Moon, H. Lim, W.-D. Kim, and H.-Y. Kim, *Water harvest via dewing.* Langmuir, 2012. **28**(27): p. 10183-10191.
8. Peters, T.B., M. McCarthy, J. Allison, F.A. Dominguez-Espinosa, D. Jenicek, H.A. Kariya, W.L. Staats, J.G. Brisson, J.H. Lang, and E.N. Wang, *Design of an Integrated Loop Heat Pipe Air-Cooled Heat Exchanger for High Performance Electronics.* IEEE Transactions on Components, Packaging and Manufacturing Technology, 2012. **2**(10): p. 1637-1648.
9. EPRI, *Water Use for Electricity Generation and Other Sectors: Recent Changes (1985–2005) and Future Projections (2005–2030)*. 2011.
10. Kenny, J.F., N.L. Barber, S.S. Hutson, K.S. Linsey, J.K. Lovelace, and M.A. Maupin, *Estimated use of water in the United States in 2005*. 2009, US Geological Survey.
11. EPA, *Cooling Water Intakes.* 2014.
12. EPA, *Federal Water Pollution Control Act.* 2002.
13. Shuster, E., *Estimating freshwater needs to meet future thermoelectric generation requirements.* National Energy Technology Laboratory–US Department of Energy, 2008.
14. Kröger, D.G., *Air-cooled heat exchangers and cooling towers*. Vol. 1. 2004: PennWell Books.
15. Zhai, H. and E.S. Rubin, *Performance and cost of wet and dry cooling systems for pulverized coal power plants with and without carbon capture and storage.* Energy Policy, 2010. **38**(10): p. 5653-5660.
16. Derby, M.M., A. Chatterjee, Y. Peles, and M.K. Jensen, *Flow condensation heat transfer enhancement in a mini-channel with hydrophobic and hydrophilic patterns.* International Journal of Heat and Mass Transfer, 2014. **68**: p. 151-160.
17. Kandlikar, S.G. and M.R. King, *Chapter 1 - Introduction*, in *Heat Transfer and Fluid Flow in Minichannels and Microchannels (Second Edition)*. 2014, Butterworth-Heinemann: Oxford. p. 1-9.
18. Taitel, Y. and A. Dukler, *A model for predicting flow regime transitions in horizontal and near horizontal gas-liquid flow.* AIChE Journal, 1976. **22**(1): p. 47-55.
19. Mandhane, J., G. Gregory, and K. Aziz, *A flow pattern map for gas—liquid flow in horizontal pipes.* International Journal of Multiphase Flow, 1974. **1**(4): p. 537-553.

20. Premoli, A., D. DiFrancesco, and A. Prina, *A dimensionless correlation for the determination of the density of two-phase mixtures.* Termotecnica,(Milan), 1971. **25**(1): p. 17-26.
21. Smith, S., *Void fractions in two-phase flow: a correlation based upon an equal velocity head model.* Proceedings of the Institution of Mechanical Engineers, 1969. **184**(1): p. 647-664.
22. Zivi, S., *Estimation of steady-state steam void-fraction by means of the principle of minimum entropy production.* Journal of heat transfer, 1964. **86**(2): p. 247-251.
23. Yashar, D., M. Wilson, H. Kopke, D. Graham, J. Chato, and T. Newell, *An investigation of refrigerant void fraction in horizontal, microfin tubes.* HVAC&R Research, 2001. **7**(1): p. 67-82.
24. El Hajal, J., J.R. Thome, and A. Cavallini, *Condensation in horizontal tubes, part 1: two-phase flow pattern map.* International Journal of Heat and Mass Transfer, 2003. **46**(18): p. 3349-3363.
25. Koyama, S., J. Lee, and R. Yonemoto, *An investigation on void fraction of vapor–liquid two-phase flow for smooth and microfin tubes with R134a at adiabatic condition.* International journal of multiphase flow, 2004. **30**(3): p. 291-310.
26. Lockhart, R. and R. Martinelli, *Proposed correlation of data for isothermal two-phase, two-component flow in pipes.* Chem. Eng. Prog, 1949. **45**(1): p. 39-48.
27. Chisholm, D., *Pressure gradients due to friction during the flow of evaporating two-phase mixtures in smooth tubes and channels.* International Journal of Heat and Mass Transfer, 1973. **16**(2): p. 347-358.
28. Friedel, L. *Improved friction pressure drop correlations for horizontal and vertical two-phase pipe flow*. in *European two-phase flow group meeting, Paper E*. 1979.
29. Hashizume, K., H. Ogiwara, and H. Taniguchi, *Flow pattern, void fraction and pressure drop of refrigerant two-phase flow in a horizontal pipe—II: Analysis of frictional pressure drop.* International journal of multiphase flow, 1985. **11**(5): p. 643-658.
30. Wang, C.-C., C.-S. Chiang, and D.-C. Lu, *Visual observation of two-phase flow pattern of R-22, R-134a, and R-407C in a 6.5-mm smooth tube.* Experimental thermal and fluid science, 1997. **15**(4): p. 395-405.
31. Hurlburt, E.T. and T.A. Newell, *Characteristics of refrigerant film thickness, pressure drop, and condensation heat transfer in annular flow.* HVAC&R Research, 1999. **5**(3): p. 229-248.
32. Chen, Y., K.-S. Yang, Y.-J. Chang, and C.-C. Wang, *Two-phase pressure drop of air–water and R-410A in small horizontal tubes.* International journal of multiphase flow, 2001. **27**(7): p. 1293-1299.
33. Wilson, M., T. Newell, J. Chato, and C.I. Ferreira, *Refrigerant charge, pressure drop, and condensation heat transfer in flattened tubes.* International journal of refrigeration, 2003. **26**(4): p. 442-451.
34. Souza, A., J. Chato, J.P. Wattelet, and B. Christofferson, *Pressure Drop During Two-Phase Flow of Pure Refrigerants and Refrigerant-Oil Mixtures in Horizontal Smooth Tubes, Proceedings of the 19 th National Heat Transfer Conference, Heat Transfer with Alternate Refrigerants, Atlanta, GA, August 8-11, 1993.* ASME Papers, 1993: p. 35-41.
35. Cavallini, A., G. Censi, D. Del Col, L. Doretti, G. Longo, and L. Rossetto, *Experimental investigation on condensation heat transfer and pressure drop of new HFC refrigerants*

(R134a, R125, R32, R410A, R236ea) in a horizontal smooth tube. International Journal of Refrigeration, 2001. **24**(1): p. 73-87.
36. Cavallini, A., G. Censi, D. Del Col, L. Doretti, G.A. Longo, and L. Rossetto, *Condensation of halogenated refrigerants inside smooth tubes.* HVAC&R Research, 2002. **8**(4): p. 429-451.
37. Cavallini, A., G. Censi, D. Del Col, L. Doretti, G. Longo, and L. Rossetto, *A tube-in-tube water/zeotropic mixture condenser: design procedure against experimental data.* Experimental thermal and fluid science, 2002. **25**(7): p. 495-501.
38. Fukano, T., A. Kariyasaki, and M. Kagawa. *Flow patterns and pressure drop in isothermal gas-liquid concurrent flow in a horizontal capillary tube*. in *ANS Proceedings of the National Heat Transfer Conference*. 1989.
39. Mishima, K. and T. Hibiki, *Some characteristics of air-water two-phase flow in small diameter vertical tubes.* International journal of multiphase flow, 1996. **22**(4): p. 703-712.
40. Triplett, K., S. Ghiaasiaan, S. Abdel-Khalik, A. LeMouel, and B. McCord, *Gas–liquid two-phase flow in microchannels: part II: void fraction and pressure drop.* International Journal of Multiphase Flow, 1999. **25**(3): p. 395-410.
41. Tran, T., M.-C. Chyu, M. Wambsganss, and D. France, *Two-phase pressure drop of refrigerants during flow boiling in small channels: an experimental investigation and correlation development.* International Journal of Multiphase Flow, 2000. **26**(11): p. 1739-1754.
42. Zhao, T. and Q. Bi, *Pressure drop characteristics of gas–liquid two-phase flow in vertical miniature triangular channels.* International journal of heat and mass transfer, 2001. **44**(13): p. 2523-2534.
43. Lee, H.J. and S.Y. Lee, *Pressure drop correlations for two-phase flow within horizontal rectangular channels with small heights.* International Journal of Multiphase Flow, 2001. **27**(5): p. 783-796.
44. Yang, C. and R. Webb, *Friction pressure drop of R-12 in small hydraulic diameter extruded aluminum tubes with and without micro-fins.* International Journal of Heat and Mass Transfer, 1996. **39**(4): p. 801-809.
45. Yan, Y.-Y. and T.-F. Lin, *Condensation heat transfer and pressure drop of refrigerant R-134a in a small pipe.* International Journal of Heat and Mass Transfer, 1999. **42**(4): p. 697-708.
46. Zhang, M. and R.L. Webb, *Correlation of two-phase friction for refrigerants in small-diameter tubes.* Experimental Thermal and Fluid Science, 2001. **25**(3): p. 131-139.
47. Garimella, S., J. Killion, and J. Coleman, *An experimentally validated model for two-phase pressure drop in the intermittent flow regime for circular microchannels.* Transactions-American Society of Mechanical Engineers Journal of Heat Transfer, 2002. **124**(1): p. 205-214.
48. Coleman, J.W. and S. Garimella, *Two-phase flow regimes in round, square and rectangular tubes during condensation of refrigerant R134a.* International Journal of Refrigeration, 2003. **26**(1): p. 117-128.
49. Garimella, S., A. Agarwal, and J.W. Coleman. *Two-phase pressure drops in the annular flow regime in circular microchannels*. in *21st IIR International Congress of Refrigeration*. 2003. International Institute of Refrigeration.
50. Kandlikar, S., S. Garimella, D. Li, S. Colin, and M.R. King, *Heat transfer and fluid flow in minichannels and microchannels*. 2005: elsevier.

51. Yang, C. and R. Webb, *Condensation of R-12 in small hydraulic diameter extruded aluminum tubes with and without micro-fins.* International Journal of Heat and Mass Transfer, 1996. **39**(4): p. 791-800.
52. Akers, W. and H. Rosson. *Condensation inside a horizontal tube*. in *Chemical Engineering Progress Symposium Series*. 1960.
53. Moser, K., R. Webb, and B. NA, *A new equivalent Reynolds number model for condensation in smooth tubes.* Journal of heat transfer, 1998. **120**(2): p. 410-417.
54. Dobson, M. and J. Chato, *Condensation in smooth horizontal tubes.* Urbana, 1998. **51**: p. 61801.
55. Traviss, D., W. Rohsenow, and A. Baron, *Forced-convection condensation inside tubes: a heat transfer equation for condenser design.* ASHRAE Trans, 1973. **79**(1): p. 157-165.
56. Shah, M.M., *An improved and extended general correlation for heat transfer during condensation in plain tubes.* Hvac&R Research, 2009. **15**(5): p. 889-913.
57. Jaster, H. and P. Kosky, *Condensation heat transfer in a mixed flow regime.* International Journal of Heat and Mass Transfer, 1976. **19**(1): p. 95-99.
58. Garimella, S., *Chapter 6 - Condensation in Minichannels and Microchannels*, in *Heat Transfer and Fluid Flow in Minichannels and Microchannels (Second Edition)*. 2014, Butterworth-Heinemann: Oxford. p. 295-494.
59. Lee, K.-Y. and M.H. Kim, *Experimental and empirical study of steam condensation heat transfer with a noncondensable gas in a small-diameter vertical tube.* Nuclear Engineering and Design, 2008. **238**(1): p. 207-216.
60. Kandlikar, S.G. *Microchannels and minichannels: history, terminology, classification and current research needs*. in *ASME 2003 1st International Conference on Microchannels and Minichannels*. 2003. American Society of Mechanical Engineers.
61. Serizawa, A., Z. Feng, and Z. Kawara, *Two-phase flow in microchannels.* Experimental Thermal and Fluid Science, 2002. **26**(6): p. 703-714.
62. Fukano, T. and A. Kariyasaki, *Characteristics of gas-liquid two-phase flow in a capillary tube.* Nuclear Engineering and Design, 1993. **141**(1-2): p. 59-68.
63. Nusselt, W., *Die Oberflachenkondesation des Wasserdamffes the surface condensation of water.* Zetrschr. Ver. Deutch. Ing., 1916. **60**: p. 541-546.
64. Chato, J.C., *Laminar condensation inside horizontal and inclined tubes*. 1960, Massachusetts Institute of Technology.
65. Rufer, C. and S. Kezios, *Analysis of two-phase, one-component stratified flow with condensation.* Journal of heat Transfer, 1966. **88**(3): p. 265-272.
66. Rosson, H. and J. Meyers. *Point values of condensing film coefficients inside a horizontal tube*. in *Chemical Engineering Progress Symposium Series*. 1965.
67. Hughmark, G., *Holdup and heat transfer in horizontal slug gas-liquid flow.* Chemical Engineering Science, 1965. **20**(12): p. 1007-1010.
68. Chen, I. and G. Kocamustafaogullari, *Condensation heat transfer studies for stratified, cocurrent two-phase flow in horizontal tubes.* International journal of heat and mass transfer, 1987. **30**(6): p. 1133-1148.
69. Shin, J.S. and M.H. Kim, *An experimental study of flow condensation heat transfer inside circular and rectangular mini-channels.* Heat transfer engineering, 2005. **26**(3): p. 36-44.
70. Agarwal, A. and S. Garimella, *Representative Results for Condensation Measurements at Hydraulic Diameters ~100 Microns.* Journal of Heat Transfer, 2010. **132**(4): p. 041010-041010-12.

71. Fang, C., J.E. Steinbrenner, F.-M. Wang, and K.E. Goodson, *Impact of wall hydrophobicity on condensation flow and heat transfer in silicon microchannels.* Journal of Micromechanics and Microengineering, 2010. **20**(4): p. 045018.
72. Matkovic, M., A. Cavallini, D. Del Col, and L. Rossetto, *Experimental study on condensation heat transfer inside a single circular minichannel.* International Journal of Heat and Mass Transfer, 2009. **52**(9–10): p. 2311-2323.
73. Yang, C.-Y. and R. Webb, *A predictive model for condensation in small hydraulic diameter tubes having axial micro-fins.* Journal of heat transfer, 1997. **119**(4): p. 776-782.
74. Kim, N.-H., J.-P. Cho, J.-O. Kim, and B. Youn, *Condensation heat transfer of R-22 and R-410A in flat aluminum multi-channel tubes with or without micro-fins.* International Journal of Refrigeration, 2003. **26**(7): p. 830-839.
75. Wang, W.W., T.D. Radcliff, and R.N. Christensen, *A condensation heat transfer correlation for millimeter-scale tubing with flow regime transition.* Experimental Thermal and Fluid Science, 2002. **26**(5): p. 473-485.
76. Garimella, S. and T. Bandhauer, *Measurement of condensation heat transfer coefficients in microchannel tubes.* ASME-PUBLICATIONS-HTD, 2001. **369**: p. 243-250.
77. Derby, M., H.J. Lee, Y. Peles, and M.K. Jensen, *Condensation heat transfer in square, triangular, and semi-circular mini-channels.* International Journal of Heat and Mass Transfer, 2012. **55**(1): p. 187-197.
78. Kim, S.-M. and I. Mudawar, *Universal approach to predicting heat transfer coefficient for condensing mini/micro-channel flow.* International Journal of Heat and Mass Transfer, 2013. **56**(1): p. 238-250.
79. Chen, X. and M.M. Derby, *Combined visualization and heat transfer measurements for steam flow condensation in hydrophilic and hydrophobic mini-gaps.* Journal of Heat Transfer, 2016. **138**(9): p. 091503.
80. Wang, H. and J.W. Rose. *Film condensation in horizontal triangular section microchannels: A theoretical model*. in *ASME 2004 2nd International Conference on Microchannels and Minichannels*. 2004. American Society of Mechanical Engineers.
81. Wang, H., J. Rose, and H. Honda, *A theoretical model of film condensation in square section horizontal microchannels.* Chemical Engineering Research and Design, 2004. **82**(4): p. 430-434.
82. Wang, H.S. and J.W. Rose, *A theory of film condensation in horizontal noncircular section microchannels.* Journal of Heat Transfer, 2005. **127**(10): p. 1096-1105.
83. Koyama, S., K. Kuwahara, and K. Nakashita. *Condensation of refrigerant in a multi-port channel*. in *ASME 2003 1st International Conference on Microchannels and Minichannels*. 2003. American Society of Mechanical Engineers.
84. Cavallini, A., L. Doretti, M. Matkovic, and L. Rossetto, *Update on condensation heat transfer and pressure drop inside minichannels.* Heat Transfer Engineering, 2006. **27**(4): p. 74-87.
85. Cavallini, A., D. Del Col, L. Doretti, M. Matkovic, L. Rossetto, and C. Zilio, *Two-phase frictional pressure gradient of R236ea, R134a and R410A inside multi-port mini-channels.* Experimental Thermal and Fluid Science, 2005. **29**(7): p. 861-870.
86. Kosky, P., *Thin liquid films under simultaneous shear and gravity forces.* International Journal of Heat and Mass Transfer, 1971. **14**(8): p. 1220-1224.

87. Zhao, T. and Q. Liao, *Theoretical analysis of film condensation heat transfer inside vertical mini triangular channels.* International journal of heat and mass transfer, 2002. **45**(13): p. 2829-2842.
88. Kim, S.-M. and I. Mudawar, *Universal approach to predicting two-phase frictional pressure drop for adiabatic and condensing mini/micro-channel flows.* International Journal of Heat and Mass Transfer, 2012. **55**(11–12): p. 3246-3261.
89. McAdams, W., W. Woods, and L. Heroman, *Vaporization inside horizontal tubes-II-benzene-oil mixtures.* Trans. ASME, 1942. **64**(3): p. 193-200.
90. Akers, W., H. Deans, and O. Crosser, *Condensing heat transfer within horizontal tubes.* Chem. Eng. Progr., 1959. **55**.
91. Cicchitti, A., C. Lombardi, M. Silvestri, G. Soldaini, and R. Zavattarelli, *Two-phase cooling experiments: pressure drop, heat transfer and burnout measurements*. 1959, Centro Informazioni Studi Esperienze, Milan.
92. Owens, W., *Two-phase pressure gradient.* International Development in Heat Transfer, 1961: p. 363-368.
93. Dukler, A., M. Wicks, and R. Cleveland, *Frictional pressure drop in two-phase flow: A. A comparison of existing correlations for pressure loss and holdup.* AIChE Journal, 1964. **10**(1): p. 38-43.
94. Beattie, D. and P. Whalley, *A simple two-phase frictional pressure drop calculation method.* International Journal of Multiphase Flow, 1982. **8**(1): p. 83-87.
95. Lin, S., C. Kwok, R.-Y. Li, Z.-H. Chen, and Z.-Y. Chen, *Local frictional pressure drop during vaporization of R-12 through capillary tubes.* International Journal of Multiphase Flow, 1991. **17**(1): p. 95-102.
96. Chisholm, D., *A theoretical basis for the Lockhart-Martinelli correlation for two-phase flow.* International Journal of Heat and Mass Transfer, 1967. **10**(12): p. 1767-1778.
97. Thome, J., A. Bar-Cohen, R. Revellin, and I. Zun, *Unified mechanistic multiscale mapping of two-phase flow patterns in microchannels.* Experimental Thermal and Fluid Science, 2013. **44**: p. 1-22.
98. Hinde, D.K., *Condensation of refrigerants 12 and 134a in horizontal tubes with and without oil*. 1992, Air Conditioning and Refrigeration Center. College of Engineering. University of Illinois at Urbana-Champaign.
99. Coleman, J.W., *Flow visualization and pressure drop for refrigerant phase change and air-water flow in small hydraulic diameter geometries.* 2000.
100. Shin, J., *A study of flow condensation heat transfer inside mini-channels with new experimental techniques.* Pohang University of Science and Technology, Korea (Ph. D. Dissertation), 2004.
101. Mitra, B., *Supercritical gas cooling and condensation of refrigerant R410A at near-critical pressures*. 2005, Georgia Institute of Technology.
102. Andresen, U.C., *Supercritical gas cooling and near-critical-pressure condensation of refrigerant blends in microchannels*. 2006, Georgia Institute of Technology.
103. Quan, X., P. Cheng, and H. Wu, *An experimental investigation on pressure drop of steam condensing in silicon microchannels.* International Journal of Heat and Mass Transfer, 2008. **51**(21): p. 5454-5458.
104. Maråk, K.A., *Condensation heat transfer and pressure drop for methane and binary methane fluids in small channels.* 2009.

105. Huang, X., G. Ding, H. Hu, Y. Zhu, Y. Gao, and B. Deng, *Two-phase frictional pressure drop characteristics of R410A-oil mixture flow condensation inside 4.18 mm and 1.6 mm ID horizontal smooth tubes.* HVAC&R Research, 2010. **16**(4): p. 453-470.
106. Dutkowski, K., *Two-phase pressure drop of air–water in minichannels.* International Journal of Heat and Mass Transfer, 2009. **52**(21): p. 5185-5192.
107. Choi, C., D. Yu, and M. Kim, *Adiabatic two-phase flow in rectangular microchannels with different aspect ratios: Part I–Flow pattern, pressure drop and void fraction.* International Journal of Heat and Mass Transfer, 2011. **54**(1): p. 616-624.
108. Rose, J., *Dropwise condensation theory and experiment: a review.* Proceedings of the Institution of Mechanical Engineers, Part A: Journal of Power and Energy, 2002. **216**(2): p. 115-128.
109. Schmidt, E., W. Schurig, and W. Sellschopp, *Versuche über die Kondensation von Wasserdampf in Film-und Tropfenform.* Technische Mechanik und Thermodynamik, 1930. **1**(2): p. 53-63.
110. Le Fevre, E. and J. Rose, *An experimental study of heat transfer by dropwise condensation.* International Journal of Heat and Mass Transfer, 1965. **8**(8): p. 1117-1133.
111. Abu-Orabi, M., *Modeling of heat transfer in dropwise condensation.* International journal of heat and mass transfer, 1998. **41**(1): p. 81-87.
112. Kim, S. and K.J. Kim, *Dropwise condensation modeling suitable for superhydrophobic surfaces.* Journal of heat transfer, 2011. **133**(8): p. 081502.
113. Lee, S., K. Cheng, V. Palmre, M.M.H. Bhuiya, K.J. Kim, B.J. Zhang, and H. Yoon, *Heat transfer measurement during dropwise condensation using micro/nano-scale porous surface.* International Journal of Heat and Mass Transfer, 2013. **65**: p. 619-626.
114. Peng, B., X. Ma, Z. Lan, W. Xu, and R. Wen, *Analysis of condensation heat transfer enhancement with dropwise-filmwise hybrid surface: Droplet sizes effect.* International Journal of Heat and Mass Transfer, 2014. **77**: p. 785-794.
115. Tanasawa, I., Y. Funawatashi, and J. Ochiai. *Experimental study on dropwise condensation-effect of maximum drop size upon the heat transfer coefficient*. in *Sixth International Heat Transfer Conference, 7-11 Aug. 1978*. 1978. Washington, DC, USA: Hemisphere Publishing Corp.
116. Tanner, D., C. Potter, D. Pope, and D. West, *Heat transfer in dropwise condensation—Part I The effects of heat flux, steam velocity and non-condensable gas concentration.* International Journal of Heat and Mass Transfer, 1965. **8**(3): p. 419IN5421-420426.
117. Hatamiya, S. and H. Tanaka, *Study on the mechanism of dropwise condensation(1st report, measurement of heat transfer coefficient of steam at low pressure).* Transactions of the Japan Society of Mechanical Engineers, 1986. **52**(476): p. 1828-1834.
118. Neumann, A., A. Abdelmessih, and A. Hameed, *The role of contact angles and contact angle hysteresis in dropwise condensation heat transfer.* International Journal of Heat and Mass Transfer, 1978. **21**(7): p. 947-953.
119. Ma, X., X.-F. Chen, T. Bai, and J.-B. Chen, *A new mechanism for condensation heat transfer enhancement: effect of the surface free energy difference of condensate and solid surface.* Journal of Enhanced Heat Transfer, 2004. **11**(4).
120. Holden, K., A. Wanniarachchi, P. Marto, D. Boone, and J. Rose, *The use of organic coatings to promote dropwise condensation of steam.* Journal of heat transfer, 1987. **109**(3): p. 768-774.

121. Haraguchi, T., R. Shimada, S. Kumagai, and T. Takeyama, *The effect of polyvinylidene chloride coating thickness on promotion of dropwise steam condensation.* International journal of heat and mass transfer, 1991. **34**(12): p. 3047-3054.
122. Koch, G., D. Zhang, and A. Leipertz, *Condensation of steam on the surface of hard coated copper discs.* Heat and mass transfer, 1997. **32**(3): p. 149-156.
123. Ma, X., J. Chen, D. Xu, J. Lin, C. Ren, and Z. Long, *Influence of processing conditions of polymer film on dropwise condensation heat transfer.* International Journal of Heat and Mass Transfer, 2002. **45**(16): p. 3405-3411.
124. Ma, X., B. Wang, D. Xu, and J. Lin, *Lifetime test of dropwise condensation on polymer-coated surfaces.* Heat Transfer—Asian Research, 1999. **28**(7): p. 551-558.
125. Ma, X., B. Tao, J. Chen, D. Xu, and J. Lin, *Dropwise condensation heat transfer of steam on a polytethefluoroethylene film.* Journal of Thermal Science, 2001. **10**(3): p. 247.
126. Zhang, B.J., C. Kuok, K.J. Kim, T. Hwang, and H. Yoon, *Dropwise steam condensation on various hydrophobic surfaces: Polyphenylene sulfide (PPS), polytetrafluoroethylene (PTFE), and self-assembled micro/nano silver (SAMS).* International Journal of Heat and Mass Transfer, 2015. **89**: p. 353-358.
127. Das, A., H. Kilty, P. Marto, G. Andeen, and A. Kumar, *The use of an organic self-assembled monolayer coating to promote dropwise condensation of steam on horizontal tubes.* Journal of heat transfer, 2000. **122**(2): p. 278-286.
128. Vemuri, S., K. Kim, B. Wood, S. Govindaraju, and T. Bell, *Long term testing for dropwise condensation using self-assembled monolayer coatings of n-octadecyl mercaptan.* Applied thermal engineering, 2006. **26**(4): p. 421-429.
129. Pang, G., J.D. Dale, and D.Y. Kwok, *An integrated study of dropwise condensation heat transfer on self-assembled organic surfaces through Fourier transform infra-red spectroscopy and ellipsometry.* International Journal of Heat and Mass Transfer, 2005. **48**(2): p. 307-316.
130. Chen, L., S. Liang, R. Yan, Y. Cheng, X. Huai, and S. Chen, *n-Octadecanethiol self-assembled monolayer coating with microscopic roughness for dropwise condensation of steam.* Journal of Thermal Science, 2009. **18**(2): p. 160-165.
131. Bonner, R.W. *Dropwise condensation life testing of self assembled monolayers*. in *2010 14th International Heat Transfer Conference*. 2010. American Society of Mechanical Engineers.
132. Yang, Q. and A. Gu, *Dropwise condensation on SAM and electroless composite coating surfaces.* Journal of chemical engineering of Japan, 2006. **39**(8): p. 826-830.
133. Rausch, M., A. Fröba, and A. Leipertz, *Dropwise condensation heat transfer on ion implanted aluminum surfaces.* International Journal of heat and Mass transfer, 2008. **51**(5): p. 1061-1070.
134. Rausch, M., A. Leipertz, and A. Fröba, *Dropwise condensation of steam on ion implanted titanium surfaces.* International Journal of Heat and Mass Transfer, 2010. **53**(1): p. 423-430.
135. Zhao, Q. and B. Burnside, *Dropwise condensation of steam on ion implanted condenser surfaces.* Heat Recovery Systems and CHP, 1994. **14**(5): p. 525-534.
136. Leipertz, A. and K.-H. Choi, *Selected adjustment of dropwise condensation on ion implanted surfaces*. 2002, Google Patents.
137. Cheng, L. and T. Chen, *Heat transfer and flow friction characteristics of a compact plate-type condenser.* ASME HEAT TRANSFER DIV PUBL HTD, 1998. **361**: p. 489-496.

138. Lan, Z., X. Ma, S. Wang, M. Wang, and X. Li, *Effects of surface free energy and nanostructures on dropwise condensation.* Chemical Engineering Journal, 2010. **156**(3): p. 546-552.
139. Izumi, M., S. Kumagai, R. Shimada, and N. Yamakawa, *Heat transfer enhancement of dropwise condensation on a vertical surface with round shaped grooves.* Experimental Thermal and Fluid Science, 2004. **28**(2-3): p. 243-248.
140. Mahapatra, P.S., A. Ghosh, R. Ganguly, and C.M. Megaridis, *Key design and operating parameters for enhancing dropwise condensation through wettability patterning.* International Journal of Heat and Mass Transfer, 2016. **92**: p. 877-883.
141. Peng, B., X. Ma, Z. Lan, W. Xu, and R. Wen, *Experimental investigation on steam condensation heat transfer enhancement with vertically patterned hydrophobic–hydrophilic hybrid surfaces.* International Journal of Heat and Mass Transfer, 2015. **83**: p. 27-38.
142. Lee, Y.-A., L.-S. Kuo, T.-W. Su, C.-C. Hsu, and P.-H. Chen, *Orientation effects of nanoparticle-modified surfaces with interlaced wettability on condensation heat transfer.* Applied Thermal Engineering, 2016. **98**: p. 1054-1060.
143. Li, X. and P. Cheng, *Lattice Boltzmann simulations for transition from dropwise to filmwise condensation on hydrophobic surfaces with hydrophilic spots.* International Journal of Heat and Mass Transfer, 2017. **110**: p. 710-722.
144. Patankar, N.A., *On the modeling of hydrophobic contact angles on rough surfaces.* Langmuir, 2003. **19**(4): p. 1249-1253.
145. Wenzel, R.N., *Surface Roughness and Contact Angle.* The Journal of Physical Chemistry, 1949. **53**(9): p. 1466-1467.
146. Cassie, A., *Contact angles.* Discussions of the Faraday Society, 1948. **3**: p. 11-16.
147. Dietz, C., K. Rykaczewski, A. Fedorov, and Y. Joshi, *Visualization of droplet departure on a superhydrophobic surface and implications to heat transfer enhancement during dropwise condensation.* Applied physics letters, 2010. **97**(3): p. 033104.
148. Le Fevre, E. and J. Rose. *A theory of heat transfer by dropwise condensation*. in *Chemical Engineering Progress*. 1966. AMER INST CHEMICAL ENGINEERS 345 E 47TH ST, NEW YORK, NY 10017.
149. Graham, C. and P. Griffith, *Drop size distributions and heat transfer in dropwise condensation.* International Journal of Heat and Mass Transfer, 1973. **16**(2): p. 337-346.
150. Tanaka, H., *A theoretical study of dropwise condensation.* ASME J. Heat Transfer, 1975. **97**(1): p. 72-78.
151. Wu, W.H. and J.R.M. Maa, *On the heat transfer in dropwise condensation.* The chemical engineering journal, 1976. **12**(3): p. 225-231.
152. Maa, J.R., *Drop size distribution and heat flux of dropwise condensation.* The Chemical Engineering Journal, 1978. **16**(3): p. 171-176.
153. Semiat, R. and Y. Galperin, *Effect of non-condensable gases on heat transfer in the tower MED seawater desalination plant.* Desalination, 2001. **140**(1): p. 27-46.
154. Othmer, D.F., *The condensation of steam*. 1929: University of Michigan.
155. Lee, W. and J. Rose, *Forced convection film condensation on a horizontal tube with and without non-condensing gases.* International journal of heat and mass transfer, 1984. **27**(4): p. 519-528.

156. Wu, T. and K. Vierow, *Local heat transfer measurements of steam/air mixtures in horizontal condenser tubes.* International journal of heat and mass transfer, 2006. **49**(15): p. 2491-2501.
157. Chantana, C. and S. Kumar, *Experimental and theoretical investigation of air-steam condensation in a vertical tube at low inlet steam fractions.* Applied Thermal Engineering, 2013. **54**(2): p. 399-412.
158. Siddique, M., M.W. Golay, and M.S. Kazimi, *Local heat transfer coefficients for forced-convection condensation of steam in a vertical tube in the presence of a noncondensable gas.* Nuclear technology, 1993. **102**(3): p. 386-402.
159. Kuhn, S.-Z., *Investigation of heat transfer from condensing steam-gas mixtures and turbulent films flowing downward inside a vertical tube*. 1995, University of California, Berkeley.
160. AKAKI, H., Y. Kataoka, and M. Murase, *Measurement of condensation heat transfer coefficient inside a vertical tube in the presence of noncondensable gas.* Journal of nuclear science and technology, 1995. **32**(6): p. 517-526.
161. Park, H.S. and H.C. No, *A condensation experiment in the presence of noncondensables in a vertical tube of a passive containment cooling system and its assessment with RELAP5/MOD3. 2.* Nuclear Technology, 1999. **127**(2): p. 160-169.
162. Kim, S.J., *Turbulent film condensation of high pressure steam in a vertical tube of passive secondary condensation system.* 2000.
163. Al-Shammari, S., D. Webb, and P. Heggs, *Condensation of steam with and without the presence of non-condensable gases in a vertical tube.* Desalination, 2004. **169**(2): p. 151-160.
164. Oh, S. and S.T. Revankar, *Effect of noncondensable gas in a vertical tube condenser.* Nuclear engineering and design, 2005. **235**(16): p. 1699-1712.
165. Zhu, A., S. Wang, J. Sun, L. Xie, and Z. Wang, *Effects of high fractional noncondensable gas on condensation in the dewvaporation desalination process.* Desalination, 2007. **214**(1-3): p. 128-137.
166. Park, H.-S., N.-H. Choi, S.-K. Chang, C.-H. Chung, S.-J. Yi, C.-K. Park, and M.-K. Chung, *Experimental study on a two-phase critical flow with a non-condensable gas at high pressure conditions.* International Journal of Multiphase Flow, 2007. **33**(11): p. 1222-1236.
167. Su, J., Z. Sun, G. Fan, and M. Ding, *Experimental study of the effect of non-condensable gases on steam condensation over a vertical tube external surface.* Nuclear Engineering and Design, 2013. **262**: p. 201-208.
168. Caruso, G. and D.V. Di Maio, *Heat and mass transfer analogy applied to condensation in the presence of noncondensable gases inside inclined tubes.* International journal of heat and mass transfer, 2014. **68**: p. 401-414.
169. Ma, X., W. Rongfu, Z. Lan, and X. Zhou, *Visual and Numerical Study for Dropwise Condensation Heat Transfer Mechanism of Steam-Air Mixture Vapor.* 2014(46552): p. V08AT10A054.
170. Sparrow, E.M., W.J. Minkowycz, and M. Saddy, *Forced convection condensation in the presence of noncondensables and interfacial resistance.* International Journal of Heat and Mass Transfer, 1967. **10**(12): p. 1829-1845.
171. Minkowycz, W.J. and E.M. Sparrow, *Condensation heat transfer in the presence of noncondensables, interfacial resistance, superheating, variable properties, and diffusion.* International Journal of Heat and Mass Transfer, 1966. **9**(10): p. 1125-1144.

172. Sparrow, E.M. and S.H. Lin, *Condensation Heat Transfer in the Presence of a Noncondensable Gas.* Journal of Heat Transfer, 1964. **86**(3): p. 430-436.
173. Sparrow, E.M. and E.R.G. Eckert, *Effects of superheated vapor and noncondensable gases on laminar film condensation.* AIChE Journal, 1961. **7**(3): p. 473-477.
174. Tang, G., H. Hu, Z. Zhuang, and W. Tao, *Film condensation heat transfer on a horizontal tube in presence of a noncondensable gas.* Applied thermal engineering, 2012. **36**: p. 414-425.
175. Rose, J., *Condensation of a vapour in the presence of a non-condensing gas.* International Journal of Heat and Mass Transfer, 1969. **12**(2): p. 233-237.
176. Rose, J., *Approximate equations for forced-convection condensation in the presence of a non-condensing gas on a flat plate and horizontal tube.* International Journal of Heat and Mass Transfer, 1980. **23**(4): p. 539-546.
177. Colburn, A.P. and O.A. Hougen, *Studies in Heat Transmission1I—Measurement of Fluid and Surface Temperatures.* Industrial & Engineering Chemistry, 1930. **22**(5): p. 522-524.
178. Peterson, P., V. Schrock, and T. Kageyama, *Diffusion layer theory for turbulent vapor condensation with noncondensable gases.* TRANSACTIONS-AMERICAN SOCIETY OF MECHANICAL ENGINEERS JOURNAL OF HEAT TRANSFER, 1993. **115**: p. 998-998.
179. Vierow, K. and V. Schrock. *Condensation in a natural circulation loop with noncondensable gases, 1*. in *Proceedings of the international conference on multiphase flows' 91-Tsukuba*. 1991.
180. Kuhn, S., V. Schrock, and P. Peterson, *An investigation of condensation from steam–gas mixtures flowing downward inside a vertical tube.* Nuclear Engineering and Design, 1997. **177**(1): p. 53-69.
181. Kedzierski, M. and J. Worthington III, *Design and machining of copper specimens with micro holes for accurate heat transfer measurements.* EXPERIMENTAL HEAT TRANSFER An International Journal, 1993. **6**(4): p. 329-344.
182. Kline, S. and F. McClintock, *Estimating the unertainty in single-sample experiments Mech.* Engng, 1953. **75**: p. 3-8.
183. Kim, S.M. and I. Mudawar, *Universal approach to predicting heat transfer coefficient for condensing mini/micro-channel flow.* International Journal of Heat and Mass Transfer, 2013. **56**(1-2): p. 238-250.
184. Wang, H.S., John W. Rose, *Film condensation in microchannels: effect of tube inclination.* Proceedings of the Fourth International Conference on Nanochannels, Microchannels and Minichannels, 2006: p. 133-137.
185. Wang, H.S. and J.W. Rose, *A theory of film condensation in horizontal noncircular section microchannels.* Journal of Heat Transfer, 2005. **127**(10): p. 1096.
186. Agarwal, A., T.M. Bandhauer, and S. Garimella, *Heat transfer model for condensation in non-circular microchannels*, in *Proceedings of the Fifth International Conference on Nanochannels, Microchannels and Minichannels*. 2007: Puebla, Mexico. p. 117-126.
187. Derby, M.M., H.J. Lee, Y. Peles, and M.K. Jensen, *Condensation heat transfer in square, triangular, and semi-circular mini-channels.* International Journal of Heat and Mass Transfer, 2012. **55**(1-3): p. 187-197.
188. Marto, P., D. Looney, J. Rose, and A. Wanniarachchi, *Evaluation of organic coatings for the promotion of dropwise condensation of steam.* International journal of heat and mass transfer, 1986. **29**(8): p. 1109-1117.

189. Rose, J., *Condensation heat transfer fundamentals.* Chemical Engineering Research and Design, 1998. **76**(2): p. 143-152.
190. Rose, J., *Dropwise condensation theory.* International Journal of Heat and Mass Transfer, 1981. **24**(2): p. 191-194.
191. Butterworth, D., *A comparison of some void-fraction relationships for co-current gas-liquid flow.* International Journal of Multiphase Flow, 1975. **1**(6): p. 845-850.
192. Soliman, H., *On the annular-to-wavy flow pattern transition during condensation inside horizontal tubes.* The Canadian Journal of Chemical Engineering, 1982. **60**(4): p. 475-481.
193. Bonner, R.W., *Correlation for dropwise condensation heat transfer: Water, organic fluids, and inclination.* International Journal of Heat and Mass Transfer, 2013. **61**: p. 245-253.
194. Carey, V.P., *Liquid-vapor phase-change phenomena.* 1992.
195. Leach, R., F. Stevens, S. Langford, and J. Dickinson, *Dropwise condensation: experiments and simulations of nucleation and growth of water drops in a cooling system.* Langmuir, 2006. **22**(21): p. 8864-8872.
196. Rose, J. and L. Glicksman, *Dropwise condensation—the distribution of drop sizes.* International Journal of Heat and Mass Transfer, 1973. **16**(2): p. 411-425.
197. Rose, J., *Further aspects of dropwise condensation theory.* International Journal of Heat and Mass Transfer, 1976. **19**(12): p. 1363-1370.
198. Lee, D.W., M. Ruths, and J.N. Israelachvili, *Surface Forces and Nanorheology of Molecularly Thin Films*, in *Nanotribology and Nanomechanics: An Introduction*, B. Bhushan, Editor. 2017, Springer International Publishing: Cham. p. 457-518.
199. Chen, Y., C. Helm, and J. Israelachvili, *Molecular mechanisms associated with adhesion and contact angle hysteresis of monolayer surfaces.* The journal of physical chemistry, 1991. **95**(26): p. 10736-10747.
200. Eral, H.B., D.J.C.M. 't Mannetje, and J.M. Oh, *Contact angle hysteresis: a review of fundamentals and applications.* Colloid and Polymer Science, 2013. **291**(2): p. 247-260.
201. Sommers, A., J. Ying, and K. Eid, *Predicting the onset of condensate droplet departure from a vertical surface due to air flow—Applications to topographically-modified, micro-grooved surfaces.* Experimental Thermal and Fluid Science, 2012. **40**: p. 38-49.
202. Israelachvili, J.N., *Intermolecular and surface forces*. 2011: Academic press.
203. Tadmor, R., P. Bahadur, A. Leh, H.E. N'guessan, R. Jaini, and L. Dang, *Measurement of lateral adhesion forces at the interface between a liquid drop and a substrate.* Physical review letters, 2009. **103**(26): p. 266101.
204. Milne, A. and A. Amirfazli, *Drop shedding by shear flow for hydrophilic to superhydrophobic surfaces.* Langmuir, 2009. **25**(24): p. 14155-14164.
205. Annapragada, S.R., J.Y. Murthy, and S.V. Garimella, *Droplet retention on an incline.* International Journal of Heat and Mass Transfer, 2012. **55**(5): p. 1457-1465.
206. Pilat, D., P. Papadopoulos, D. Schaffel, D. Vollmer, R. Berger, and H.-J. Butt, *Dynamic measurement of the force required to move a liquid drop on a solid surface.* Langmuir, 2012. **28**(49): p. 16812-16820.
207. Antonini, C., F. Carmona, E. Pierce, M. Marengo, and A. Amirfazli, *General methodology for evaluating the adhesion force of drops and bubbles on solid surfaces.* Langmuir, 2009. **25**(11): p. 6143-6154.
208. Brown, R., F. Orr, and L. Scriven, *Static drop on an inclined plate: analysis by the finite element method.* Journal of Colloid and Interface Science, 1980. **73**(1): p. 76-87.

209. ElSherbini, A. and A. Jacobi, *Liquid drops on vertical and inclined surfaces: II. A method for approximating drop shapes.* Journal of colloid and interface science, 2004. **273**(2): p. 566-575.
210. Volynskii, M., *Study of droplet breakings in a gas flow.* DAN SSSR, 1949. **18**(2).
211. Lane, W., *Breakup of droplets in an air flow.* Industrial and Engng. Chem, 1951. **43**(6).
212. Morsi, S. and A. Alexander, *An investigation of particle trajectories in two-phase flow systems.* Journal of Fluid mechanics, 1972. **55**(02): p. 193-208.
213. Xu, H., Z. Sun, H. Gu, and H. Li, *Forced convection condensation in the presence of noncondensable gas in a horizontal tube; experimental and theoretical study.* Progress in Nuclear Energy, 2016. **88**: p. 340-351.
214. Ma, X.-H., X.-D. Zhou, Z. Lan, L. Yi-Ming, and Y. Zhang, *Condensation heat transfer enhancement in the presence of non-condensable gas using the interfacial effect of dropwise condensation.* International Journal of Heat and Mass Transfer, 2008. **51**(7): p. 1728-1737.
215. Ogg, D.G., *Vertical downflow condensation heat transfer in gas-steam mixtures*. 1991: University of California, Berkeley.
216. Caruso, G., D.V. Di Maio, and A. Naviglio, *Condensation heat transfer coefficient with noncondensable gases inside near horizontal tubes.* Desalination, 2013. **309**: p. 247-253.
217. Gambill, W., *How to estimate mixtures viscosities.* Chemical Engineering, 1959. **66**: p. 151-152.